Aus der Medizinischen Klinik und Poliklinik II Großhadern
der Ludwig-Maximilians-Universität München
Direktor: Prof. Dr. med. Alexander L. Gerbes

A synthetic lethal screen identifies ATR-inhibition as a novel therapeutic approach for *POLD1*-deficient cancers

Dissertation
zum Erwerb des Doktorgrades der Naturwissenschaften
an der Medizinischen Fakultät
der Ludwig-Maximilians-Universität München

vorgelegt von
Sandra Hocke

aus Zittau
2016

Gedruckt mit Genehmigung der Medizinischen Fakultät
der Ludwig-Maximilians-Universität München

Berichterstatter:	Priv. Doz. Dr. rer. nat. Andreas Herbst
Mitberichterstatter:	Prof. Dr. rer. nat. Peter B. Becker Prof. Dr. rer. nat. Olivier Gires
Dekan:	Prof. Dr. med. dent. Reinhard Hickel
Tag der mündlichen Prüfung:	11.08.2016

DECLARATION

I hereby declare that the thesis is my original work and I have not received outside assistance. All the work and results presented in the thesis were performed independently. Anything from the literature was cited and listed in the reference.

All the data presented in the thesis will not be used in any other thesis for scientific degree application.

The work for the thesis began November 2012 with the supervision from PD. Dr. med. Eike Gallmeier and PD Dr. rer. nat. Andreas Herbst in Medizinischer Klinik und Poliklinik II Großhadern, Ludwig-Maximilians University Munich, Germany.

Eching, 31.08.2016 _____ (Sandra Hocke)

To my parents and Martin

ABSTRACT

ATR (Ataxia Telangiectasia-mutated and Rad3-related) kinase acts as a central regulator and mediator of the replication checkpoint in response to DNA damage and replication stress. To initiate DNA repair, ATR induces a G2/M cell cycle arrest and stabilizes the replication fork during DNA synthesis. Pharmacological inhibition of ATR has recently been demonstrated to eliminate tumor cells in colorectal cancers (CRCs) but the underlying genetic determinants remain unexplained. Identification of these determinants is essential to develop novel tumor therapy strategies. Due to ATRs` essential role in DNA repair, synthetic lethal interactions of DNA repair mechanisms with *ATR* are suggested to mediate ATR-inhibitor specific tumor cell killing.

Using the concept of synthetic lethality, a synthetic lethal screen was conducted in a genetically well-defined *ATR* knock-in model of DLD1 CRC cells to identify potential genetic determinants eliciting ATR inhibitor-specific tumor cell killing. Applying a siRNA library directed against 288 DNA-repair genes, a set of DNA-repair genes was identified whose knockdown caused either the selective killing of DLD1 *ATR*-deficient cells (n=6) or an *ATR* genotype-independent cell killing of DLD1 *ATR*-proficient and DLD1 *ATR*-deficient cells (n=20).

The strongest synthetic lethal effect was observed between *ATR* and *POLD1* confirmed by kinetic and titration analysis upon *POLD1* knockdown in *ATR*-deficient cells. *ATR* genotype-dependent *POLD1* knockdown-induced cell killing was reproducible pharmacologically in *POLD1*-depleted DLD1 as well as a panel of other CRC cell lines by using chemical inhibitors of ATR or of its major effector kinase CHK1. Mechanistically, POLD1 depletion in DLD1 *ATR*-deficient cells caused caspase-dependent apoptosis without preceding cell cycle arrest and increased DNA damage along with impaired DNA repair, as demonstrated by elevated and sustained levels of γ-H2AX focus formation and pan-nuclear γ-H2AX staining. Irradiation-induced spatial co-localization of POLD1 with ATR as well as of POLD1 with γ-H2AX at sites of DNA damage was further detected.

Notably, inactivating *POLD1* mutations have recently been described in four families with multiple colorectal adenomas and CRC. In three of these families endometrial tumors were diagnosed. Considering that whole genome-sequencing might determine the *POLD1* mutation rates in different tumor entities, our data could have clinical implications in tumor genotype-based cancer therapy with regard to patients harboring those *POLD1*-deficient tumors, which might respond to chemical inhibition of the ATR/CHK1-axis. *POLD1* deficiency might thus represent a predictive marker for treatment response towards ATR- or CHK1-inhibitors, which are currently tested in clinical trials. Long-term, the development of selective POLD1-targeted drugs might further broaden the applicability of the identified synthetic lethality with ATR-inhibitors.

ZUSAMMENFASSUNG

DNA-Schäden lösen umfangreiche intrazelluläre Signaltransduktionskaskaden zur Erhaltung der genomischen Integrität aus. Die Kinase ATR (Ataxia Telangiectasia-mutated and Rad3-related) vermittelt dabei die Aktivierung und Regulierung des Replikationscheckpunkts zum Anhalten des Zellzyklus sowie die Stabilisierung der Replikationsgabel, um eine gezielte DNA-Reparatur gewährleisten zu können. Eine pharmakologische Inhibition von ATR führte bereits zum Absterben von Tumorzellen in kolorektalen Tumoren, wobei die zugrundeliegenden genetischen Determinanten noch nicht identifiziert werden konnten. Aufgrund der zentralen Funktionen von ATR im Rahmen der DNA-Reparatur liegt jedoch nahe, dass insbesondere veränderte DNA-Reparaturmechanismen in diesen Tumoren hier eine Rolle im Sinne synthetisch letaler Beziehungen mit *ATR* spielen könnten. Die Identifizierung dieser Determinanten könnte daher als Basis für neue Tumortherapie-konzepte dienen.

Im Rahmen dieser Arbeit wurde ein Screening einer siRNA-Bibliothek, basierend auf dem Prinzip der synthetischen Letalität, mit 288 DNA-Reparaturgenen in einem genetischen *ATR*-Knock-in-Modellsystem humaner kolorektaler Tumorzellen durchgeführt. Das Ziel war die Identifizierung genetischer Determinanten, die mit *ATR* synthetisch letal wirken. Es konnten mehrere DNA-Reparaturgene identifiziert werden, deren Ausschaltung das selektive Absterben von *ATR*-defizienten Tumorzellen induzierte (n=6). Desweiteren wurden auch DNA-Reparaturgene gefunden, deren Ausschalten zu einem *ATR*-unabhängigen Absterben von kolorektalen Tumorzellen (n=20) führte.

Das Ausschalten von *POLD1* zeigte den stärksten Effekt in *ATR*-defizienten Tumorzellen, der mittels Kinetik- und Titrationsexperimente bestätigt wurde. Potentiell klinische Relevanz erhalten diese Daten dadurch, dass die beobachteten Effekte nicht nur durch genetische *ATR*-Inhibition, sondern auch durch pharmakologische Inhibition sowohl von ATR selbst als auch seiner Haupt-Effektorkinase CHK1 in ähnlichem Maße ausgelöst werden konnten. Diese Daten ließen sich durch Untersuchung weiterer Tumorzelllinien generalisieren.

Weiterführende Untersuchungen zum zugrunde liegenden Wirkmechanismus konnten ein vermehrtes Auftreten von DNA-Schäden und eine beeinträchtige DNA-Reparatur zeigen, dargestellt durch eine erhöhte und anhaltende Anzahl an γ-H2AX Foci sowie einer Caspase-abhängige Apoptose ohne vorhergehenden Zellzyklusarrest in *ATR*-defizienten Tumorzellen nach dem Ausschalten von *POLD1*. Die zusätzlich nachgewiesene Ko-Lokalisation von POLD1 mit ATR sowie POLD1 mit γ-H2AX an Positionen mit DNA-Schäden nach IR in Tumorzellen unterstützt unsere Hypothese zum Wirkmechanismus (Apoptose als Folge von erhöhten DNA-Schäden bzw. verringerter DNA-Reparatur).

Mutationen in *POLD1* wurden bereits in niedriger Mutationsfrequenz in Patienten mit kolorektalen und endometrialen Tumoren beschrieben. Die hier erzeugten Daten könnten

daher als Basis zur Patientenstratifizierung für derzeit in klinischen Studien befindliche ATR/CHK1-Inhibitoren dienen und somit zur Individualisierung klinischer Therapieansätze beitragen. Langfristig könnte die Entwicklung spezifischer POLD1-Inhibitoren dazu dienen, die hier identifizierte synthetische Letalität als Kombinationstherapie mit ATR-Inhibitoren einem größeren Patientenkollektiv zugänglich zu machen.

CONTENTS

I List of contents

II. List of figures

III. List of tables

IV. Abbreviations

AKT	V-akt murine thymoma viral oncogene homolog 1, serine/threonine kinase
APC	Adenomatous polyposis coli
ATM	Ataxia telangiectasia mutated
ATR	Ataxia telangiectasia and Rad3 related
ATRIP	ATR interacting protein
BER	base-excision repair
BRAF	B-Raf proto-oncogene, serine/threonine kinase
BSA	Bovine serum albumin
$C_6H_5Na_3H_7 \times 2H_2O$	Trisodiumcitratedihydrate
CDC25	Cell division cycle
CDK1	Cyclin-dependent kinase 1
CHK1	Checkpoint kinase 1
CHK2	Checkpoint kinase 2
CIMP	CpG island methylator phenotype
CIN	Chromosomal instability
CRC	Colorectal cancer
DDR	DNA damage response
DNA-PKcs	DNA-dependent protein kinase catalytic subunit
dNTPs	Deoxynucleotides
DSB	Double-strand breaks
EDTA	Ethylenediaminetetraaceticacid
EGF	Epidermal growth factor
FANC	Fanconi anemia
H2AX	Histone variant H2AX
HR	Homologous recombination
ICL	Interstrand crosslink
IgG1/2	Immunoglobulin G 1/2
IR	Ionizing radiation
KRAS	Kirsten rat sarcoma viral oncogene homologue
LOH	Loss of heterozygosity
MAPK	Mitogen-activated protein kinase
MGMT	O^6-methylguanine DNA methyltransferase
MLH1	MutL homolog 1
MMR	Mismatch repair

MSI	Microsatellite instability
MSS	Microsatellite stable
mTOR	Mammalian target of rapamycin
NaCl	Sodium chloride
NAF	Sodium fluoride
$Na_4P_2O_7$	Sodium pyrophosphate
Na_3VO_4	Sodium orthovanadate
NER	Nucleotide-excision repair
NHEJ	Non-homologous end joining
P/S	Penicillin-Streptomycin
PARP	Poly(ADP-ribose)-Polymerase
PI3K	Phosphatidylinositol-4,5-bisphosphate 3-kinase
PI3KCA	Phosphatidylinositol-4,5-bisphosphate 3-kinase, catalytic subunit
PTEN	Phosphatase and tensin homolog
ROS	Reactive oxygen species
RPA	Replication factor A
RSR	Replication stress response
RS	Replication stress
RT	Room temperature
SMAD2/4	SMAD family member 2/4
SMG1	Suppressor with morphological effect on genitalia family member
SRC	SRC proto-oncogene, non-receptor tyrosine kinase
SSB	Single-strand breaks
SSBR	Single-strand break repair
TOPBP1	Topoisomerase (DNA) II binding protein 1
TS	Thymidylate synthase
UV	Ultraviolet
VEGF	Vascular endothelial growth factor
w/o	without
XP	Xeroderma pigmentosum

1. INTRODUCTION

1.1. The DNA damage response (DDR)

1.1.1. DDR-mediated signal transduction

Each of the ~10^{13} cells of the human body is persistently challenged by up to 10^5 DNA lesions per day (1). These damages are caused by exogenous (environmental) or endogenous (spontaneous) stress. Environmental-induced DNA lesions can be generated chemically (chemicals, anti-tumor agents) or physically (ultraviolet (UV) light, ionizing radiation (IR)). Endogenously-induced DNA alterations are elicited by depurination, cytosine deamination or oxidation via reactive oxygen species (ROS) (2; 3). These DNA lesions activate a complex DNA damage response (DDR) network. The DDR coordinates DNA replication and repair, cell cycle transition and apoptosis to ensure genome integrity and cell viability (4). The classical DDR pathways lead to the activation of a signal transduction cascade including DNA damage and replication stress detection, information transduction and execution of DDR functions by different repair mechanisms (5; 6) (**Fig. 1**).

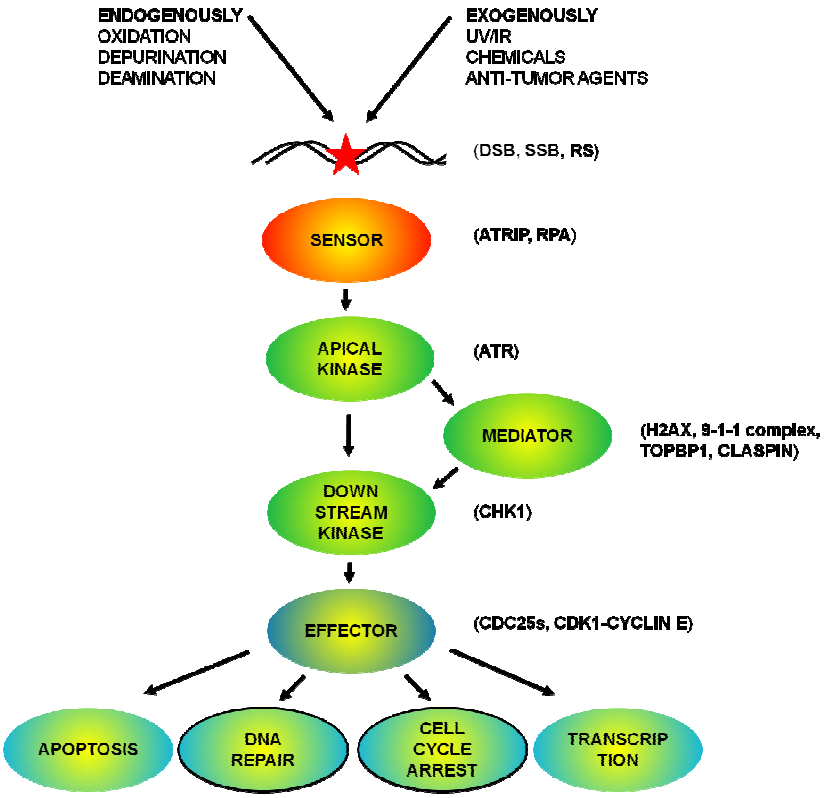

Figure 1: Schematic representation of DDR pathways. The DDR network is activated by exogenously- and endogenously-induced DNA lesions leading to stalled replication forks (and subsequent replication stress (RS)), single-strand breaks (SSBs) and double-strand breaks (DSBs). Signaling of DNA lesions comprises consecutive activation of sensor, transducer (apical kinases, mediators, downstream kinases) and effector proteins. Proteins involved in ATR-mediated DDR signaling are exemplarily listed in brackets. ATR activation directly effects DNA-repair and cell cycle progression/arrest (illustrated by black-bordered circles). Figure modified according to (5; 7).

1.1.2. DDR-mediated activation of DNA-repair pathways

Once a DNA lesion is sensed by DDR, different DNA-repair pathways depending on the source of DNA damage, exogenously- or endogenously-induced, are activated (**Table 1**).

Table 1: DNA-repair mechanisms in DDR.

DNA-repair mechanism	DNA lesion	Inducer of DNA lesions	DNA-repair mediators; Comments	References
Homologous recombination (HR)	• DSBs* • Stalled replication forks	• Unrepaired SSBs	• BRCA1/2 • FA protein • Error-free • Intact sister chromatid template required • S and G2/M cell cycle phase association	(8-11)
Non-homologous end joining (NHEJ)	• DSBs*	• ROS • IR	• Core proteins KU70/KU80 • Not error-free • No sequence homology required • Predominantly G0/ G1	(8-11)
Single-strand break repair (SSBR)**	• SSBs	• IR	• PARP proteins • XRCC1 • DNA polymerase δ/ε	(10)
Nucleotide-excision repair (NER)	• Helix-distorting lesions (large DNA adducts, base modifications) • Intrastrand and interstrand crosslinks (ICLs)	• UV, tobacco smoke, afflatoxin • Platinum-based agents	• XP proteins • ERCC1 • XRCC1 • DNA polymerase δ/ε	(12)
Base-excision repair (BER)**	• Non-helix-distorting • DNA strands with damaged bases • SSBs	• Base modification (deamination, loss) • ROS • IR	• PARP proteins • XRCC1 • DNA polymerase δ/ε	(10)
Mismatch repair (MMR)	• Mismatched nucleotides • Insertions • Deletions	• Replication errors*** • Base deamination	• MSH • MLH • PCNA proteins • DNA polymerase δ	(13; 14)
O^6-methylguanine DNA methyl-transferase (MGMT)	• Erroneous alkylation at the O^6- position of guanine	• SAM	• DNA methyltransferase • Direct reversal of DNA lesions	(10)

* DSBs display the most difficult DNA lesions.
** BER and SSBR are often assumed to be synonymous but differ in initial DNA lesion recognition. Whereas BER generates a SSB after removing of a damaged base, existing SSBs directly induce SSBR.
*** Replication errors are induced by insufficient intrinsic proofreading activity of DNA polymerases during DNA synthesis.
SSBs, single-strand breaks; DSBs, double-strand breaks; SAM, S-adenosyl methionine; ROS, Reactive oxygen species, UV, ultraviolet light; IR, ionized radiation; XP, xeroderma pigmentosum; FA, Fanconi anemia

1.1.3. Targeting DNA-repair pathways for cancer therapy

DDR and repair mechanisms are essential to cope with exogenously and endogenously-induced DNA lesions to maintain genomic stability. In order to exploit the DDR and DNA repair mechanisms for anticancer therapeutic approaches, different aspects have to be taken into consideration.

Firstly, chemo- and radiotherapy cause massive unspecific DNA damage. Their cytotoxic effects depend on the cellular DDR and DNA-repair mechanisms. Secondly, vice versa, an increased DNA-repair activity is suggested to be correlated with resistance to chemo- and radiotherapy, which represents one major obstacle in cancer treatment. Thirdly, predisposition to cancer can be associated with germline and infrequently arising somatic mutations of DDR genes, alterations of DDR proteins and epigenetic changes. Loss of function or down-regulation of DNA-repair genes in cancer results in hypersensitivity to DDR protein-targeted drugs. Fourthly, the loss of a distinct DDR pathway can activate tumor-specific compensatory DNA-repair mechanisms (15).

The understanding of DDR network along with the identification of potentially druggable DNA-repair proteins have provided the basis to exploit cancer-associated DDR alterations. DNA-repair inhibitors are often used in a combination therapy with chemo- or radiosensitizers to potentiate cytotoxicity. In solid cancer treatment, platinum chemotherapeutics (cisplatin, oxaliplatin, carboplatin) are known to form DNA adducts but are often associated with resistance, which is caused by an increased cellular repair activity. It has been shown that a combination therapy with PARP inhibitors (16) or the protein kinase inhibitor UCN-01 (17) can circumvent platinum resistance. In radiotherapy, it has been reported that the DNA-dependent protein kinase inhibitor NU7441 sensitizes cancer cells to IR. Inhibition of NHEJ by NU7441 prevents IR-induced DSBs repair (18). Furthermore, several PARP inhibitors undergo clinical testing as a single agent cancer therapy (10). However, the administration of DNA-repair inhibitors as monotherapy entails advantages and limitations. In general, single-agent therapies increase treatment selectivity, thus reduce unspecific side effects. Nevertheless, cross-talk between overlapping DNA-repair pathways also reduces single-agent activity and promotes acquisition of resistance mechanisms. To overcome cross-talk-induced resistance, the exploitation of synthetic lethal interactions is a possible concept to increase DNA-repair inhibitor selectivity and potency to achieve an exclusive cancer cytotoxicity (9). The principle of synthetic lethality is described in paragraph 1.3.

1.2. Ataxia telangiectasia mutated and RAD3-related (ATR)

1.2.1. ATR-mediated checkpoint signaling and DDR

The DDR network senses DNA damage and replication stress leading to a signal cascade activation primarily mediated by apical kinases of the phosphoinositide 3-kinase (PI3K)-related protein kinase (PIKK) family. These serine/threonine kinases include DNA-PKcs, mTOR, SMG1, ATM and ATR (19). The following part will focus on the role of ATR in cell cycle checkpoint signaling and DDR, as illustrated in Figure 1.

ATR is essential for the viability of replicating cells (20) due to its influences in cell cycle checkpoint signaling and DNA-damage repair (21). Although ATR-mediated DDR is initiated by single-stranded DNA structures, arising at double-strand breaks (DSBs), base adducts and crosslinks (19), ATR is mainly a replication stress (RS)-response kinase (4). Despite the different types of DNA lesions and RS events, single-stranded DNA (ssDNA) is suggested to be responsible for ATR activation (22). ssDNA is sensed and rapidly coated by RPA proteins. The ATRIP protein directly binds to RPA and recruits ATR to ssDNA (23). An RPA-coated ssDNA might be sufficient for ATR-ATRIP complex recruitment, however its interaction is not sufficient to activate ATR (4). Therefore, ATR signaling requires primed ssDNA with free 5´primer ends (24) and co-localization of the RAD9-RAD1-HUS1 (9-1-1) protein complex (19). The 9-1-1 complex recruits the critical ATR activator TOPBP1, containing an ATR activation domain (AD).

Once activated, ATR promotes transient cell cycle arrest, DNA-repair, replication fork stabilization and restart via its downstream targets (4). In detail, ATR signaling is mediated by phosphorylation of its major downstream kinase CHK1. ATR-CHK1 interaction is regulated by the adaptor protein CLASPIN (25). CHK1 activation mainly leads to the phosphorylation of CDC25 phosphatases (CDC25A-C), which inhibits their own activity. In detail, CDC25A phosphorylation inhibits replication origin firing during S-phase, which results in DNA replication slowdown and ensures proper DNA-repair conditions as a consequence of exogenously- or endogenously-induced DNA damage. The cell cycle S-phase is re-activated by CDC25A degradation and CDK1-CYCLIN E kinase regulation (4; 21). Further, G2/M cell cycle checkpoint signaling is regulated by CHK1-dependent CDC25A and CDC25C phosphorylation, which prevents premature mitosis entry (4).

Overall, ATR activation mediates S-phase arrest ensuring DNA repair by slowing DNA replication progress and preventing premature entry into mitosis, which is defined as ATR-induced replication stress response (RSR) (26).

1.2.2. Development of ATR-inhibitors for cancer therapy

Since ATR has been identified as an essential gene in mouse early embryogenesis (27), pharmacological inactivation of ATR was not taken into further consideration for specific inhibitor development.

Currently, it is believed that only hypomorphic or heterozygous ATR mutations with haploinsufficient features are compatible with cell viability (28). Based on this assumption, a human hypomorphic ATR mutation has been reported to cause the rare hereditary Seckel syndrome disorder (29). Studies of a mouse model harboring Seckel syndrome mutation could show that hypomorphic ATR depletion increases sensitivity of cancer cells to oncogene-induced replication stress (30). This finding reconsidered ATR inhibition as possible cancer strategy promoting ATR-inhibitor development.

Different studies identified the role of ATR in tumorigenesis. During early lesions, the ATR-dependent RSR prevents tumor growth, while in advanced stages, ATR activation promotes tumor progression (28; 31). Therefore, exploitation of the ATR-dependent RSR might be a potent strategy in cancer therapy.

The first available small molecule ATR-inhibitor was caffeine, which lacked potency and selectivity (32). Recently, several compounds were identified as effective ATR-inhibitors, e.g. VE-821 or AZ20. The further development of these ATR-targeting drugs and investigations in ongoing clinical trials show the potential of ATR inhibition, e.g. for VE-822 or AZD6738 (**Table 2**).

1.2.3. Targeting ATR in mono-and combination cancer therapy

ATR inhibition is considered to be a promising therapeutic target in combination with chemo- and radiotherapy. It has been reported, that various chemotherapeutics with different mode of actions sensitize cells to ATR inhibition, e.g. gemcitabine, 5-fluorouracil (5-FU) and platinum derivates. Gemcitabine, a cytidine analogue, misincorporates into the DNA and elicit DNA damage and replication fork stalling. Platinum chemotherapeutics form intra- and interstrand DNA adducts that result in bulky distortion of the DNA (33). However, in the clinical setting, a potent and selective monotherapy of DDR-targeted drugs, with few side effects, is aspired. Single agent activity has been exclusively reported for the ATR-inhibitors AZ20 and AZD6738 in either *MRE11*- or *ATM*-deficient cells so far (34; 35). VE-822, AZD6738 and NVP-BEZ235 are as yet the only ATR-inhibitors undergoing clinical testing (**Table 2**).

Table 2: Recently identified and developed ATR-inhibitors.

ATR inhibitor	Inhibitory effect	Comments	Reference
NU6027	• Originally developed as CDK2 inhibitor • Phosphorylation inhibition of CHK1 at Ser345	• Sensitivity in µM range • Lacks selectivity • Sensitivity to DNA-damaging agents/IR	(36)
VE-821	• Phosphorylation inhibition of CHK1 at Ser345	• Sensitivity in µM range • Potent and selective • Sensitivity to DNA-damaging agents/IR • Single agent activity in hypoxic cells	(37-39)
VE-822 (VX-970)	• Analogue of VE-821 • Phosphorylation inhibition of CHK1 at Ser345	• Sensitivity in nM range • Increased potency and selectivity • Improved pharmacokinetic properties • Sensitivity to DNA-damaging agents/IR/gemcitabine • 1st ATR inhibitor entering clinical trials	(33) (40) (ClinicalTrials.gov: NCT02157792)
AZ20	• Phosphorylation inhibition of CHK1 at Ser345	• Sensitivity in nM range • Potent and selective • Single agent activity *in vivo*	(34)
AZD6738	• Analogue of AZ20 • Phosphorylation inhibition of CHK1 at Ser345	• Increased potency and selectivity • Improved pharmacokinetic properties • Single agent activity *in vivo* • Sensitivity to IR and carboplatin • Clinical trial phase I investigations	(35) (Clinical Trials. gov: NCT02223 9239)
ETP-46464	• Leading to stalled replication fork breakage	• Sensitivity in nM range • Potent and selective	(41)
NVP-BEZ235	• Originally developed as a dual PI3K and mTOR inhibitor • Destabilization of stalled replication forks	• Sensitivity in nM range • Potent and selective • Clinical trial phase I investigations	(41) (42)

1.3. Synthetic lethality

Synthetic lethality is defined as interaction of two non-lethal mutations incompatible with cell viability (43; 44) and is induced by either classical gene knockout (**Fig. 2A**) or chemical inhibitor treatment (**Fig. 2B**). Genome-wide RNA interference screens are presently used to identify unknown synthetic lethal gene interactions in cancer cells harboring ´non-druggable oncogenes´ or ´absent tumor suppressors´ with new or already known and druggable gene targets, which are not previously associated with cancer (45; 46). These synthetic lethal approaches have the advantage to elicit tumor specificity because non-cancer cells harbor at least one functional gene of the targeted synthetic lethal gene interaction. In clinical application, synthetic lethality exploits tumor-associated alterations and has the ability to potentiate a weak single-agent anticancer activity in certain subpopulations of patients. Furthermore, this concept represents a more selective and tumor-specific anticancer therapy besides the classical less-selective chemo- and radiotherapy having a narrow therapeutic window and causing tissue-independent toxicity and patient-dependent side effects (45; 46). Therefore, synthetic lethal approaches provide a promising and powerful tool for anticancer therapy in personalized medicine.

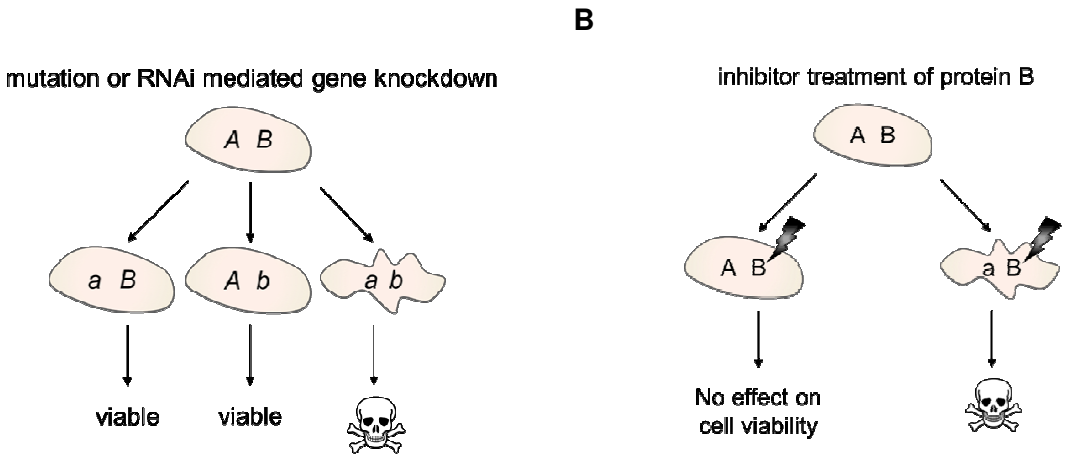

Figure 2: The principle of synthetic lethality. A synthetic lethal interaction of two genes is elicited, if two non-lethal mutations are incompatible with cell viability. Concerning therapeutic approaches, synthetic lethality is induced by (**A**) classical gene knockdown or (**B**) chemical inhibition.

1.3.1. Exploitation of deregulated DDR by synthetic lethality

Alterations in DDR pathways lead to genomic instability and predispose cells to exogenous and endogenous genotoxic stress, which is often linked to tumor development and progression (9; 47). Whereas down-regulation of DDR genes sensitizes cancer cells to some DDR-inhibitors, up-regulation of DDR genes can cause resistance to chemo- and

radiotherapy (10). The loss of a DDR pathway can lead to a compensatory DNA-repair gene activation (9). These compensatory pathways are particularly exploitable in DDR-defective tumors through synthetic lethal approaches. Utilizing the concept of synthetic lethality, one of the most striking examples for this approach is illustrated by the inhibition of *PARP* in *BRCA1* and *BRCA2*-deficient cancers (48; 49). Several other synthetic lethal interactions of DDR pathway genes have been reported so far (reviewed in (9; 11)).

1.3.2. Synthetic lethal interactions of ATR with DDR-associated and other genes

To date, little is known about synthetic lethal interactions between *ATR* and DDR genes. ATR inhibition induces synthetic lethality with *ATM*, encoding another apical kinase of the DDR network (38), *XRCC1*, encoding a component of the BER and NER pathways (50) and *ERCC1*, a gene, which is mainly associated with NER and further with HR and single-strand annealing (51). ATR-inhibitors also exhibit synthetic lethality with *p53* deficiency (38) as well as with oncogenic *RAS* and *CYCLIN E* overexpression (41; 52).

Genome-wide functional screens and the development of specific ATR inhibitors will promote the identification of novel synthetic lethal interaction partners of *ATR*. For clinical application, patient stratification regarding already known *ATR* synthetic lethal interactors and the improvement of ATR-inhibitors with regard to therapeutic efficacy and pharmacological properties might improve clinical trial designs and might benefit the clinical outcome in personalized cancer therapy.

1.4. Colorectal cancer (CRC)

1.4.1. Epidemiology of CRC

With over one million cases per year, CRC is one of the major cancer-related diseases worldwide (53). In men, CRC is the third most common malignancy after lung and prostate cancer. In women, CRC is registered as second most common malignancy after breast cancer (54). The CRC incidence rate varies widely and depends on age, socioeconomic status connected with 'modern lifestyle' and geographic area distribution as well as disease predisposition. A low CRC incident rate is seen up to 50 years of age, however with advanced age, the number of CRC patients is increasing (54). In Europe and in the US, the incidence rate is 10-fold higher compared to African and Asian countries, which is associated with the socioeconomic status of industrial and developing countries. 13% of the European and 8% of men and women from the US with CRC have an estimated mortality rate of 12% and 9%, respectively (55; 56). In 5-10% of all CRC cases, hereditary syndromes are associated with CRC development, such as HNPCC (hereditary non-polyposis CRC) and FAP (familial adenomatous polyposis) (57). Furthermore, 20% of CRCs occur among the patient's first-degree family members (54), whereas inflammatory diseases, such as ulcerative colitis and Crohn's disease, are main predisposing factors to CRC (58). However, the vast majority of CRC cases are of sporadic origin with no identifiable genetic risk factor.

1.4.2. Genetic and epigenetic patterns in CRC pathogenesis

CRC is defined as a heterogeneous disease caused by genetic (sporadic and hereditary origin) and epigenetic changes (59). Although 15-30% of CRC patients harbor hereditary components, the majority of colorectal tumors arise through sporadic accumulation of different gene mutations (60). In 1990, a genetic model for colorectal neoplasia was proposed by Fearon and Vogelstein describing oncogene activation (e.g. *RAS*) coupled with tumor suppressor gene inactivation (e.g. *p53*) as potential tumor promoting factors (61) leading to an increased clonal cell expansion, which promotes invasive cancer growth (60). Currently, three major CRC pathogenesis mechanisms have been identified as being the chromosomal instability (CIN) with an incidence of 60-80% (62; 63), the microsatellite instability (MSI) with an 13-20% incidence (62; 64; 65) and CpG island methylator phenotype (CIMP) with a frequency of 5-15% (59; 65). New insights into CRC pathogenesis imply that CRC does not arise by one distinct genetic mechanism, e.g. the mutual exclusiveness of MSI or CIN (53). Several studies associated different genetic and epigenetic CRC characteristics together with molecular profiles (different gene mutations) and clinical-pathological features (tissue morphology and location), which underlines the complexity of CRC tumorigenesis and progression (65-69).

The most common form of genomic instability in CRC is CIN characterized by aneuploidy, activation of proto-oncogenes, such as *KRAS*, *c-MYC, c-SRC*, *PI3KCA*, inactivation of tumor suppressor genes, such as *APC* and *p53*, and loss of heterozygosity for the long arm of chromosome 18 (18q LOH) (63; 70; 71). (**Fig. 3A**). Usually, mutations in *APC* initiate CRC tumorigenesis (72).

In a subgroup of patients, CRC is related to MSI caused by defects in the DNA mismatch repair (MMR) response. MSI is related to aberrant CpG promoter methylation of *MLH1* or point mutations in MMR genes (60). In detail, cells with impaired MMR tend to accumulate frameshift mutations (insertions, deletions) in microsatellite regions encoding small repetitive non-coding DNA sequences, which subsequently lead to genomic instability. (**Fig. 3B**). MSI is classified into MSI-high (MSI-H, ≥30%), MSI-low (MSI-L, 10-30%) and MSS (microsatellite stable).

MSI and CIN correlate with the CIMP status in CRC. CIMP is defined as hypermethylation of aberrant promoter sequences, which results in transcriptional silencing of tumor suppressor genes and DNA-repair genes, such as *MLH1* (**Fig. 3C**). Further, CIMP correlates with significant mutations in *BRAF* (69) and is classified into different subgroups (CIMP-high, CIMP-low, CIMP negative) (73).

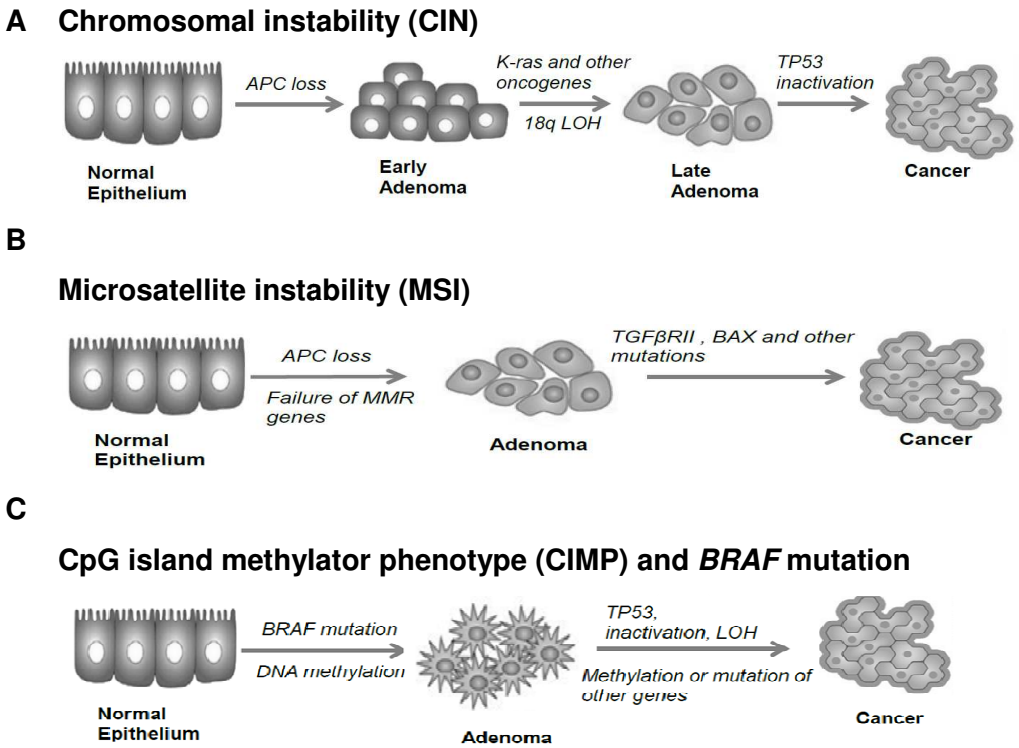

Figure 3: Genetic and epigenetic events involved in CRC pathogenesis. Three distinct pathways are associated with CRC tumorigenesis: (**A**) Chromosomal instability (CIN), (**B**) Microsatellite instability (MSI) and (**C**) CpG island methylator phenotype (CIMP), accompanied by gene mutations of *APC* (**A**+**B**), *p53* (**A**+**C**), *KRAS* (**A**) and *BRAF* (**C**). Figure modified according to (60).

1.4.3. Predictive and prognostic markers for CRC therapy

An ongoing challenge is to translate CRC-related genomics and epigenomics into clinical prognosis and prediction (**Table 3**). Currently, the assessment of the patients' clinical-pathological stage is based on the tumor-node-metastasis (TNM) classification, which remains the gold standard for prognosis (74). Nevertheless, the identification and validation of new prognostic and predictive genetic markers can improve and individualize a patient-specific therapy concerning drug efficacy maximization and cytotoxic side effect minimization (75).

Table 3: Clinically applicable prognostic and predictive genetic markers in CRC.

Genetic marker	Prognosis/Prediction	References
Prognostic		
Chromosome 18q	• LOH associated with a poorer prognosis • Worse prognosis for down-regulated *SMAD 2* and *SMAD4* (located on chromosome 18q)	(76)
APC mutation	• High risk of CRC development with *APC* germline mutations • *APC* mutations in 90% of CRC patients • Prophylactic colectomy or proctocolectomy in patients with germline *APC* mutations	(59; 77)
KRAS mutation	• Worse prognosis for substitution in codon 12 (G->V)	(78; 79)
BRAF mutation	• Poorer prognosis for V600E mutation • KRAS downstream signaling to BRAF	(79)
EGFR	• Poorer prognosis for *EGFR* overexpression	(80)
Thymidylate synthase (TS)	• Poorer prognosis for *TS* overexpression	(81)
Predictive		
KRAS mutation	• No response to EGFR inhibitor therapy (panitumumab and cetuximab)	(82; 83)
BRAF mutation	• V600E mutation • KRAS downstream signaling to BRAF • No response to EGFR inhibitor therapy (panitumumab and cetuximab)	(84)
Thymidylate synthase (TS)	• Decreased survival for patients highly expressing TS with 5-FU therapy	(85)

Prognostic markers provide information about the disease-related history and the likely course in non-treated individuals. For prognosis, germline mutations in tumor suppressor genes, such as *APC*, *MLH1* and *MSH2*, are associated with a high risk of CRC (77; 86). MSI is correlated with a favorable prognosis (86; 87), whereas CRC patients with a CIN pattern show a worse survival (88). In contrast, predictive markers correlate with the response and the impact to a specific drug treatment to evaluate patient-specific benefit (53). An established marker for prediction is *KRAS* associated with resistance to EGFR-inhibitor therapy (82; 83).

1.4.4. Treatment strategies in CRC therapy

Different types of treatment strategies are available for CRC patients. The most important strategy to improve survival of patients is the early detection of CRC. The most efficient treatment for early stage colon cancer is the removal of polyps by colonoscopy or by abdominal surgery (partial colectomy). Classical surgical resection is accompanied by adjuvant treatment with radio- and chemotherapy to control and restrict tumor growth as well as to reduce tumor recurrence after resection (74). However, radio- and chemotherapy are limited by a narrow therapeutic window and tissue-independent toxicity causing unselective side effects. Currently, new therapeutic strategies in the form of humanized monoclonal antibodies are developed to specifically affect molecular pathways critical for tumor growth and survival (74). However, therapies applying humanized monoclonal antibodies are likely to be more beneficial for CRC patients in combination with basic chemotherapies (89). Nonetheless, potent and selective monotherapies with few side effects are aspired in the clinical setting. New technologies like blood-based screenings of biomarkers with high CRC specificity are also currently under development (90) and should further improve early CRC detection, prognosis and prediction of treatment responses.

Table 4: Chemotherapeutic agents in systematic CRC treatment. Monoclonal antibody, noted mAb.

Therapeutic agent	Comment	Mechanism of action	References
Bevacizumab (Avastin®)	• Targeted therapy • Anti-VEGF mAb (humanized antibody against all VEGF-A isoforms)	• Antiangiogenesis (Prevention of VEGF receptor 2 signaling through VEGF-A antibody binding)	(91)
Cetuximab (Erbitux®)	• Targeted therapy • Anti-EGFR mAB (IgG1 subclass, chimeric mouse/human antibody)	• Antineoplastic • Inhibition of EGF receptor downstream signaling including RAS-RAF-MAPK axis (cell proliferation) and PI3K-PTEN-AKT axis (cell survival)	(92)
Irinotecan (Camptosar®)	• Derivate of camptothecin (topoisomerase I inhibitor),small molecule	• Antineoplastic • Inhibition of topoisomerase I • Increased DNA fragmentation and apoptosis induction	(93)
Fluorouracil (Fluoroplex®)	• fluorinated pyrimidine, small molecule	• Antineoplastic • Inhibition of thymidylate synthase	(89)
Oxaliplatin (Eloxatin®)	• Platinum derivate, small molecule	• Antineoplastic • DNA adduct formation, impaired DNA synthesis/replication and apoptosis induction	(94)
Panitumumab (Vectibix®)	• Targeted therapy • Anti-EGFR mAB (IgG2 subclass, fully human antibody)	• Antineoplastic • Inhibition of EGF receptor downstream signaling including RAS-RAF-MAPK axis (cell proliferation) and PI3K-PTEN-AKT axis (cell survival)	(92)

Various drugs already in clinical application (**Table 4**), e.g. irinotecan, 5-FU and oxaliplatin, are currently undergoing randomized clinical studies as single agent or combination therapy with chemotherapeutics already used in clinical CRC treatment (74) targeting DNA synthesis or DNA-repair mechanisms (10). DNA damage is detected and resolved by a complex genome maintenance system to permit high rates of spontaneous mutations in each cell generation (10). If DNA lesions are not removable, cells are forced into apoptosis (6), which serves as natural barrier to tumorigenesis (95). However, cancer cells developed different strategies to restrict or circumvent DNA damage-induced apoptosis in order to achieve replicative immortality, a hallmark of cancer (96), e.g. the activation of compensatory DNA-repair mechanisms (9). Thus, targeting DNA-damage signaling and repair proteins is a promising rationale in colorectal anti-cancer treatment strategies.

1.5. Aim of the project

ATR (Ataxia Telangiectasia-mutated and Rad3-related) kinase acts as central regulator and mediator of the replication checkpoint in response to DNA damage and replication stress. To initiate DNA repair, ATR induces a S-phase arrest and stabilizes the replication fork during DNA synthesis. Pharmacological inhibition of ATR has been reported to specifically eliminate tumor cells in colorectal cancers (CRCs) but the underlying genetic determinants remain unexplained. Based on ATRs' central role in DNA damage response, synthetic lethal interactions with DNA-repair genes might provide the underlying genetic mechanism leading to ATR inhibitor-specific tumor cell killing. Therefore, the purpose of this study was to clarify the genetic background of ATR inhibitor-specific tumor cell killing and to introduce novel therapeutic strategies with ATR-targeting drugs. The specific aims of this project are:

1. To identify potential synthetically lethal interactions between *ATR* and DNA-repair genes by applying a siRNA library screening approach of all major DNA-repair genes in a genetically well-defined *ATR* knock-in DLD1 CRC cell model.

2. To analyze the underlying mechanisms mediating the synthetic lethal interactions between *ATR* and the identified DNA-repair genes.

3. To test whether the pharmacological inhibition of ATR or its major effector kinase CHK1 elicits similar synthetically lethal effects as genetic *ATR* inactivation does, using common preclinically and clinically used ATR- and CHK1-targeting agents.

2. MATERIAL AND METHODS

2.1. Material

2.1.1. Chemicals

5-fluorouracile (5-FU)	Medac, Wedel, Germany
Acetic acid	Merck, Chemicals, Darmstadt, Germany
Acryl-bisacrylamide	Bio-Rad Laboratories GmbH, Munich, Germany
Actinomycin D	Sigma-Aldrich GmbH, Steinheim, Germany
β-Mercaptoethanol	Sigma-Aldrich GmbH, Steinheim, Germany
Bovine serum albumin (BSA)	Carl Roth GmbH & Co. KG, Karlsruhe, Germany
Bromophenol blue	Serva, Heidelberg; Germany
Dimethyl sulfoxide	Carl Roth GmbH & Co. KG, Karlsruhe, Germany
DN/RNase free H_2O	Qiagen GmbH, Hilden, Germany
dNTPs (dATP, dTTP, dGTP, dCTP)	KapaBiosystems Ltd., London, UK
Ethylenediaminetetraacetic acid (EDTA)	Merck KGaA, Darmstadt, Germany
Ethanol	Merck, Chemicals, Darmstadt, Germany
Hoechst 33342	Sigma-Aldrich GmbH, Steinheim, Germany
Ficoll® PM 400 Type 400	Sigma-Aldrich GmbH, Steinheim, Germany
Glycerol	Carl Roth GmbH & Co. KG, Karlsruhe, Germany
β-Glycerophosphate	Sigma-Aldrich GmbH, Steinheim, Germany
Glycine	Carl Roth GmbH & Co. KG, Karlsruhe, Germany
Methanol	Carl Roth GmbH & Co. KG, Karlsruhe, Germany
Mitomycin C (MMC)	Sigma-Aldrich GmbH, Steinheim, Germany
Non-fat dry milk	Bio-Rad Laboratories GmbH, Munich, Germany
Orange G	Sigma-Aldrich GmbH, Steinheim, Germany
Oxaliplatin	Accord Healthcare, Freilassing, Germany
Pierce ECL Western Blotting Substrate	Thermo Scientific, Rockford, IL, USA
Propidium iodide	Sigma-Aldrich GmbH, Steinheim, Germany
Sodium dodecyl sulfate (SDS)	Carl Roth GmbH & Co. KG, Karlsruhe, Germany
Sodium chloride	Sigma-Aldrich GmbH, Steinheim, Germany
Sodium fluoride	Sigma-Aldrich GmbH, Steinheim, Germany
Sodium orthovanadate	Sigma-Aldrich GmbH, Steinheim, Germany
Sodium pyrophosphate	Sigma-Aldrich GmbH, Steinheim, Germany
Sodium hydroxide	Merck, Chemicals, Darmstadt, Germany
SuperSignal West Dura Chemoluminescent Substrate	Thermo Scientific, Rockford, IL, USA

SuperSignal West Pico Chemoluminescent Substrate	Thermo Scientific, Rockford, IL, USA
SYBR Green Nucleic Acid Gel Stain	Lonza, Fisher Scientific GmbH, Schwerte, Germany
TEMED	Bio-Rad Laboratories GmbH, Munich, Germany
TNFα	Perbio Science AB, Helsingborg, Sweden
Tris-Base	Roche Diagnostics GmbH, Mannheim, Germany
Tris-HCl	Roche Diagnostics GmbH, Mannheim, Germany
Triton X-100	Carl Roth GmbH & Co.KG, Karlsruhe, Germany
Trypan blue	Sigma-Aldrich GmbH, Steinheim, Germany
Tween®20	Sigma-Aldrich GmbH, Steinheim, Germany

2.1.2. Biochemical reagents

Agarose (Crystal Agarose)	Carl Roth GmbH & Co. KG, Karlsruhe, Germany
Ethidiumbromide (10 mg/mL)	Carl Roth GmbH & Co. KG, Karlsruhe, Germany
Oligofectamin™ Reagent	Invitrogen, Life Technologies GmbH, Darmstadt, Germany

2.1.3. Antibodies

The following antibodies were used for immunoblotting detection.

2.1.3.1. Primary Antibodies

anti-β-ACTIN (Host: mouse)	Sigma-Aldrich GmbH, Steinheim, Germany
anti-ATR (N-19, sc-1887, Host: goat)	Santa Cruz Biotechnologies Inc., Heidelberg, Germany
anti-CASPASE3 (Host: rabbit)	Cell Signaling Technology, Boston, MA, USA
anti-CASPASE8 (Host: rabbit)	R&D Systems, Inc., Abingdon, UK
anti-CASPASE9 (Host: rabbit)	Cell Signaling Technology, Boston, MA, USA
anti-PARP (Host: rabbit)	Cell Signaling Technology, Boston, MA, USA
anti-phosphoH2AX (Ser139, 20E3, Host: rabbit)	Cell Signaling Technology, Boston, MA, USA
anti-phosphoH2AX (Ser139, Host: mouse)	Upstate Biotechnology Inc., NY, USA
anti-POLD1 (DNA pol # cat, sc-8797, Host: goat)	Santa Cruz Biotechnologies Inc., Heidelberg, Germany

2.1.3.2. Secondary Antibodies

2.1.3.2.1. HRP-conjugated antibodies

anti-mouse HRP-conjugated	GE Healthcare, PAA Laboratories GmbH, Pasching, Austria
anti-goat IgG-HRP (sc-2352, Host: bovine)	Santa Cruz Biotechnologies Inc., Heidelberg, Germany
anti-rat HRP-conjugated	GE Healthcare, PAA Laboratories GmbH, Pasching, Austria

2.1.3.2.2. Fluorochrome-conjugated antibodies

anti-goat Alexa Fluor®488 (Host: donkey)	Life Technologies GmbH, Darmstadt, Germany
anti-goat Rhodamine Red™-X-conjugated (Host: donkey)	Jackson ImmunoResearch Laboratories, Inc., West Grove, PA, USA
anti-mouse Alexa Fluor® 488 (Host: goat)	Life Technologies GmbH, Darmstadt, Germany

2.1.4. Antibiotics

Penicillin-Streptomycin (P/S)	PAA Laboratories GmbH, Pasching, Austria

2.1.5. Inhibitors

2.1.5.1. ATR inhibitors

NU6027	Merck, Darmstadt, Germany
VE-822	MedKoo Bioscience, Chapel Hill, NC, USA
CHK1 inhibitors	
LY2603618	Selleckchem, Munich, Germany
UCN-01	Sigma-Aldrich GmbH, Steinheim, Germany

2.1.5.2. Protease inhibitor

Protease Inhibitor Cocktail Set 1	Calbiochem, Merck, Darmstadt, Germany

The ready-to-use Protease Inhibitor Cocktail Set 1 was dissolved in 1 mL ddH_2O, aliquoted to 50 µL samples and stored at -20 °C. Ingredients of the Protease Inhibitor Cocktail Set 1 are listed in Table 5.

Table 5: Content of Protease Inhibitor Cocktail Set 1.

Inhibitor	Concentration (1x)	Target Protease
AEBSF	500 µM	Serine Proteases
Aprotinin	150 nM	Serine Proteases and Esterases
E-64	1 µM	Cysteine Proteases
EDTA	0.5 mM	Metalloproteases
Leupeptin	1 µM	Cysteine Proteases and Trypsin-like Proteases
Hemisulfate	1 µM	Cysteine Proteases and Trypsin-like Proteases

2.1.6. siRNA oligonucleotide

2.1.6.1. Single siRNA oligonucleotide

All siRNA oligonucleotide samples (1 nmol), except anti-β Gal siRNA 1 (Dharmacon Lafayette, Co, USA) were purchased from Qiagen GmbH, Hilden, Germany, diluted to a stock concentration of 20 µM and stored at -20 °C, according to the Qiagen siRNA protocol. Targeted sequences of all siRNAs are shown in Table 6.

Table 6: siRNA oligonucleotides and their target sequences.

siRNA oligonucleotide	Target sequence
anti-β Gal siRNA 1	5'-TTATGCCGATCGCGTCACATT-3
Hs_G22P1_3 (XRCC6)	5'-GAGGATCATGCTGTTCACCAA-3
Hs_POLD1_2	5'-CGGGACCAGGGAGAATTAATA-3
Hs_PRIM1_4	5'-AGCCTTGTAAAGGGTGGTCAA-3
Hs_RAD51AP1_3	5'-ATGGCATATGTCTCCGATTTA-3
Hs_RPA3_1	5'-AAGGGAGTAAATCGACCCTCA-3
Hs_SEPT9_10	5'-CTCAGAGCCCATGGTAACGAA-3
Hs_XRCC1_4	5'-AAGCCTGAAGTATGTGCTATA-3
Hs_XRCC5_6	5'-AAGCATAACTATGAGTGTTTA-3

2.1.6.2. siRNA Library

A FlexiPlate siRNA library containing 864 validated siRNAs targeting 288 DNA-repair genes in triplicates was purchased from QIAGEN, Hilden, Germany (catalog no. 1027411-385), diluted to a stock concentration of 1 µM and stored at -20 °C, according to the Qiagen siRNA protocol.
All 288 DNA-repair genes are listed in 7.1.

2.1.7. Cancerous cell lines

The following colorectal carcinoma cell lines were used.

Table 7: Colorectal cancer cell lines and their culture conditions.

Cell line	Characteristics*	Medium	Origin
DLD1	ATCC® CCL-211™ Dukes' type C, colorectal adenocarcinoma	Standard DMEM culture medium	American TypeCulture Collection, LGC Standards, Wesel Germany
DLD1 ATR	ATCC® CCL-221™ Dukes' type C, colorectal adenocarcinoma	Standard DMEM culture medium	(97) Gallmeier, Hermann et al. (2011)
HCT116	ATCC® CCL-221™ Dukes' type C, colorectal adenocarcinoma	Standard DMEM culture medium	European Collection of Cell Culture, Sigma-Aldrich GmbH, Steinheim, Germany
HT29	ATCC® HTB-38™ Colorectal adenocarcinoma	McCoys medium + 10% FCS + 1% P/S	European Collection of Cell Culture, Sigma-Aldrich GmbH, Steinheim, Germany
LS513	ATCC® CRL2134™ Dukes' type C, colorectal carcinoma	Standard RPMI culture medium	European Collection of Cell Culture, Sigma-Aldrich GmbH, Steinheim, Germany
RKO	ATCC® CRL-2577™ Colon carcinoma	Standard DMEM culture medium	European Collection of Cell Culture, Sigma-Aldrich GmbH, Steinheim, Germany
SW480	ATCC® CCL-288™ Dukes' type B, colorectal adenocarcinoma	Standard DMEM culture medium	European Collection of Cell Culture, Sigma-Aldrich GmbH, Steinheim, Germany

* Reference: American Type Culture Collection ATCC

2.1.8. Cell culture media, buffers and solutions

Dulbecco´s minimal essential medium (DMEM) high Glucose (4.5 g/l)	GE Healthcare, PAA Laboratories GmbH, Pasching, Austria
Dulbecco´s PBS (w/o Mg^{2+}, w/o Ca^{2+})	Sigma-Aldrich GmbH, Steinheim, Germany
Fetal bovine serum Superior (FBS)	Biochrom AG, Berlin, Germany
OptiMEM® Reduced Serum	Gibco, Life Technologies GmbH Darmstadt, Germany
RPMI medium	GE Healthcare, PAA Laboratories GmbH, Pasching, Austria
Trypsin/EDTA (0.25 %/0.02 %	PAA Laboratories GmbH, Pasching, Austria

2.1.8.1. Preparation of cell culture media, buffers and solutions

Standard DMEM culture medium	DMEM 10% FCS 1% P/S → Stored at 4 °C
Standard RPMI culture medium	RPMI

	10% FCS 1% P/S → Stored at 4 °C
Freezing medium	Standard DMEM/RPMI culture medium 5% DMSO

2.1.8.2. Further preparations of buffers, solutions and gels

2.1.8.2.1. Preparation of solutions

BSA solution (1 mg/mL)	10 mg BSA 10 mL ddH_2O → Stored at -20 °C
Caspase lysis buffer	200 mM HEPES 84 mM KCl 10 mM $MgCl_2$ 0.2 mM EDTA 0.2 mM EGTA 0.5% NP 40 (IGEPAL)

Additionally, the following protease and phosphatase inhibitors were immediately added to caspase lysis buffer before usage.

	1 mM PMSF 1 mM DTT 1 µg/mL Pepstatin 5 µg/mL Aprotinin
NaCl solution (5 M)	146.1 g NaCl 450 mL ddH_2O → Stored at RT
Nicoletti staining solution	228 mg $C_6H_5Na_3H_7$ x $2H_2O$ 189 µL Triton X-100 10 mL 50 µg/mL propidium iodide

PCR loading dye solution (10x)	0.05 g Orange G 1.5 g Ficoll® (type 400) 1 mL 0.5 M EDTA (pH 8) Add to 10 mL ddH_2O → Stored at RT
Resolving gel solution	10 mL 10% SDS 250 mL 1.5 M Tris pH 8.8 400 mL ddH_2O → Stored at 4 °C
SDS solution (10 %)	10 g SDS 90 mL ddH_2O → Stored at RT
Stacking gel solution	5 mL 10% SDS 62.5 mL 1 M Tris pH 6.8 → Stored at 4 °C

2.1.8.3. Preparation of buffers

Blocking buffer	5% (w/v) non-fat milk powder TBST buffer (1x)
p38 protein lysis buffer	40 mg $Na_4P_2O_7$ 68 mg NaF 440 mg β-Glycerophosphate 0.8 mL Triton X-100 0.8 mL 100 mM Na_3VO_4 1.6 mL 2 mM EDTA 2.4 mL 5 M NaCl 16 mL 100 mM Tris Base, pH 7.4 → Stored at 4 °C

Additionally, 50 µL of the Protease Inhibitor Cocktail Set 1 (see 2.1.5.3) were immediately added to 5 mL of p38 protein lysis buffer before usage.

Sample loading buffer (Laemmli buffer, 5x)	10 mg Bromophenol blue 1 g SDS 2.5 mL SDS-PAGE Stacking gel buffer, pH 6.8 2.5 mL β-Mercaptoethanol 5 mL Glycerol →Stored at -20 °C
SDS-PAGE electrophoresis running buffer (10x)	10 g SDS 30 g Tris Base 144 g Glycine Add to 1 l ddH_2O → Stored at RT
SDS-PAGE resolving gel buffer	181.7 g 1.5 M Tris Base 900 mL ddH_2O → Adjust pH to 8.8 and add ddH_2O to 1 L. → Stored at RT
SDS-PAGE stacking gel buffer	181.7 g 0.5 M Tris Base 900 mL ddH_2O → Adjust pH to 6.8 and add ddH_2O to 1 L. → Stored at RT
TBS buffer (10x)	24.1 g Tris Base 80 g NaCl 800 mL ddH_2O → Adjust pH to 7.6 and add ddH_2O to 1 L. → Stored at RT
TBST buffer (1x)	1 mL Tween20 100 mL 10x TBS 800 mL ddH_2O → Stored at RT
Transfer buffer (10x)	30 g Tris Base 144 g Glycine Add to 1 L ddH_2O → Stored at RT

Transfer buffer (1x)	100 mL 10x Transfer buffer 200 mL Methanol 700 mL ddH_2O → Stored at RT

2.1.8.4. Gels

Agarose gel (2%)	4 g Agarose 200 mL ddH_2O → Stored at 4 °C
SDS-PAGE resolving gel (8%)	0.006 mL TEMED 0.1 mL 10% Ammonium persulfate 0.1 mL 10% SDS 2.5 mL 1.5 M Tris (pH 8.8) 2.7 mL 30% Acryl-bisacrylamide mix 4.6 mL ddH_2O → Used directly
SDS-PAGE resolving gel (10%)	0.004 mL TEMED 0.1 mL 10% Ammonium persulfate 0.1 mL 10% SDS 2.5 mL 1.5 M Tris (pH 8.8) 3.3 mL 30% Acryl-bisacrylamide mix 4.0 mL ddH_2O → Used directly
SDS-PAGE stacking gel (5%)	0.005 mL TEMED 0.05 mL 10% Ammonium persulfate 0.05 mL 10% SDS 0.63 mL 1.5 M Tris (pH 6.8) 0.83 mL 30% Acryl-bisacrylamide mix 3.4 mL ddH_2O → Used directly

2.1.9. Primer

The following primers (Metabion international AG, Munich, Germany) were used for KAPATaq DNA Polymerase Standard PCR.

Table 8: Primer for KAPATaq DNA Polymerase Standard PCR.

Primer	Target sequence
Forward MycoPrimer	5'-GGGAGCAAACAGGATTAGATACCCT-3'
Reverse MycoPrimer	5'-TGCACCATCTGTCACTCCGTTAACCTC-3'

2.1.10. Standards

2.1.10.1. Standards for agarose gel electrophoresis

Low Molecular Weight DNA Ladder	New England Biolabs GmbH, Frankfurt am Main, Germany
O'GeneRuler™ 1 kb Plus DNA Ladder	Fermentas Life Science, Fisher Scientific GmbH, Schwerte, Germany

2.1.10.2. Standards for SDS-PAGE

MagicMark™ XP Western Protein Standard	Life Technologies, Darmstadt, Germany
Precision Plus Protein™Standards	Bio-Rad Laboratories, Munich, Germany

2.1.11. Kits

Apo-One Homogenous Caspase3 Kit	Promega GmbH, Mannheim, Germany
KAPATaq PCR Kit KK1015	KapaBiosystems Ltd., London, UK

2.1.12. Consumables

Adhesive PCR Film	PeQLab Biotechnologies GmbH, Erlangen, Germany
Cell Scraper (16 cm)	Sarstedt AG & Co. KG, Nümbrecht, Germany
Cover glass	Fisher Scientific GmbH, Schwerte, Germany
Cover slips	Thermo Scientific, Langenselbold, Germany
CryotubesCryo.S™	Greiner Bio-One GmbH, Frickenhausen, Germany

Culture dishes (10 cm)	BD Biosciences, San Jose, CA, USA
Culture plates (6-/96-well plate)	BD Biosciences, San Jose, CA, USA
Cuvettes	Sarstedt AG & Co. KG, Nümbrecht, Germany
Gloves	Semperit GmbH, Vienna, Austria
Microtubes (1.5 mL)	Sarstedt AG & Co. KG, Nümbrecht, Germany
Microtubes (2 mL)	Eppendorf Vertrieb Deutschland GmbH, Wesseling-Berzdorf, Germany
Non-pyrogenic serological pipette	Sigma-Aldrich GmbH, Steinheim, Germany
PARAFILM® M	Sigma-Aldrich GmbH, Steinheim, Germany
Pasteur pipettes	Brand GmbH, Wertheim, Germany
PCR soft tubes	Fisher Scientific GmbH, Schwerte, Germany
Pipette tips	VWR International GmbH, Darmstadt, Germany
PVDF membranes	Zefa-Laboratories GmbH, Harthausen, Germany
Ranin tips	Mettler-Toledo, LLC, Columbus, USA
Sterile filter	PeskeGmbH, Aindling-Pichl, Germany
Tubes (15/50 mL)	BD Biosciences, San Jose, CA, USA
X-ray film	Fuji Film Europe GmbH, Düsseldorf, Germany

2.1.13. Instruments

Accuri C6 Flow Cytometer® (FACS)	BD Biosciences, San Jose, CA, USA
Airfuge® Air-Driven Ultracentrifuge	Beckman Coulter GmbH, Krefeld, Germany
Cell counting chamber (0.0025 mm^2/ 0.1 mm)	Carl Roth GmbH & Co. KG, Karlsruhe, Germany
Centrifuge ROTANTA	HettichGmbH& Co. KG, Tuttlingen, Germany
Refrigerated centrifuge	Eppendorf Vertrieb Deutschland GmbH, Wesseling-Berzdorf, Germany

CytoFluor 4000 plate reader	Per-SeptiveBiosystems, Framingham, MA, USA
Electrophoresis transfer unit	PeQLab Biotechnologies GmbH, Erlangen, Germany
Electrophoresis transfer chamber + power supply	Bio-Rad Laboratories GmbH, Munich, Germany
Inverted Fluorescence Microscope Axiovert 135	Carl Zeiss Jena GmbH, Jena, Germany
HERA cell culture incubator	Fisher Scientific GmbH, Schwerte, Germany
Laminar Hood	Fisher Scientific GmbH, Schwerte, Germany
Mini Spin Centrifuge	Eppendorf Vertrieb Deutschland GmbH, Wesseling-Berzdorf, Germany
Olympus CK2 Inverted Microscope	Olympus Optical Co. GmbH, Planegg, Germany
PCR cycler	Eppendorf Vertrieb Deutschland GmbH, Wesseling-Berzdorf, Germany
PCR gel electrophoresis chamber	Bio-Rad Laboratories GmbH, Munich, Germany
PCR gel electrophoresis chamber power supply	Bio-Rad Laboratories GmbH, Munich, Germany
pH meter	Inolab®-WTW GmbH, Weilheim, Germany
Pipettes (10/20/200/1000 µL)	Eppendorf Vertrieb Deutschland GmbH, Wesseling-Berzdorf, Germany
Ranin multichannel pipettes (300 µL)	Mettler-Toledo, LLC, Columbus, USA
Ranin pipettes (2/10/20/200/1000/2000 µL)	Mettler-Toledo, LLC, Columbus, USA
Refrigerators (4/-20 °C)	LIEBHERR, Hamburg, Germany
Thermomixer comfort	Eppendorf Vertrieb Deutschland GmbH, Wesseling-Berzdorf, Germany
UV/Vis Spectrophotometer Ultraspec 3100 pro	Amersham Biosciences, Freiburg, Germany
Vortex Mixer VM-300	NeoLabMigge, Heidelberg, Germany
Water bath	Labortechnik Medingen, Arnsdorf, Germany
Western Blot Gel making unit	Bio-Rad Laboratories GmbH, Munich, Germany

2.1.14. Software

CFlow Plus BD Accuri Software	BD Biosciences, San Jose, CA, USA
IBM SPSS Statistics 21	SPSS Inc., Chicago, IL, USA
Microsoft Office 2007/2010	Microsoft, Redmond, WA, USA
Prism/GraphPad	GraphPad Software Inc., La Jolla, CA, USA
Zeiss Axio Vision Rel. 4.8	Carl Zeiss Jena GmbH, Jena, Germany

2.2. Methods

2.2.1. Cell culture methods

2.2.1.1. Standard cell culture conditions and subculturing

All cells (see 2.1.7) were grown in standard DMEM/RPMI culture medium (see 2.1.8.1) in a humidified incubator under standard culture conditions (37 °C, 5% CO_2). Cells were checked microscopically to ensure viability and confluence. Cells were assessed regularly for mycoplasma contamination by PCR (see 2.2.4). For subculturing, all media, additives, buffers and trypsin were preheated before using. Every 2 to 3 days, cells were washed once in sterile PBS, trypsinized for an appropriate time at 37 °C and subcultured.

2.2.1.2. Thawing and freezing (cryopreservation) of cells

Immediately after thawing, cells were added to cold standard DMEM/RPMI culture medium, centrifuged (1200 rpm, 10 min, RT) and re-suspended in fresh standard DMEM/RPMI culture medium.
To freeze cells, cell confluence was 80-90%. The cells were washed in PBS and trypsinized. After centrifugation (1200 rpm, 10 min, RT) in standard culture media, the cell pellet was resuspended in freezing medium, aliquoted in cryovials and stored at -80 °C for 24 h before transferring into liquid nitrogen. Cells were periodically frozen to maintain original cell conditions.

2.2.1.3. Determination of cell numbers

The number of cells were determined prior to every experiment in order to maintain equal cell amounts required for each experiment. After the cells have been trypsinized and resuspended in standard culture medium, a volume of 10 µL of cell suspension was mixed with 10 µL trypan blue and analyzed in a cell counting chamber. Cells in 4 quadrates were counted. The average cell number was multiplied by 10^4 to obtain the final cell number per mL.

2.2.1.4. Cell cycle analysis by flow cytometry

Cells were grown in 6-well plates. At 80% confluence, the cells were trypsinized, collected, washed with sterilized, ice-cold PBS once and incubated in Nicoletti staining solution (light sensitive) according to the method by Nicoletti (98). Quantification of cell cycle distribution and subG1-cell fraction were analyzed by flow cytometry and CFlow Plus software. Per sample, 20.000 events were analyzed.

2.2.2. RNA interference experiments

2.2.2.1. siRNA library transfection

A siRNA library was used containing 288 validated DNA-repair genes each targeted by 3 different siRNAs (QIAGEN, Hilden, Germany). 800 to 1,000 cells/well were seeded in 96-well plates to reach confluence at day 7. 24 h later, transfection was performed in a supplementary-free medium with the respective siRNAs or no siRNA at a final concentration of 10 nM using Oligofectamin (Invitrogen, Darmstadt, Germany) in OptiMEM (Gibco, Life Technologies GmbH, Darmstadt, Germany). 4 h after transfection, serum-containing medium was added to the cells. 120 h after transfection, cells were washed, lysed in 100 µL H_2O and 0.2% SYBR®Green (Lonza, Cologne, Germany) was added. Fluorescence was measured using a CytoFluor Series 4000 plate reader (PerseptiveBiosystems, Framingham, MA, USA) (**Fig. 4**).

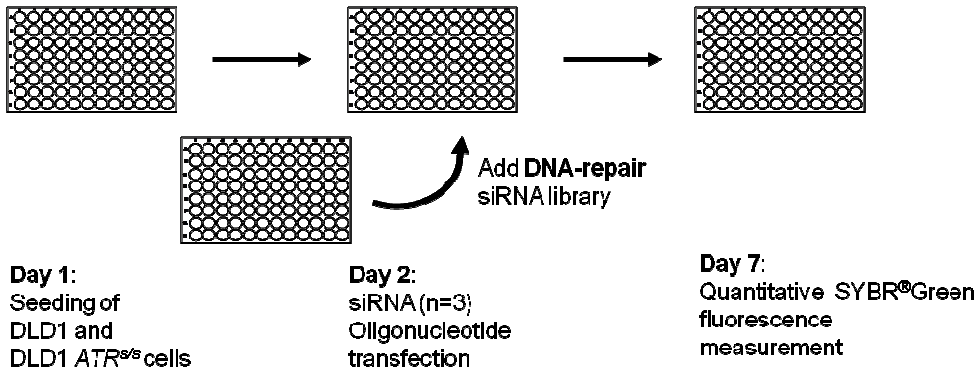

Figure 4: Experimental procedure of the siRNA library screen. DLD1 parental and DLD1 *ATR*$^{s/s}$ cells were transfected with 288 DNA-repair genes targeted by three different siRNAs or no siRNA.

Four independent siRNA library screens were performed with each siRNA data point reflecting triplicate wells. The proliferation inhibition was determined by dividing each siRNA-treated value by the average of 12 untreated control values for both DLD1 parental and DLD1 *ATR*$^{s/s}$ cells. The proliferation inhibition ratio was calculated by dividing the growth inhibition value of DLD1 parental by the value of DLD1 *ATR*$^{s/s}$ cells. The mean proliferation inhibition ratio and the standard error of the mean were determined from four individual proliferation inhibition ratio values that each represented triplicates from three different oligonucleotides targeting one particular gene. DNA-repair genes were classified into hit categories defined as either "*ATR*-genotype dependent" or "*ATR*-genotype independent" proliferation inhibition. DNA-repair genes were scored as "*ATR*-genotype dependent" hits if the mean growth inhibition ratio was >1.50 and the average relative survival of DLD1 parental cells was >0.45. Gene targets causing comparable growth inhibitions in DLD1 parental and DLD1 *ATR*$^{s/s}$ cells were scored as "*ATR*-genotype independent" hits. The

average relative survival of DLD1 parental and DLD1 *ATR*$^{s/s}$ cells was ≤0.45, respectively, calculated by the mean of four individual proliferation inhibition values for each cell line from three different oligonucleotides targeting one particular gene. Further, Δ-values of the average relative survival of DLD1 parental and DLD1 *ATR*$^{s/s}$ cells were calculated by subtracting the average relative survival of DLD1 parental and DLD1 *ATR*$^{s/s}$ cells, respectively, and scored as "*ATR*-genotype dependent" DNA-repair genes with Δ-values of ≥0.3 and "*ATR*-genotype independent" DNA-repair genes with Δ-values of <0.3. As preliminary experiments confirmed no relevant proliferation differences between untreated and mock-transfected cells, untreated cells were used as controls in the following screening experiments.

2.2.2.2. siRNA oligonucleotide transfection

Cells at 30-50% confluence were transiently transfected in supplementary-free DMEM/RPMI medium using oligofectamin in OptiMEM and siRNA directed against a single gene or a non-coding sequence of *ß*-galactosidase (*ß*GAL) or no siRNA (mock-transfected). siRNAs were used at final concentrations of 2.5, 5, 10, 20, 40 and 80 nM. The transfection proceeded for 4 h before adding serum-containing standard DMEM/RPMI culture medium. After different incubation times from 24 to 120 h, protein depletion was either quantified by immunoblotting (2.2.5.1) or cell proliferation differences were assessed by quantitative SYBR®Green fluorescence measurement (2.2.2.1).

2.2.2.3. Cell proliferation assay

Cell proliferation assays were performed over a broad range of concentrations covering 100% to 0% cell survival. 800 to 3,000 cells/well were seeded in 96-well plates to reach confluence on day 7. After settling, the cells were incubated with various drugs at multiple concentrations. Following incubation for 120 h, the cells were washed with sterilized, ice-cold PBS, lysed in 100 µL sterilized ddH_2O and 0.2% SYBR®Green was added. Fluorescence was measured using a CytoFluor Series 4000 plate reader and proliferation inhibition was calculated as compared to the untreated control samples. At least three independent experiments were performed per drug, with each data point reflecting triplicate wells. Error bars represent standard deviation from three experiments.

2.2.3. Molecular biological methods

2.2.3.1. Detection of Mycoplasma contamination

PCR technique was used to detect mycoplasma contamination in cell culture supernatants. After 72 h incubation, cell culture supernatants were analyzed according to KAPATaq DNA Polymerase Standard PCR protocol (**Fig. 5**) using Forward/Reverse MycoPrimer (see 2.1.10).

Ingredients	**Master Mix (1x)**
Cell culture supernatant	1.0 µL
KAPA B buffer (10x)	1.0 µL
dNTP-Mix (1 mM)	0.2 µL
Forward MycoPrimer	0.1 µL
Reverse MycoPrimer	0.1 µL
DMSO	0.2 µL
KAPATaq polymerase (5 U/µL)	0.04 µL
ddH_2O	7.36 µL
	10 µL

Cycling instructions			
1.	95 °C	2 min	
2.	95 °C	30 min	35 cycles
3.	62 °C	30 sec	
4.	72 °C	∞ 40 sec	
4.	72 °C	∞ 2 min	
5.	4 °C	∞	

Figure 5: KAPATaq Standard PCR protocol.

2.2.4. Biochemical methods

2.2.4.1. Cell lysate preparation for protein quantification

Cells were trypsinized and centrifugated (1200 rpm, 10 min, RT). The supernatant was discarded and cells were washed with ice-cold PBS twice. After centrifugation (1200 rpm, 10 min, RT), PBS was removed and the cell pellet was lysed in freshly prepared p38 protein lysis buffer including protease inhibitor cocktail Set 1 (Calbiochem, 30 min, on ice). The cell pellet was centrifuged (10,000 rpm, 10 min, 4 °C) and the supernatant containing protein lysate was stored at -20 °C.

2.2.4.2. Protein quantification

To adjust similar protein amounts for SDS-PAGE, Bradford protein assay was used to measure protein concentrations of lysates according to manufacturer´s recommendations (99). Bradford reagent was diluted 1:5 in ddH_2O. Afterwards, 1 µL diluted BSA protein standard (0.2, 0.4, 0.6, 0.8 mg/mL) or 1 to 5 µL protein lysate were mixed in 1000 µL diluted Bradford reagent. The mixture was shortly incubated (5 min, RT) and the absorbance was measured at 595 nm wave length at a spectrophotometer. Lysate concentrations were calculated on the basis of the linear regression obtained from protein standard values.

2.2.4.3. One dimensional SDS polyacrylamide gel electrophoresis (SDS-PAGE)

SDS-PAGE was conducted as described previously (100). In short, Laemmli buffer (5x) was added to concentration-adjusted lysates. Samples were boiled (10 min, 95 °C), centrifuged briefly before separating 20 to 60 µg of cell extracts by SDS-PAGE using 5% (w/v) acrylamide stacking gel and 8 to 10% (w/v) acrylamide resolving gel (see 2.1.9.3). Gels were run in SDS electrophoresis running buffer (1x) at 80 V for 30 min throughout the stacking gel and further 1 h at 120 V.

2.2.4.4. Fluorometric CASPASE3 activity assay

Detection of CASPASE3-like DEVDase activity was described previously (101). In short, cells were seeded in 96-well plates to reach confluence at day 5 and lysed in caspase lysis buffer including protease and phosphatase inhibitors (30 min, on ice). Protein concentration was measured by Bradford protein assay as described before. Caspase activity was determined from 20 µg protein lysate by incubation with 50 µM of the fluorogenic substrate peptide Ac-DEVD-AMC in 200 µL caspase lysis buffer. Cleavage of Ac-DEVD-AMC peptide by CASPASE3 releases the fluorophore 7-amino-4-methylcoumarin, which was measured in a kinetic assay by spectrofluorometry using an excitation wavelength of 360 nm and an emission wavelength of 460 nm. The level of caspase enzymatic activity is directly proportional to the fluorescence signal. Caspase activity was determined as slope of the resulting linear regression.

2.2.5. Immunological methods

2.2.5.1. Immunoblotting

Proteins were transferred onto a PVDF membrane (102) (120 mA, 1 h) using a semi-dry blot device in the presence of transfer buffer (1x) for immunoblot analysis.

2.2.5.2. Immunoblot staining and detection

Blotted membranes were blocked in blocking buffer (1 h, RT) prior to primary antibody exposure (o/n, 4 °C) followed by the appropriate secondary antibody incubation (2 h, RT). Antibodies were diluted 1:1,000 to 1:10,000 in blocking buffer. Target proteins were identified using horseradish peroxidase (HRP) conjugated secondary anti-IgG antibodies and ECL Western Blotting Substrate according to the manufacturer´s instructions. Semi-quantitative analysis for protein expression levels was performed by densitometry.

2.2.5.3. Immunofluorescence microscopy for co-localization analysis

To study γ-H2AX focus formation, cells were grown on coverslips in 6-well plates. At 60% confluence, the cells were irradiated at a dose of 4 Gy using a Mueller RT-250 γ-ray tube (200 kV and 10 mA, Thoraeus filter, 1 Gy in 1 min 52 s). Consecutively, treated cells were washed with sterilized, ice-cold PBS, fixed in 3.7% formaldehyde (10 min, RT) and methanol (1 min, RT). After permeabilization in TBS/0.5% Triton X-100 (10 min, RT) and blocking in TBS/2% BSA/0.5% Triton X-100 (30 min, RT), cells were incubated with an anti-ATR (1:200), anti-phosphoH2AX (1:200) or anti-POLD1 (1:200) antibody in TBS/2% BSA/0.5% Triton X-100 (2 h, RT). Afterwards, the cells were washed with sterilized, ice-cold PBS and incubated with their corresponding fluorochrome-conjugated antibodies (1:200, see 2.1.3.2.2) in TBS/2% BSA/ 0.5% Triton X-100 (2 h, RT). After washing with sterilized, ice-cold PBS, nuclei were counterstained with Hoechst 33258 at 10 µg/mL in TBS/0.5% Triton X-100 (10 min, RT). Slides were mounted with VECTASHIELD mounting medium and analyzed using a Axiovert fluorescence microscope (Zeiss) and the AxioVision Re.4.8 software. Exposure time and settings were kept constant for all samples within each experiment.
For co-localization study, the cells were fixed at 4 h post IR. For foci quantification, 45 and 30 nuclei were scored for ATR-POLD1 and γ-H2AX-POLD1 co-localization analysis, respectively, in one single experiment. Values represent the standard deviation of two independent experiments.

2.2.6. Statistical methods

2.2.6.1. Statistical analysis by SPSS

All statistical analyses were performed using IBM SPSS Statistics 21. Error bars represent standard deviation from at least three experiments. FACS and spatial co-localization data were statistically interpreted using a paired Student's *t*-test. *P*-values (**$p < 0.01$, ***$p < 0.001$) were considered statistically significant.

3. RESULTS

3.1. siRNA library screening of DNA-repair genes

3.1.1. Verification of ATR-Seckel phenotype in DLD1 cancer cells.

Prior to siRNA library screening on human *ATR*-proficient DLD1 parental and *ATR*-deficient DLD1 CRC cells, both cell lines were verified on the ATR protein level to ensure cell line identity. DLD1 *ATR*-deficient cells homozygously harboring the hypomorphic Seckel mutation (*ATR*$^{s/s}$) have been described previously (97; 103; 104). This mutation causes strongly reduced but not absent ATR protein levels without significant impairment of cell proliferation or survival (103). For protein synthesis analysis, immunoblotting demonstrated ATR protein suppression below the detection limit in DLD1 *ATR*$^{s/s}$ cells (**Fig. 6A**). *ATR* deficiency of DLD1 *ATR*$^{s/s}$ cells was further verified functionally through the confirmation of hypersensitivity towards the DNA interstrand crosslinking (ICL) agent mitomycin C (MMC, IC50 ratio 3.5-fold) (**Fig. 6B**), as reported before (103; 105).

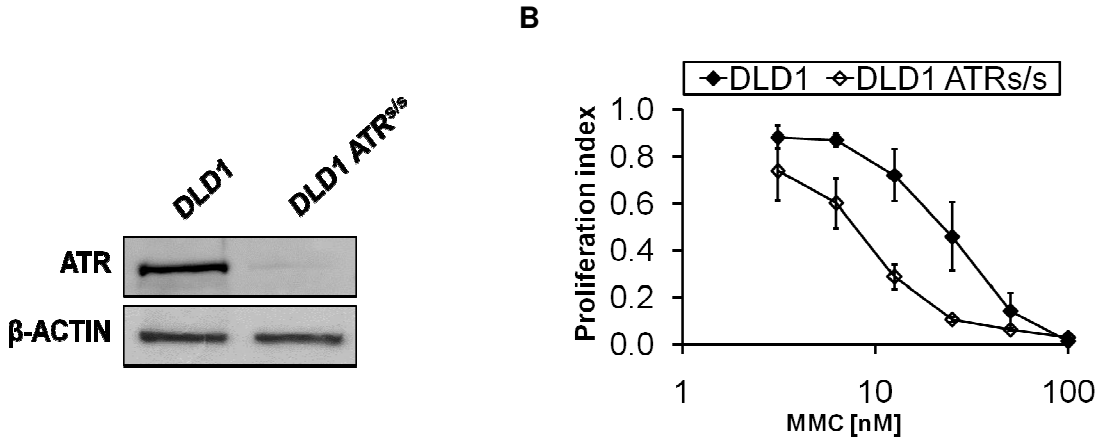

Figure 6: *ATR* deficiency-induced phenotype in DLD1 CRC cells. (**A**) ATR protein synthesis was assessed in DLD1 parental and DLD1 *ATR*$^{s/s}$ cells by immunoblotting. β-ACTIN served as loading control. (**B**) Mitomycin C (MMC) sensitivity of DLD1 parental and DLD1 *ATR*$^{s/s}$ cells was assessed at 120 h after treatment by proliferation assay. Error bars represent standard deviation of three independent experiments with each data point representing triplicate wells.

3.1.2. siRNA library screening to identify synthetic lethal interactions between *ATR* and DNA-repair genes in DLD1 cells.

ATR-inhibition has recently been demonstrated to induce the elimination of tumor cells in CRCs (104; 106) but the underlying genetic determinants are still insufficiently defined. Therefore, a siRNA library screening approach was conducted using the well-defined genetic *ATR* knock-in model (*ATR*$^{s/s}$) of human DLD1 CRC cells (97) to identify potential synthetically lethal interactions between *ATR* and DNA-repair genes. A focused siRNA library directed against 288 DNA-repair genes each targeted by three different siRNAs was used. The experimental screening design is schematically outlined in **Fig. 4** and **Fig. 7**. In short, DLD1 parental and DLD1 *ATR*$^{s/s}$ cells were transfected simultaneously using a previously established siRNA library at a final siRNA concentration of 10 nM. At 120 h post transfection, proliferation differences between DLD1 parental and DLD1 *ATR*$^{s/s}$ cells were assessed. This primary screen was independently performed twice and generated 26 primary hits (hit rate = 9%), which were again tested twice in the confirmatory screen and classified into hit categories as selective *ATR* genotype-dependent and *ATR* genotype-independent proliferation inhibition according to the criteria described in the Material & Methods section. After the screening, each candidate gene was validated based on the average proliferation inhibition ratio of four independent experiments.

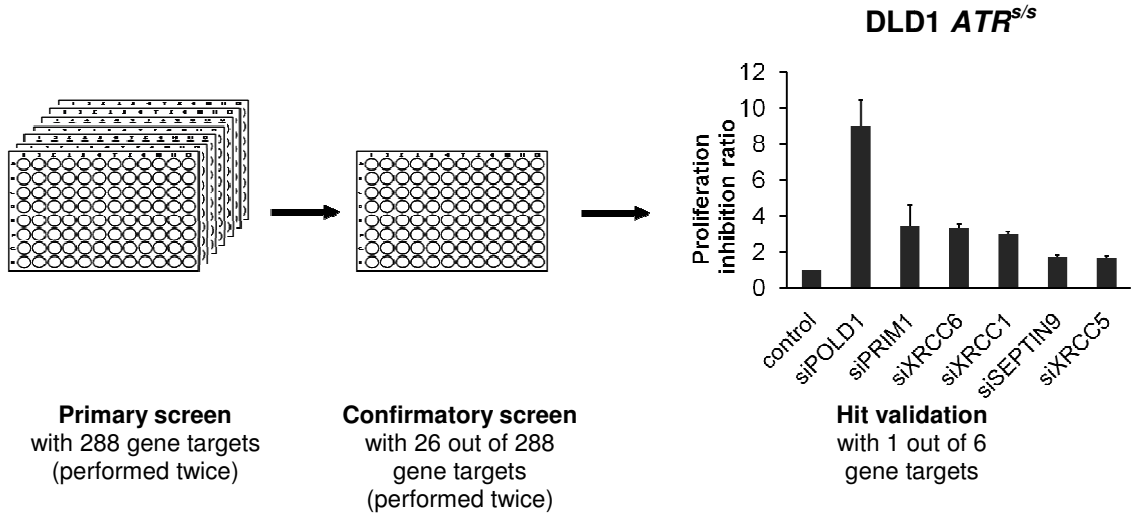

Figure 7: Screening process of the siRNA library. Multiple siRNA screens gradually identified the top six candidate genes exhibiting synthetic lethal interactions with *ATR*. Error bars represent standard error of the mean of four independent experiments with each data point representing triplicate wells.

DNA-repair genes were scored as selective *ATR*-genotype dependent hits if the mean proliferation inhibition ratio was >1.50, the average relative survival of DLD1 parental cells was >0.45 and the Δ-values of the average relative survival of DLD1 parental and DLD1 *ATR*$^{s/s}$ cells were ≥0.3. The screening identified six genes eliciting selective *ATR*-genotype dependent proliferation inhibition in DLD1 *ATR*$^{s/s}$ cells (**Fig. 7**, **Table 9**). The strongest effects

specifically on DLD1 *ATR*$^{s/s}$ cells were observed for *POLD1* knockdown causing a 9-fold proliferation inhibition ratio with an average relative survival of 5% (Δ-value = 0.42) at 120 h post transfection. A 3-fold proliferation inhibition ratio on DLD1 *ATR*$^{s/s}$ cells was induced upon *PRIM1* (Δ-value = 0.30), *XRCC6* (Δ-value = 0.38) and *XRCC1* knockdown (Δ-value = 0.40) with an average relative survival of ≤30% of cells, respectively.

Table 9: Identified *ATR* genotype-dependent DNA-repair genes. *ATR*-dependent sensitivity upon siRNA-mediated DNA-repair gene knockdown was assessed in DLD1 parental and DLD1 *ATR*$^{s/s}$ cells. Proliferation inhibition and the average relative survival of DLD1 parental and DLD1 *ATR*$^{s/s}$ cells of four independent screens were analyzed at 120 h.

Rank	Gene target	Proliferation inhibition ratio *	Average relative survival DLD1	Average relative survival DLD1 *ATR*$^{s/s}$	Δ-value Average relative survival of DLD1 to DLD1 *ATR*$^{s/s}$ **
1	***POLD1***	9.04±1.42	0.47	0.05	0.42
2	***PRIM1***	3.43±1.15	0.47	0.17	0.30
3	***XRCC6 (Ku70)***	3.34±0.23	0.68	0.30	0.38
4	***XRCC1***	3.03±0.12	0.60	0.20	0.40
5	***SEPT9***	1.74±0.11	0.73	0.42	0.31
6	***XRCC5 (Ku80)***	1.66±0.12	0.64	0.38	0.26

** The proliferation inhibition ratio was calculated by dividing the proliferation inhibition value of DLD1 parental by the value of DLD1 ATR$^{s/s}$ cells. The mean proliferation inhibition ratio and standard error of the mean were determined from four individual proliferation inhibition ratio values that each represent triplicates from three different oligonucleotides targeting one particular gene.*

*** Δ-values of the average relative survival of DLD1 parental and DLD1 ATR$^{s/s}$ cells were calculated by subtracting the average relative survival of DLD1 parental and DLD1 ATR$^{s/s}$ cells, respectively.*

3.1.3. *ATR*-genotype independent DNA-repair gene knockdown-induced detrimental effects on DLD1 cells.

The DNA-repair gene siRNA library screen identified potential synthetic lethal interactions between *ATR* and DNA-repair genes (**Table 9**). In addition, *ATR*-genotype independent DNA-repair gene knockdown-induced detrimental effects were identified (**Table 10**).

Table 10: Identified *ATR* genotype-independent DNA-repair genes. *ATR*-independent sensitivity upon siRNA-mediated DNA-repair gene knockdown was assessed in DLD1 parental and DLD1 $ATR^{s/s}$ cells. Proliferation inhibition and the average relative survival of DLD1 parental and DLD1 $ATR^{s/s}$ cells of four independent screens were analyzed at 120 h.

Rank	Gene target	Proliferation inhibition ratio*	Average relative survival DLD1	Average relative survival DLD1 $ATR^{s/s}$	Average relative survival of DLD1 and DLD1 $ATR^{s/s}$**	IΔI Average relative survival of DLD1 to DLD1 $ATR^{s/s}$***
1	***XAB2***	1.40±0.46	0.06	0.05	0.06	0.01
2	***PLK1***	2.51±1.86	0.12	0.03	0.08	0.09
3	***RPL35***	0.58±0.17	0.07	0.14	0.11	0.07
4	***PSMC4 (TBP7)***	1.73±1.14	0.16	0.11	0.14	0.05
5	***RPL27***	0.21±0.07	0.04	0.23	0.14	0.19
6	***NUP205***	2.85±2.29	0.18	0.15	0.17	0.03
7	***RRM1***	1.75±1.04	0.22	0.11	0.17	0.11
8	***POLE***	1.63±0.80	0.22	0.12	0.17	0.10
9	***RRM2***	1.40±0.39	0.23	0.15	0.19	0.08
10	***PSMA1***	0.61±0.24	0.27	0.11	0.19	0.16
11	***POLA1***	1.66±1.13	0.22	0.18	0.20	0.04
12	***RPA2 (RPA32)***	1.68±0.32	0.26	0.15	0.21	0.11
13	***RPA1 (RPA70)***	0.93±0.34	0.22	0.21	0.22	0.01
14	***SNRPF (SMF)***	1.06±0.63	0.23	0.21	0.22	0.02
15	***ENDOV***	0.74±0.10	0.24	0.35	0.30	0.11
16	***FBXO18 (FBH1)***	0.85±0.21	0.27	0.35	0.31	0.08
17	***PMS2P5***	1.66±1.02	0.41	0.20	0.31	0.21
18	***PARP4 (VPARP)***	1.60±0.62	0.40	0.23	0.32	0.17
19	***FEN1***	0.70±0.17	0.28	0.41	0.35	0.13
20	***PCNA***	1.83±1.00	0.45	0.25	0.35	0.20

** The proliferation inhibition ratio was calculated by dividing the proliferation inhibition value of DLD1 parental by the value of DLD1 $ATR^{s/s}$ cells. The mean proliferation inhibition ratio and standard error of the mean were determined from four individual proliferation inhibition ratio values that each represent triplicates from three different oligonucleotides targeting one particular gene.*

*** The average relative survival of DLD1 parental and DLD1 ATR$^{s/s}$ cells, respectively, was calculated by the mean of four individual growth inhibition values for each cell line from three different oligonucleotides targeting one particular gene.*

**** Δ-values of the average relative survival of DLD1 parental and DLD1 ATR$^{s/s}$ cells were calculated by subtracting the average relative survival of DLD1 parental and DLD1 ATR$^{s/s}$ cells, respectively.*

These DNA-repair genes were scored as *ATR*-genotype independent hits if the average relative survival of DLD1 parental and DLD1 *ATR*$^{s/s}$ cells was ≤0.45 and Δ-values of the average relative survival of DLD1 parental and DLD1 *ATR*$^{s/s}$ cells were low (<0.3) at 120 h post transfection. siRNA-mediated knockdown of *XAB2* caused a virtually complete loss of proliferation shown in an average relative survival in both DLD1 parental and DLD1 *ATR*$^{s/s}$ cells of <10% (Δ-value = 0.01). siRNA-mediated knockdown of *PLK1* and *RPL35* displayed an average relative survival in both DLD1 parental and DLD1 *ATR*$^{s/s}$ cells of <15% (Δ-value = 0.09/0.07). The results indicate that these genes execute essential functions at least in DLD1 CRC cells.

These *ATR*-genotype independent effects were not the focus of this study. Consequently, these DNA-repair genes were not further examined.

3.1.4. Confirmation of potential synthetic lethal interactions between *ATR* and DNA-repair genes identified by siRNA library screening.

The siRNA library screen identified DNA-repair genes eliciting a selective *ATR* genotype-dependent proliferation inhibition upon their knockdown. To verify these potential synthetic lethal interactions, the siRNA-mediated DNA-repair gene knockdown was analyzed by dose titration experiments in DLD1 *ATR*$^{s/s}$ cells. The siRNA-targeted sequences were chosen based on the strongest effect in the siRNA library screen. A dose-dependent knockdown effect was confirmed upon *POLD1*, *PRIM1* and *XRCC6* depletion in DLD1 *ATR*$^{s/s}$ cells at 120 h post transfection (**Fig. 8A-C**). Upon siRNA-mediated *XRCC1* and *XRCC5* knockdown, a weak dose-dependent proliferation inhibition was elicited in DLD1 *ATR*$^{s/s}$ cells at 120 h post transfection (**Fig. 8D, F**). However, data were not reproducible for the potential synthetic lethal interaction between *ATR* and *SEPT9* (**Fig. 8E**).

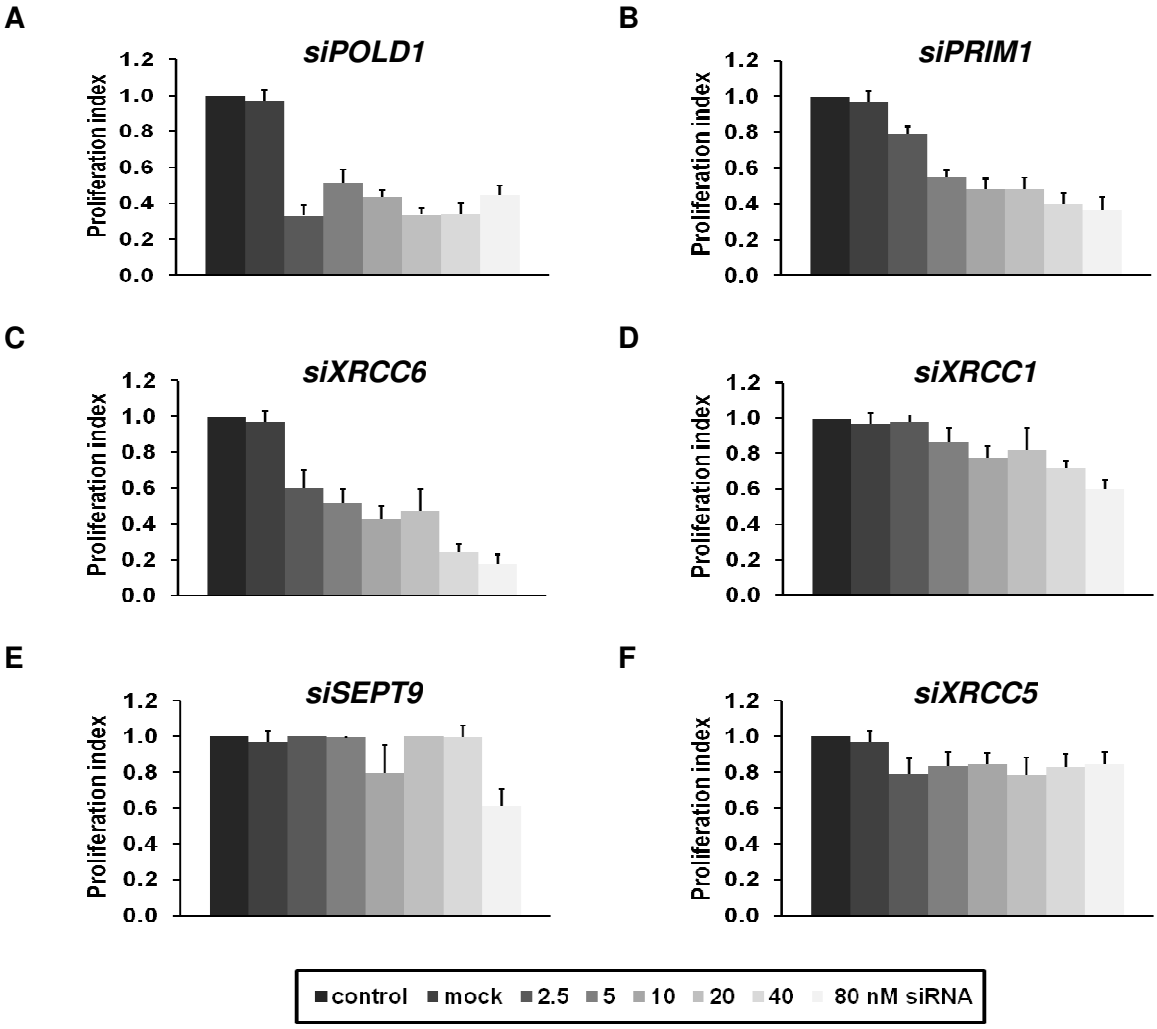

Figure 8: *siRNA* dose-dependent knockdown effect of DNA-repair genes in DLD1 *ATR*$^{s/s}$ cells. Proliferation inhibition upon incremental concentrations, starting from 2.5 to 80 nM, of transfected siRNA directed against (**A**) *POLD1*, (**B**) *PRIM1*, (**C**) *XRCC6*, (**D**) *XRCC1*, (**E**) *SEPT9* and (**F**) *XRCC5* was analyzed in DLD1 *ATR*$^{s/s}$ cells at 120 h. Error bars represent standard deviation from three independent experiments with each data point representing triplicate wells.

In summary, the siRNA screen of 288 DNA-repair genes identified potential knockdown-induced synthetic lethal interactions of *POLD1*, *PRIM1*, *XRCC6*, *XRCC1*, *SEPT9* and *XRCC5* in DLD1 *ATR*$^{s/s}$ cells (**Table 9**). Dose titration experiments confirmed siRNA-mediated gene knockdown effects of *POLD1*, *PRIM1*, *XRCC6*, *XRCC1* and *XRCC5* on proliferation in DLD1 *ATR*$^{s/s}$ cells (**Fig. 8**).

However, the strongest effect specifically on DLD1 *ATR*$^{s/s}$ cells was observed and confirmed for *POLD1* knockdown. Therefore, *POLD1* was primarily picked for a more detailed analysis in the following experiments.

3.2. Synthetic lethal interaction between *ATR* and *POLD1*

3.2.1. Validation of synthetic lethality between *ATR* and *POLD1* in DLD1 *ATR*$^{s/s}$ cells.

To further substantiate the synthetic lethal interaction between *ATR* and *POLD1*, dose titration and time kinetic experiments were performed upon *POLD1* knockdown in DLD1 *ATR*$^{s/s}$ cells. A siRNA-mediated dose-dependent knockdown effect upon constantly increasing *siPOLD1* concentrations was exclusively shown in DLD1 *ATR*$^{s/s}$ but not in DLD1 parental cells at 120 h post transfection (**Fig. 10A**). Expectedly, *ATR*-genotype independent proliferation inhibition was observed in both DLD1 parental and DLD1 *ATR*$^{s/s}$ cells upon *siPOLD1* treatment at higher and likely toxic siRNA concentrations starting from 80 nM.

Detrimental effects of siRNA-mediated *POLD1* knockdown (10 nM) selectively on DLD1 *ATR*$^{s/s}$ cells were time-dependent, as shown by a proliferation inhibition of at least 50%, starting at 96 h and peaking at 120 h post transfection, as compared to mock-transfected and control DLD1 *ATR*$^{s/s}$ cells (**Fig. 10B**). The efficient siRNA-mediated *POLD1* knockdown was confirmed on the protein level in DLD1 parental and DLD1 *ATR*$^{s/s}$ cells at 96 h post transfection (**Fig. 10C**). Clonally selected heterozygous DLD1 *ATR*$^{+/s}$ cells remained unaffected by POLD1 depletion excluding artefacts due to clonal variability (data not shown).

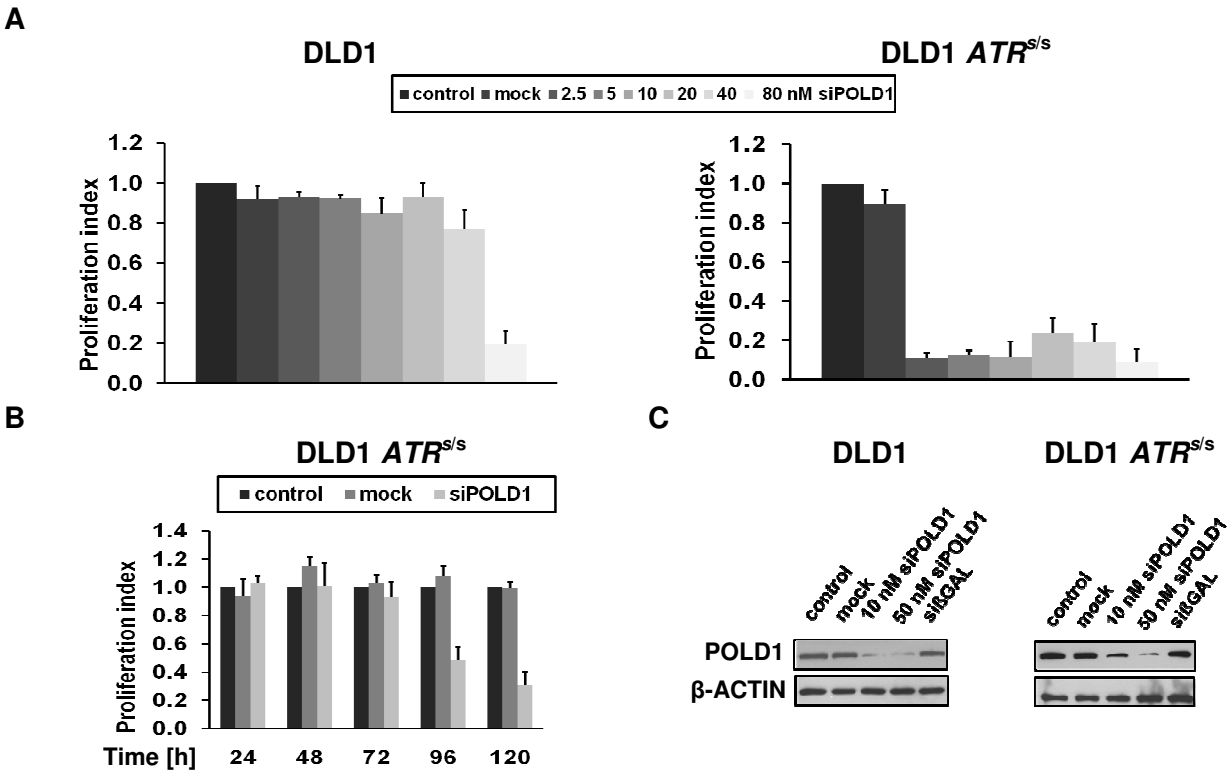

Figure 9: Characterization of *POLD1* knockdown in DLD1 cells. (**A**) Dose-dependent knockdown upon increasing concentrations of *siPOLD1*, starting from 2.5 to 80 nM, was analyzed in DLD1 parental and DLD1 *ATR*$^{s/s}$ cells at 120 h. (**B**) Time-dependent knockdown upon 10 nM *siPOLD1* was studied in DLD1 *ATR*$^{s/s}$ cells. Error bars represent standard deviation of three independent experiments with each data point representing triplicate wells. (**C**) Effective siRNA-mediated knockdown of *POLD1* at 10 nM and 50 nM was confirmed at 96 h in DLD1 parental and DLD1 *ATR*$^{s/s}$ cells. *siβGAL* at 50 nM served as transfection control, β-ACTIN as loading control.

3.2.2. *POLD1* knockdown-mediated sensitivity towards chemical inhibition of the ATR/CHK1-axis.

Targeting ATR is a promising strategy in cancer therapy but the majority of ATR-inhibitors is currently still in pharmacological development (33; 34; 36; 38; 39; 107; 108). Targeting ATRs' major downstream kinase CHK1 might therefore represent a more attractive approach as CHK1-inhibitors already undergo clinical trials (109-111).

Thus, it was analyzed whether *siPOLD1*-mediated effects in DLD1 $ATR^{s/s}$ cells were similarly chemically reproducible through chemical inhibition of ATR as well as CHK1 in DLD1 parental cells. Various ATR (NU6027, VE-822)- and CHK1 (UCN-01, LY2603618)-inhibitors were applied in cell proliferation assays to analyze proliferation differences between POLD1-depleted and mock-transfected DLD1 parental cells. Targeting ATR with NU6027 was reported to sensitize different cancer cells to DNA damaging agents (36). The ATR-inhibitor VE-822, a more potent analogue of VE-821 (33; 108), is the first ATR-targeting drug entering clinical development (ClinicalTrials.gov: NCT02157792). The CHK1-inhibitors UCN-01 and LY2603618 were chosen because their application were already tested in different cancer identities, e.g. pancreatic and lung cancer, of phase 2 clinical trials (ClinicalTrials.gov: NCT00045747, NCT00072189, NCT00082017, NCT01296568, NCT00988858).

Upon *POLD1* knockdown, a significant hypersensitivity towards NU6027 (IC50 ratio 4-fold), VE-822 (IC50 ratio 5-fold) and UCN-01 (IC50 ratio 8-fold) was observed in POLD1-depleted but not in mock-transfected and control DLD1 parental cells at 120 h (**Fig. 10A**).

To exclude a general unspecific hypersensitivity phenotype upon *POLD1* knockdown, POLD1-depleted, mock-transfected and control DLD1 parental cells were treated with commonly used chemotherapeutics including ICL- and non-ICL-chemotherapeutics (MMC, oxaliplatin, 5-fluorouracil (5-FU)). No significant proliferation differences between POLD1-depleted, mock-transfected and control DLD1 parental cells were detected upon treatment with any of these agents (**Fig. 10B**).

A

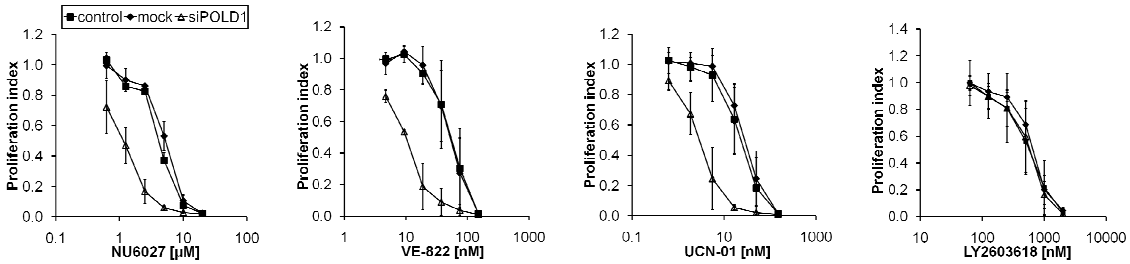

B

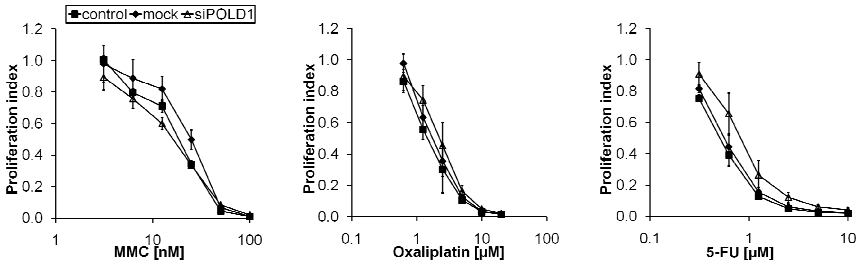

Figure 10: ATR-/CHK1-dependent proliferation inhibition upon *POLD1* knockdown in DLD1 cancer cells. Effects on proliferation of (**A**) ATR- and CHK1-inhibitors or (**B**) common chemotherapeutics were assessed at 120 h after treatment in control, mock-transfected or *siPOLD1*-transfected (10 nM) DLD1 parental cells. Error bars represent standard deviation of three independent experiments with each data point representing triplicate wells.

3.2.3. *POLD1* knockdown-mediated apoptosis in DLD1 *ATR*$^{s/s}$ cells.

The DNA-repair siRNA screen identified detrimental effects on proliferation upon *POLD1* knockdown in DLD1 *ATR*$^{s/s}$ cells. Furthermore, POLD1-depleted DLD1 parental cells showed hypersensitivity towards chemical inhibition with ATR- and CHK1-targeting drugs.

To elucidate the mechanism underlying the identified synthetic lethal interaction of *ATR* with *POLD1*, cell cycle distribution and sub-G1 cell fraction were assessed upon *siPOLD1* transfection (10 nM) by flow cytometry in DLD1 *ATR*$^{s/s}$ versus DLD1 parental cells in a time-dependent manner. The experimental set-up is schematically depicted in **Fig. 11A**. No significant baseline differences in cell cycle profiles or sub-G1 content were depicted among *siPOLD1*-transfected, mock-transfected and control DLD1 parental cells up to 72 h (**Fig. 11B**). In contrast, DLD1 *ATR*$^{s/s}$ but not DLD1 parental cells displayed a slightly increased sub-G1 fraction at 96 h post *siPOLD1*-transfection (10%, **Fig. 11B**), which strongly and exclusively increased at 120 h (40%, **Fig. 11C-D**) indicating an induction of cell death mechanisms.

The two major types of cell death are apoptosis and necrosis, both morphologically distinguishable. Apoptosis is characterized by cell shrinkage with an intact plasma membrane, chromatin condensation and nuclear fragmentation. The cytoplasm retains in membrane-bounded apoptotic bodies (112). On the contrary, necrotic cells swell, the plasma membrane is disrupted and cytoplasm release follows (112; 113). With regard to morphological changes, an obvious cell shrinkage (**Fig. 12A**, **left panel**) along with chromatin condensation and apoptotic body formation (**Fig. 12A**, **right panel**) were observed for POLD1-depleted but not control DLD1 *ATR*$^{s/s}$ cells indicating a *POLD1* knockdown-mediated apoptosis induction in DLD1 *ATR*$^{s/s}$ cells.

To validate and confirm *POLD1* knockdown-induced apoptosis, suggested by the increased subG1-fraction in the cell cycle experiments and morphological changes in light and fluorescence microscopy observations, apoptosis-involved caspases were analyzed. A general apoptosis activation is indicated by cleaved Poly (ADP-ribose) polymerase (PARP) as well as the initiator caspases CASPASE8, CASPASE9 and the central effector CASPASE3. (112) Thus, these proteins were assessed on protein level in DLD1 *ATR*$^{s/s}$ versus DLD1 parental cells upon *siPOLD1* transfection (10 nM). Consistently, a cleavage of PARP, CASPASE3 and CASPASE9 but not CASPASE8 was selectively observed in DLD1 *ATR*$^{s/s}$ but not in DLD1 parental cells upon *POLD1* knockdown (**Fig. 12B**).

To show that the extrinsic apoptotic pathway is inducible in DLD1 parental and DLD1 *ATR*$^{s/s}$ cells, the tumor necrosis factor α (TNFα) and actinomycin D (AcD) were applied. TNFα as corresponding ligand of TNF receptor 1 (TNFR1) triggers extrinsic apoptosis induction through initiator CASPASE8 activation (114). A synergistic toxic effect of TNFα and AcD, a pro-apoptotic drug, sensitizes cells to TNFα-mediated apoptosis (115). In concordance with

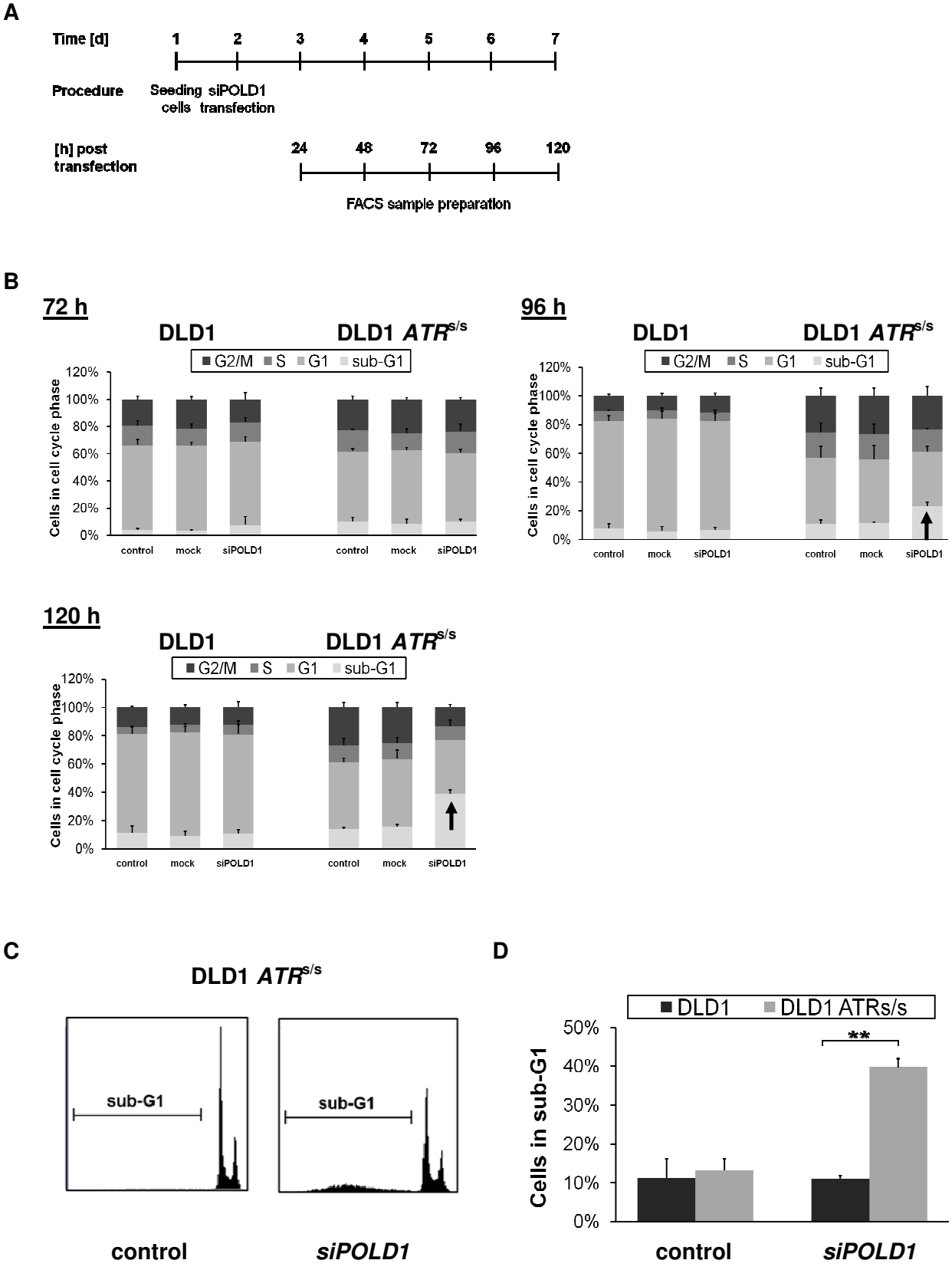

Figure 11: POLD1 depletion-induced apoptosis without preceding cell cycle arrest. Cell cycle analysis was performed upon siRNA-mediated *POLD1* knockdown at 10 nM in DLD1 parental and DLD1 *ATR*$^{s/s}$ cells. (**A**) Timeline depicting experimental procedure. (**B**) Representative cell cycle distribution, (**C**) histograms of sub-G1 fraction of one experiment at 120 h and (**D**) statistical analysis from three independent experiments at 120 h are shown. Error bars represent standard deviation of three experiments. Asterisks mark statistical significance between two samples using the Student's t-test (**$p < 0.01$).

these data, application of TNFα and AcD activates extrinsic apoptosis in DLD1 parental and DLD1 *ATR*$^{s/s}$ cells, as illustrated by CASPASE8 cleavage (**Fig. 12C**, **upper panel**).

To show that the intrinsic apoptotic pathway is inducible in DLD1 parental and DLD1 *ATR*$^{s/s}$ cells, CASPASE9 activation was analyzed upon irradiation (IR) and etoposide treatment in both cells. An IR-induced CASPASE9 activation was shown at 20 Gy in DLD1 parental and DLD1 *ATR*$^{s/s}$ cells (**Fig. 12C**, **middle panel**). In addition, etoposide-induced CASPASE9 activity was detected (**Fig. 12C**, **lower panel**), as described before (116).

Caspase cascade activity was further verified by CASPASE3-dependent cleavage of the fluorogenic CASPASE3-specific substrate Ac-DEVD-AMC in DLD1 *ATR*$^{s/s}$ versus DLD1 parental control cells at 96 h post *siPOLD1* transfection. POLD1-depleted DLD1 *ATR*$^{s/s}$ cells exhibited a 6-fold increase in DEVDase activity, corresponding to CASPASE3 activity, compared to DLD1 parental cells (**Fig. 12D**).

These data suggest that DLD1 cancer cells with depletion of ATR and POLD1 undergo cell death through apoptosis.

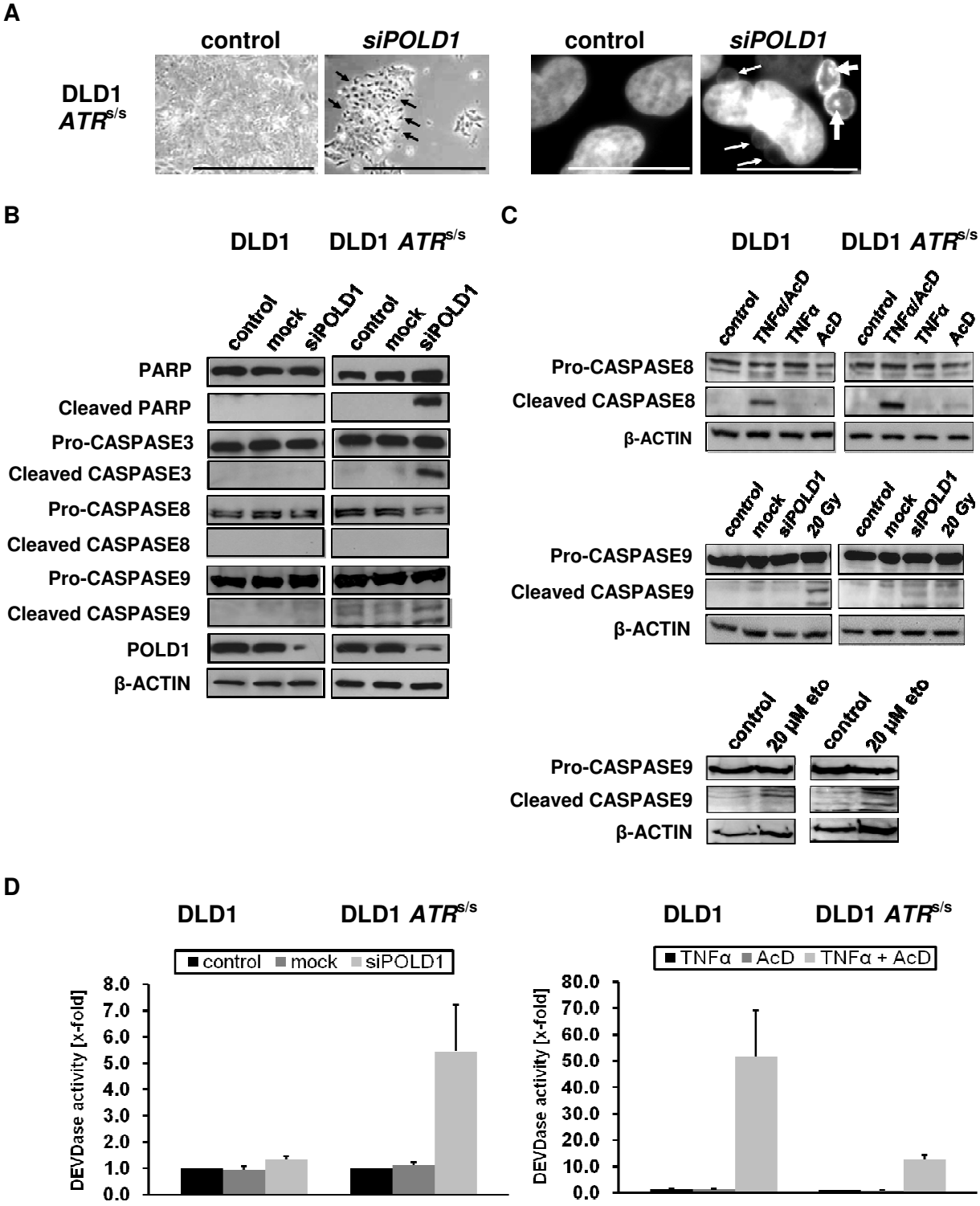

Figure 12: Caspase-dependent apoptosis induction upon POLD1 depletion. siRNA-mediated *POLD1* knockdown was performed at 10 nM in DLD1 parental and DLD1 *ATR*$^{s/s}$ cells. (**A**) Morphological changes observed by light microscopy (**left panel**) and nuclear staining by Hoechst 33258 (**right panel**) in control and *siPOLD1*-transfected DLD1 *ATR*$^{s/s}$ cells at 120 h. Black arrows, cell shrinkage; white thin arrows, apoptotic bodies; white thick arrows, chromatin condensation. Scale bar left panel, 50 µm; Scale bar right panel, 5 µm. (**B**) PARP and Caspase activation was analyzed by immunoblotting. (**C**, **upper panel**) CASPASE8-mediated extrinsic apoptosis induction through TNFα (25 ng/mL) and AcD (200 ng/mL) treatment at 6 h and (**C**) CASPASE9-mediated intrinsic apoptosis induction upon (**C**, **middle panel**) irradiation at 20 Gy at 24 h and (**C**, **lower panel**) etoposide (eto) at 20 µM at 6 h. β-ACTIN detection was used as loading control. (**D**) Fluorometric analysis of intracellular CASPASE3-mediated DEVDase activity was analyzed at 96 h (**D**, **left panel**). Administration of TNFα (25 ng/mL) and AcD (200 ng/mL) served as positive control to show DEVDase activity corresponding to CASPASE3 activity (**D**, **right panel**). Error bars represent standard deviation of two experiments, independently performed in triplicates.

3.2.4. Effects of combined POLD1- and ATR-depletion on H2AX phosphorylation in DLD1 cancer cells upon genotoxic stress.

DLD1 *ATR*$^{s/s}$ cells undergo apoptosis upon *POLD1* knockdown. To clarify the underlying mechanisms, DNA damage- and DNA-repair kinetics were assessed using intranuclear γ-H2AX focus formation, elimination and pan-nuclear staining as surrogate markers. The spotted phosphorylation of H2AX at Ser-139 to γ-H2AX illustrates one of the earliest response events at sites of DNA double-strand breaks (41; 117; 118) formed as consequence of irradiation or chemotherapeutic agents (119). In contrast, pan-nuclear staining is defined as diffuse phosphorylation of H2AX in the whole nucleus and indicates replication stress (41). Experimentally, *ATR* and *POLD1* were down-regulated in DLD1 parental and DLD1 *ATR*$^{s/s}$ cells, either alone or in combination. Both cells were additionally treated with ionizing gamma-radiation (IR), etoposide or left untreated.

3.2.4.1. POLD1 and ATR depletion-induced γ-H2AX focus formation upon IR-stress.

After verification of an effective siRNA-mediated *POLD1* knockdown at 96 h post transfection (**Fig. 9C**), DLD1 parental and DLD1 *ATR*$^{s/s}$ cells with or without *POLD1* knockdown were treated with IR at a sub-lethal dose of 4 Gy or left untreated (experimental set-up schematically depicted in **Fig. 13A**). The sub-lethal dose of 4 Gy was defined using a dose titration study (data not shown). Subsequently, γ-H2AX focus formation, elimination and pan-nuclear staining were quantified at multiple time points ranging from 0.5 to 120 h. Control DLD1 parental and DLD1 *ATR*$^{s/s}$ cells displayed no significant γ-H2AX focus formation or pan-nuclear staining. Upon *POLD1* knockdown, a fraction of DLD1 parental cells exhibited increased γ-H2AX focus formation (21% of cells showing >10 foci/cell), whereas no significant pan-nuclear staining was observed. In contrast, DLD1 *ATR*$^{s/s}$ cells displayed a large fraction of cells that exhibited either an increased γ-H2AX focus formation (36% of cells showing >10 foci/cell) or high levels of pan-nuclear staining (36% of cells) upon *POLD1* knockdown (**Fig. 13B**+**C**). In general, distinct γ-H2AX foci are rapidly formed within minutes, peak at 0.5 to 1 h and recover within 24 h in response to IR (120; 121). Upon treatment with IR, a large fraction of γ-H2AX foci-positive cells was expectedly observed at 0.5 h for control (63% of cells showing >10 foci/cell) and POLD1-depleted DLD1 parental cells (65%) and an even higher fraction for control and POLD1-depleted DLD1 *ATR*$^{s/s}$ cells (approximately 90%), which is consistent with the known *ATR* deficiency-mediated radio-sensitivity (33). However, POLD1-depleted DLD1 *ATR*$^{s/s}$ cells additionally exhibited an increased fraction of H2AX-positive cells also at 24 h and even at 120 h after IR, including cells with increased γ-H2AX focus formation (63% at 24 h / 41% at 120 h) and pan-nuclear staining (23% at 24 h /7% at 120 h) (**Fig. 13D**+**E**).

A

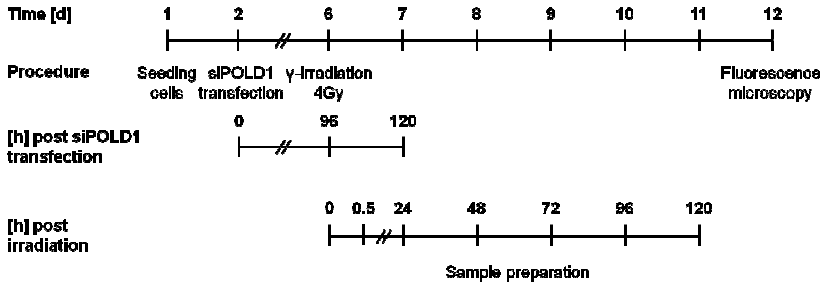
Time [d]
1
2
6
7
8
9
10
11
12
Procedure
Seeding cells
siPOLD1 transfection
γ-Irradiation 4Gy
Fluorescence microscopy
[h] post siPOLD1 transfection
0
96
120
[h] post irradiation
0
0.5
24
48
72
96
120
Sample preparation

B

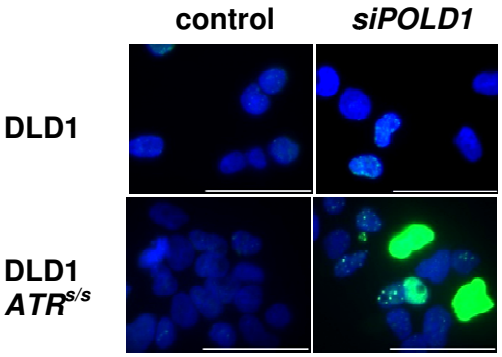
control
siPOLD1
DLD1
DLD1 ATR s/s

C

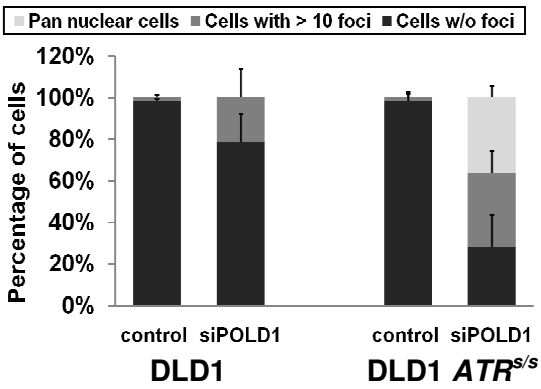
Pan nuclear cells
Cells with > 10 foci
Cells w/o foci
Percentage of cells
120%
100%
80%
60%
40%
20%
0%
control
siPOLD1
control
siPOLD1
DLD1
DLD1 ATR s/s

D

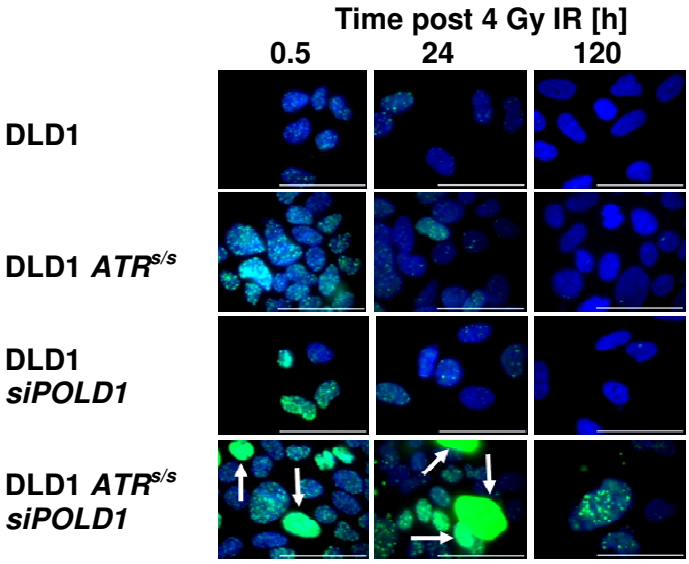
Time post 4 Gy IR [h]
0.5
24
120
DLD1
DLD1 ATR s/s
DLD1
siPOLD1
DLD1 ATR s/s
siPOLD1

E

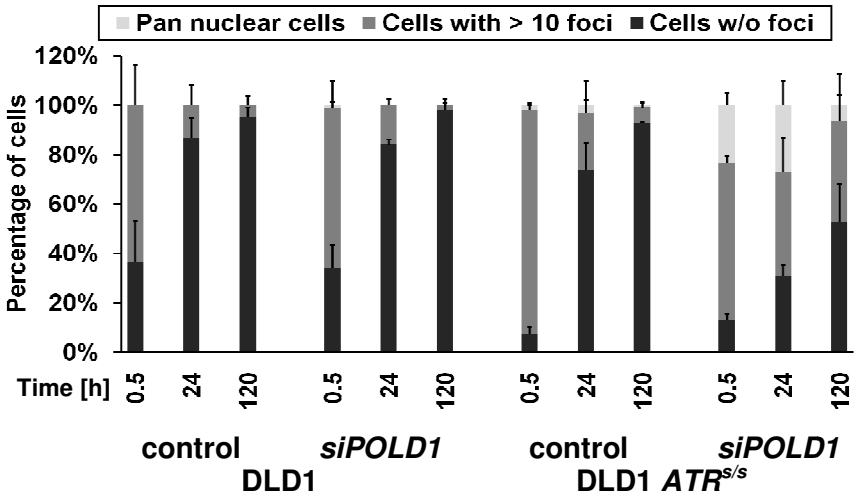
Pan nuclear cells
Cells with > 10 foci
Cells w/o foci
Percentage of cells
120%
100%
80%
60%
40%
20%
0%
Time [h]
0.5
24
120
0.5
24
120
0.5
24
120
0.5
24
120
control
siPOLD1
control
siPOLD1
DLD1
DLD1 ATR s/s

3.2.4.2. POLD1 and ATR depletion-induced γ-H2AX focus formation upon etoposide

DNA damage and repair were further examined upon etoposide treatment in *POLD1*- and *ATR*-deficient DLD1 parental and DLD1 *ATR*$^{s/s}$ cells. The etoposide concentration used was determined by dose titrations using FACS analysis in DLD1 parental and DLD1 *ATR*$^{s/s}$ cells. A sub-lethal dose of 0.25 µM etoposide was defined displaying no cell cycle phase alterations at 24 h post treatment in both cells (data not shown).

The experimental set-up was based on previous experiments (see 3.2.4.1) and is schematically depicted in **Fig. 14A**. Efficient siRNA-mediated *POLD1* down-regulation was verified (**Fig. 9C**). As shown before, *POLD1*-knockdown induced detrimental DNA damage was confirmed in DLD1 parental and DLD1 *ATR*$^{s/s}$ cells persistently showing γ-H2AX focus formation (29%/41% of cells showing >10 foci/cell) and occasional pan-nuclear staining (4%/7%) at 24 h (**Fig. 14B**+**C**), compared to their untreated controls (**Fig. 14B**).

Etoposide inhibits topoisomerase II activity eliciting DNA DSBs, which rapidly triggers H2AX phosphorylation (122). In response to etoposide treatment, a low level of γ-H2AX was displayed at 24 h in DLD1 parental (9% of cells showing >10 foci/cell) and an increased fraction of γ-H2AX in POLD1-depleted DLD1 parental and DLD1 *ATR*$^{s/s}$ cells (27%/34% of cells showing >10 foci/cell). Of note, virtually no DNA damage in these three cell lines was detectable at 120 h, indicating an efficient DNA repair system. In contrast, POLD1-depleted DLD1 *ATR*$^{s/s}$ cells exhibited an elevated fraction of H2AX-positive cells at 24 h and even at 120 h after etoposide treatment, displayed by cells with γ-H2AX focus formation (30% at 24 h/48% at 72 h/42% at 120 h), pan-nuclear staining (13% at 24 h/16% at 72 h/9% at 120 h) along with apoptotic body formation (**Fig. 14D**+**E**).

In conclusion, massive DNA damage induced by concomitant depletion of ATR and POLD1 was confirmed in DLD1 cells. Furthermore, IR, referred to paragraph 3.2.4.1, and etoposide treatment similarly elicited detrimental and sustained DNA damage with an impaired or at least decelerated DNA-repair machinery specifically in cells with combined ATR- and POLD1-defects, as compared to control cells and cells harboring only one of these defects.

Figure 13: *ATR* and *POLD1* knockdown-dependent γ-H2AX formation upon IR stress (see page 49). DLD1 parental and DLD1 *ATR*$^{s/s}$ cells were grown on coverslips, treated with *siPOLD1* at 10 nM or left untreated, then irradiated (4 Gy) and stained with an anti-γ-H2AX antibody (green). Nuclei were counterstained with Hoechst 33258 (blue).(**A**) Timeline depicting experimental procedure. (**B**+**D**) Representative fluorescence images and (**C**+**E**) γ-H2AX quantification of control versus *siPOLD1*-treated DLD1 parental and DLD1 *ATR*$^{s/s}$ cells, respectively, are shown (**B**+**C**) at 120 h after transfection without irradiation and (**D**+**E**) upon irradiation at 0.5 h, 24 h and 120 h. Arrows indicate pan-nuclear γ-H2AX staining. A scale bar (10 µm) is depicted. (**C**+**D**) For quantification, at least 50 cells of each cell line and condition were scored in two independent experiments. Error bars represent standard deviation of two experiments.

A

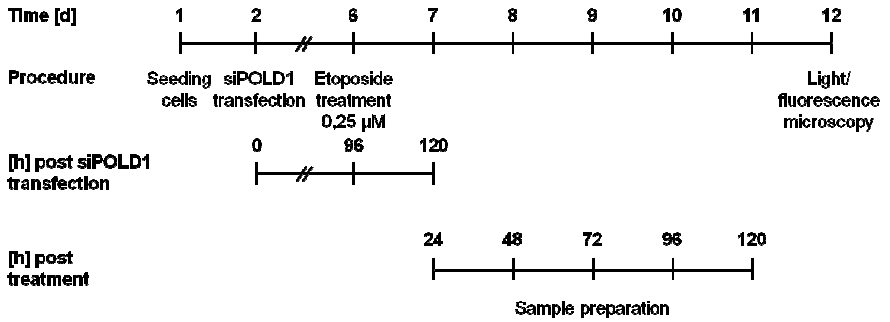
Time [d]
1
2
6
7
8
9
10
11
12
Procedure
Seeding cells
siPOLD1 transfection
Etoposide treatment 0,25 µM
Light/ fluorescence microscopy
[h] post siPOLD1 transfection
0
96
120
[h] post treatment
24
48
72
96
120
Sample preparation

B

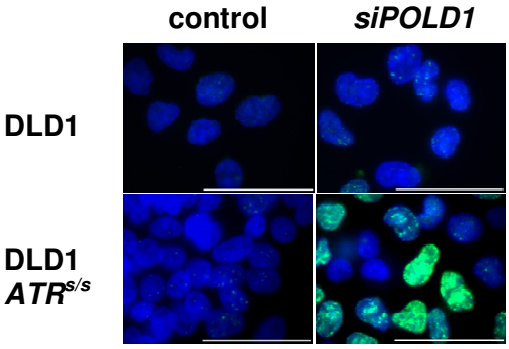
control
siPOLD1
DLD1
DLD1 ATR s/s

C

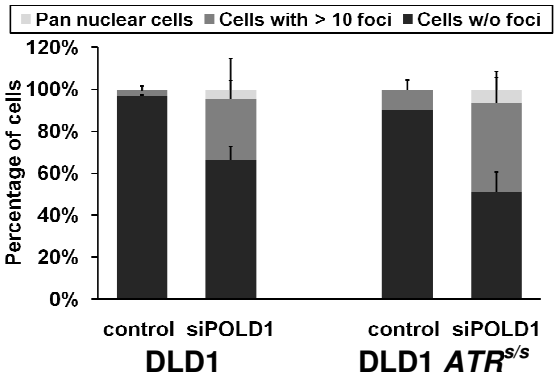
Pan nuclear cells
Cells with > 10 foci
Cells w/o foci
120%
100%
80%
60%
40%
20%
0%
Percentage of cells
control
siPOLD1
control
siPOLD1
DLD1
DLD1 ATR s/s

D

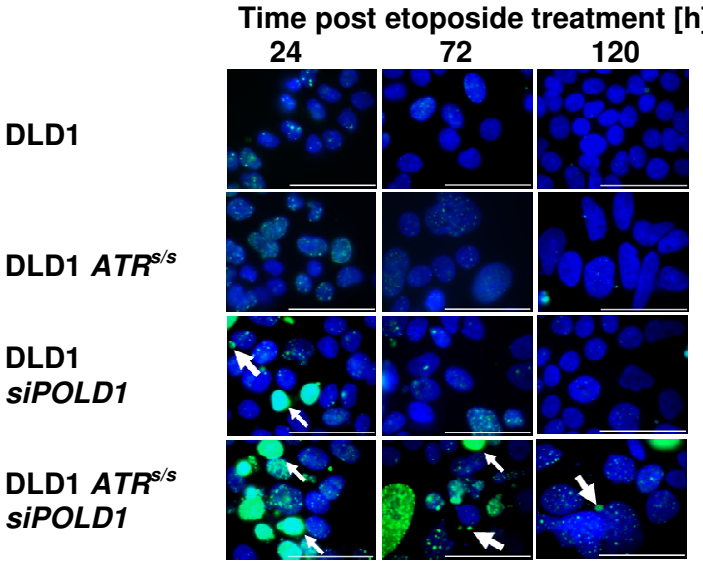
Time post etoposide treatment [h]
24
72
120
DLD1
DLD1 ATR s/s
DLD1
siPOLD1
DLD1 ATR s/s
siPOLD1

E

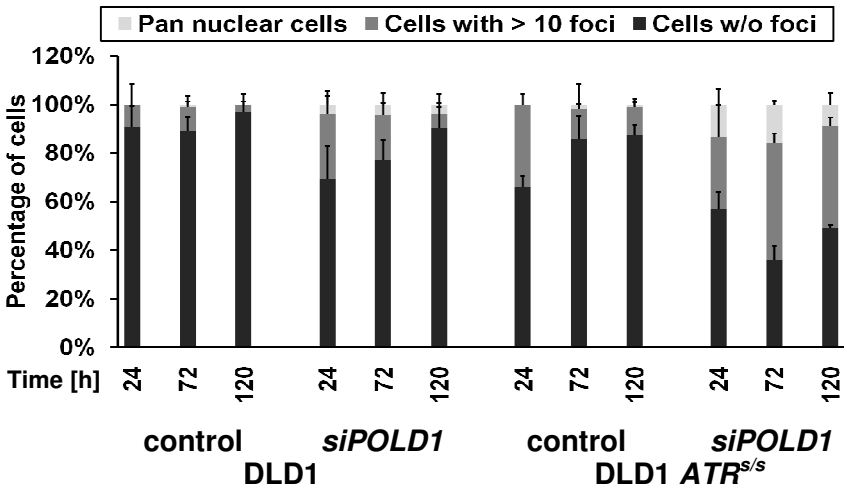
Pan nuclear cells
Cells with > 10 foci
Cells w/o foci
120%
100%
80%
60%
40%
20%
0%
Percentage of cells
Time [h]
24
72
120
24
72
120
24
72
120
24
72
120
control
siPOLD1
control
siPOLD1
DLD1
DLD1 ATR s/s

3.2.5. IR-induced co-localization of POLD1 with ATR and γ-H2AX.

To test whether ATR and POLD1 co-localize at sites of DNA damage, spatial localization of ATR, POLD1 and γ-H2AX was assessed upon IR stress, using co-immunostaining analysis. DLD1 parental cells were irradiated at 4 Gy and POLD1, ATR and γ-H2AX localization were examined by fluorescence microscopy at 4 h post IR using fluorescence-coupled antibodies directed against the targeted proteins. Co-localization of ATR and POLD1 was depicted in cell nucleus partially in untreated DLD1 parental cells (2.9 ± 1.6 co-localized foci) and with a 9.7-fold increase of spatial overlap (27.6 ± 8.9 co-localized foci) upon IR (**Fig. 15A+C,D**). Further, POLD1 relocalization to sites of DNA damage visualized by γ-H2AX focus formation was assessed upon irradiation. POLD1 clearly co-localized with γ-H2AX foci with a 14.2-fold increase in irradiated DLD1 parental cells (9.0 ± 2.3 co-localized foci) in comparison to untreated DLD1 parental cells (0.6 ± 0.2 co-localized foci) as illustrated by yellow-colored foci (**Fig. 15B+C,D**).

Figure 14: *ATR* and *POLD1* knockdown-dependent γ-H2AX formation upon etoposide stress (see page 51). DLD1 parental and DLD1 *ATR*$^{s/s}$ cells were grown on coverslips, treated with *siPOLD1* at 10 nM or left untreated, then treated with etoposide (0,25 µM) and stained with an anti-γ-H2AX antibody (green). Nuclei were counterstained with Hoechst 33258 (blue).(**A**) Timeline depicting experimental procedure. (**B**+**D**) Representative fluorescence images and (**C**+**E**) γ-H2AX quantification of control versus *siPOLD1*-treated DLD1 parental and DLD1 *ATR*$^{s/s}$ cells, respectively, are shown (**B**+**C**) at 120 h after transfection without etoposide and (**D**+**E**) upon etoposide treatment at 24 h, 72 h and 120 h. Thin arrows indicate pan-nuclear γ-H2AX staining, thick arrows apoptotic bodies. A scale bar (10 µm) is depicted. (**C**+**D**) For quantification, at least 50 cells of each cell line and condition were scored in two independent experiments. Error bars represent standard deviation of two experiments.

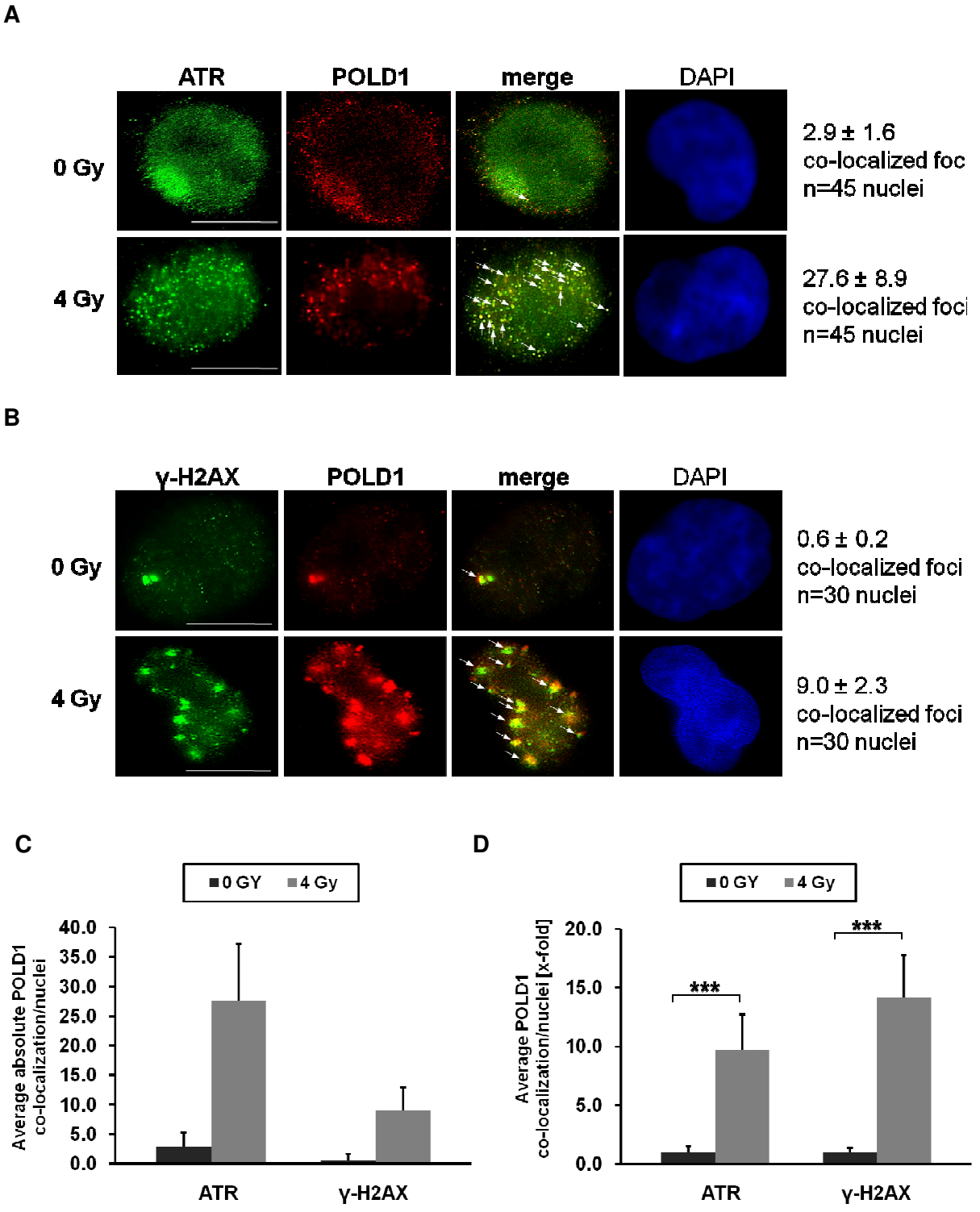

Figure 15: Spatial co-localization of POLD1 with ATR and γ-H2AX upon IR stress. DLD1 cells were grown on coverslips and irradiated at 4 Gy. Cells were co-immunostained with (**A+B**) anti-POLD1 (red) and (**A**) anti-ATR (green) or (**B**) anti-γ-H2AX (green) antibody at 4 h post irradiation. Nuclei were counterstained with Hoechst 33258 (blue). Merged images are shown for (**A**) ATR and POLD1 and (**B**) γ-H2AX and POLD1 signals. (**C**) Average absolute number of co-localized foci and (**D**) fold change of average number of co-localized foci between POLD1 and ATR or γ-H2AX per nuclei at 4 h post irradiation are shown. Fold change was normalized to untreated (0 Gy) DLD1 parental cells. 45 nuclei were scored for POLD1-ATR co-localization and 30 nuclei for POLD1-γ-H2AX co-localization, for each condition, at 4 h post irradiation per experiment. Values represent the mean (n=45/30) ± standard deviation of two independent experiments. Arrow denotes protein co-localization. Error bars represent standard deviation of two independent experiments. Scale bar, 3 µm. Asterisks mark statistical significance between two samples using the Student's t-test (***$p < 0.001$).

3.3. Generalization of *siPOLD1*-mediated sensitivity towards ATR- and CHK1-inhibitors using a panel of CRC cell lines

In an effort to generalize the data of *siPOLD1*-mediated sensitivity towards ATR- and CHK1-inhibitors beyond one single cancer cell line (DLD1), a panel of different CRC cell lines were analyzed. These cells lines were characterized by microsatellite instability (MSI; HCT116, RKO, (DLD1); **Fig. 16A**) as well as chromosomal instability (CIN; HT29, LS513, SW480; **Fig. 16B**) (123-125). Prior to inhibitor treatment, POLD1 protein depletion was quantified by immunoblotting for each cell line (**Fig. 16**). There was virtually no detectable POLD1 protein observed for RKO, LS513 and SW480 cells indicating an efficient *POLD1* down-regulation. However, *POLD1* knockdown failed for HCT116 and HT29 cells. Therefore, generalization of si*POLD1* knockdown-mediated sensitivity upon ATR- and CHK1-inhibitors was studied in RKO, LS513 and SW480 cells.

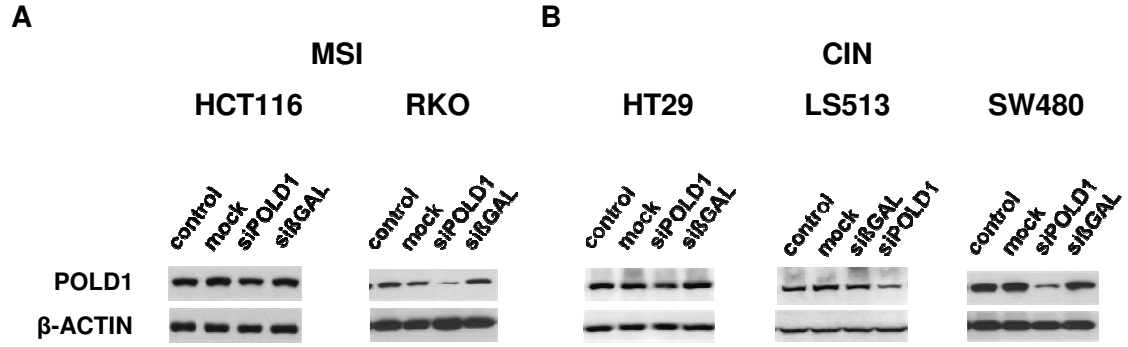

Figure 16: siRNA-mediated knockdown of *POLD1* in a panel of different CRC cell lines. Efficient siRNA-mediated (50 nM) POLD1 protein depletion was confirmed at 96 h post transfection in (**A**) MSI defined HCT116 and RKO cells and in (**B**) CIN defined HT29, LS513 and SW480 by immunoblotting. *siβGAL* at 50 nM served as transfection control, β-ACTIN as loading control.

For pharmacological generalization of *siPOLD1*-mediated sensitivity in RKO, LS513 and SW480 cells, ATR- and CHK1-inhibitors were applied, which were already described in 3.2.2. Inhibitor treatment was conducted at time points of the most efficient *POLD1* knockdown (**Fig. 16**). As compared to mock-transfected and control cells, POLD1 depletion sensitized RKO cells to NU6027 (IC50 ratio 3-fold), VE-822 (IC50 ratio 2-fold) and LY2603618 (IC50 ratio 3-fold) (**Fig. 17**, **upper panel**), SW480 cells to NU6027 (IC50 ratio 2-fold) and UCN-01 (IC50 ratio 2-fold) (**Fig. 17, middle panel**) and LS513 cells to all inhibitors used (IC50 ratio 2- to 3-fold) (**Fig. 17, lower panel**).

To exclude general and POLD1-independent hypersensitivity phenotypes, all cell lines were additionally treated with MMC, oxaliplatin and 5-FU upon *POLD1*-knockdown. As already shown for DLD1 cells, no significant proliferation differences among POLD1-depleted, mock-

transfected and control RKO, SW480 and LS513 cells were detected upon treatment with any of these agents (**Fig. 18**).

RKO

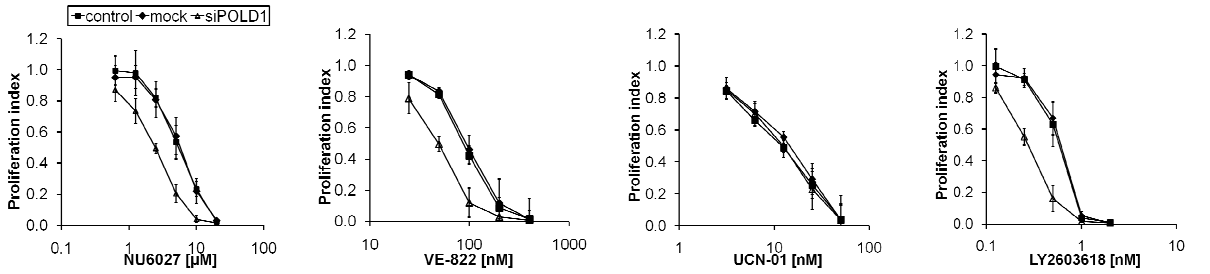

SW480

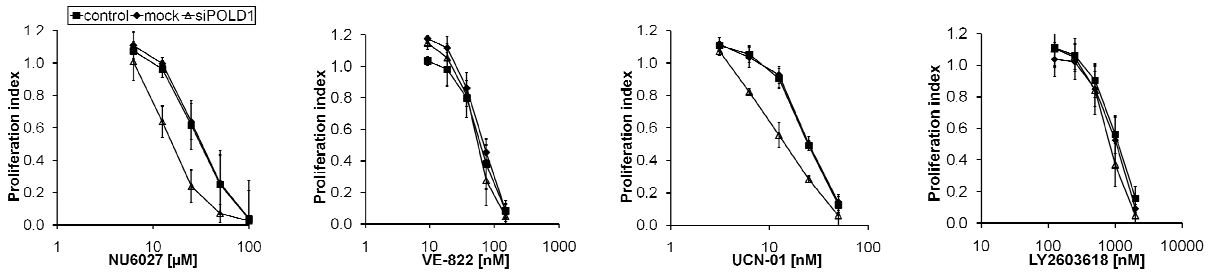

LS513

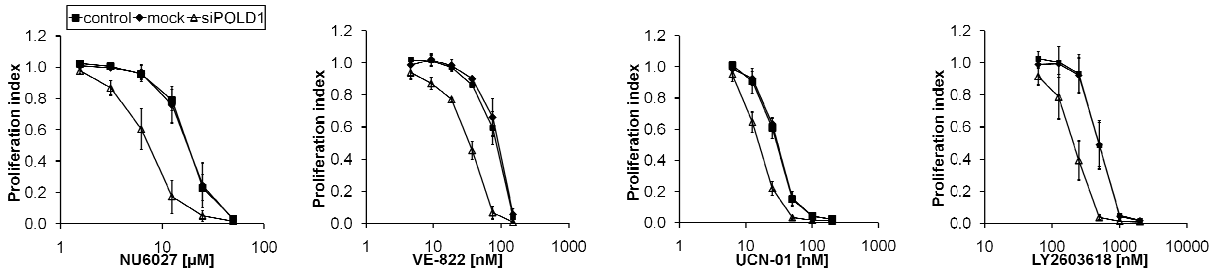

Figure 17: ATR-/CHK1-dependent proliferation inhibition upon *POLD1* knockdown in a panel of CRC cell lines. Effects on proliferation of ATR- and CHK1-inhibitors were assessed at 120 h after treatment in control, mock-transfected or *siPOLD1*-transfected (50 nM) RKO, SW480 and LS513 cells. Error bars represent standard deviation of three independent experiments with each data point representing triplicate wells.

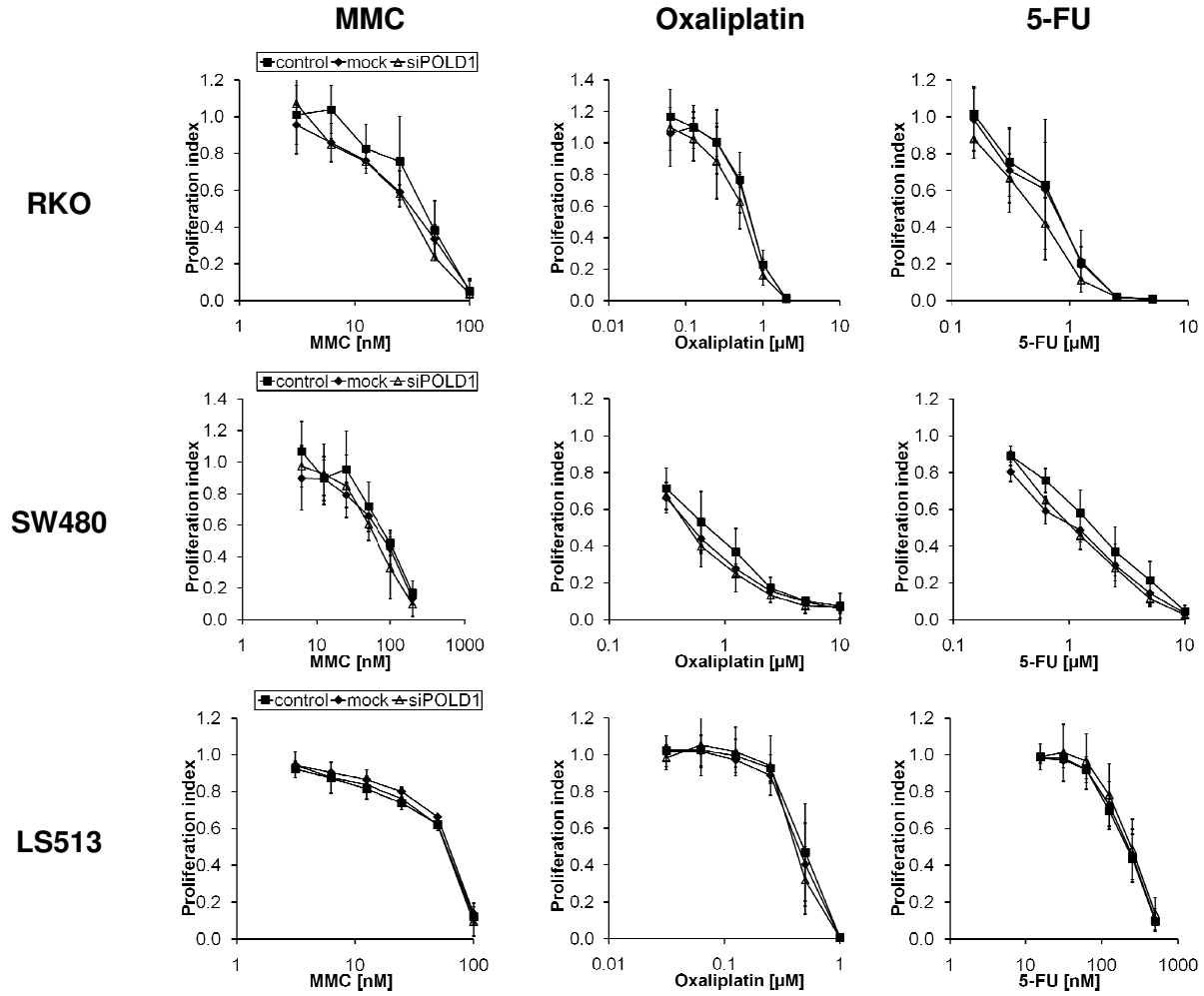

Figure 18: Chemotherapeutic-independent proliferation of CRC cells upon POLD1 depletion. Effects on proliferation of common chemotherapeutics (MMC, oxaliplatin and 5-FU) were assessed at 120 h after treatment in control, mock-transfected or *siPOLD1*-transfected (50 nM) RKO, SW480 and LS513 cells. Error bars represent standard deviation of three independent experiments with each data point reflecting triplicate wells.

4. DISCUSSION

In response to DNA damage and replication stress, ATR acts as a central checkpoint regulator and mediator of the DNA-repair machinery by homologous recombination (4). ATR-inhibition has recently been demonstrated to induce the elimination of tumor cells in CRCs (104; 106) but the underlying genetic determinants are still insufficiently defined. Using a well-defined genetic *ATR* knock-in model of human CRC cells (97), a siRNA library screening approach was conducted to identify potential synthetically lethal interactions between *ATR* and DNA-repair genes. Six DNA-repair genes exhibiting synthetically lethal interactions with *ATR* and 20 genes displaying *ATR* genotype-independent knockdown-induced cell killing were identified. Among the identified genes exhibiting synthetically lethal interactions with *ATR*, the most profound effects were observed for *POLD1* and were further characterized.

4.1. DLD1 *ATR*$^{s/s}$ cells as ideally-suited model for DNA-repair siRNA library screening

ATR is an essential gene (126) and consequently, few cellular models exist to investigate its complete disruption. However, the bi-allelic hypomorphic *ATR* splice site mutation 2101$^{A\rightarrow G}$, naturally found in Seckel syndrome patients (29), results in a subtotal ATR protein depletion without significant effects on cancer cell growth or viability (97). The human CRC line DLD1 engineered to homozygously harbor this mutation (termed *ATR*$^{s/s}$ cells) (97; 104; 127) thus represents an ideally-suited model system for our question, as subtotal ATR protein depletion likely mimics the incomplete inhibition of ATR achievable through pharmacological means more closely than the complete and in most instances lethal *ATR* gene knockout (126). Preliminary experiments confirmed that DLD1 *ATR*$^{s/s}$ cells display suppression of ATR protein below the detection limit of our assay as well as increased sensitivity towards MMC, as previously described (97; 103).

In this screen, 26 out of 288 DNA-repair genes were identified, whose knockdown elicited either selective *ATR* genotype-dependent or -independent detrimental effects. Hit rates did not systematically differ between DLD1 parental and DLD1 *ATR*$^{s/s}$ cells (hit rate = 9%) ruling out the systematic error of a general siRNA-transfection-mediated cell killing of DLD1 *ATR*$^{s/s}$ cells. In addition, the screening validity was confirmed by a z factor of >0.5 (128). The sensitivity of this approach was illustrated by the re-identification of the previously described synthetically lethal interactions of *XRCC1* or *PRIM1* with *ATR* (50; 129). In addition, very recent data published during the writing of this PhD thesis confirmed some of the hits obtained in our genetic *ATR* model including especially *POLD1* and *PRIM1* (130). Mohni and colleagues used a less *ATR*-specific synthetic lethal screening system applying the ATR-inhibitor VE-821. VE-821 was described as less specific than its further developed

analogue VE-822 showing elevated potency, less cell and tissue toxicity and improved pharmacokinetic features (33). VE-822 was used in our study for pharmacological reproduction of synthetic lethal interactions of *ATR* with *POLD1*. Further, siRNA-library screening was conducted in a well-defined *ATR* knock-in model excluding unspecific inhibitor side effects as well as ensuring that effects specifically results from ATR protein depletion. While Mohni et al. described synthetically lethal effects only in one cell line (U2OS bone osteosarcoma cells) (130), our study provides data on the specific killing of cells harboring *ATR* and *POLD1* deficiency in several CRC cell lines along with different ATR- and CHK1-inhibitors (**Fig. 10**, **Fig 17**) confirming our screening data.

4.2. *ATR* genotype-independent effects in DLD1 cancer cells

Our screen identified 20 DNA-repair genes (**Table 10**), whose knockdown led to proliferation inhibition in DLD1 parental and DLD1 $ATR^{s/s}$ cells independently of *ATR* status (hit rate = 7%) indicating essential functions of these genes at least in DLD1 cells. The strongest *ATR* genotype-independent effects were observed for *XAB2* and *PLK1* knockdown, both of which resulted in a virtually complete proliferation loss. Consistently, homozygous *XAB2* and *PLK1* knockout mice display an early embryonic lethal phenotype (131; 132) and knockdown of *XAB2* was reported to induce widespread cell death in human bladder, cervix and pancreatic cancer (133). However, these *ATR*-genotype independent effects were not the focus of this study. Consequently, these DNA-repair genes were not further examined.

4.3. *ATR* genotype-dependent effects identified synthetic lethal interactions with DNA-repair genes in DLD1 cancer cells

Five genes interplaying in DNA repair as well as in DNA replication at the DNA replication fork were identified, whose knockdown led to proliferation inhibition selectively of DLD1 $ATR^{s/s}$ but not of DLD1 parental cells (hit rate = 2%) (**Table 9**, **Fig. 19**). The strongest effects selectively on DLD1 $ATR^{s/s}$ cells were observed for *POLD1* and *PRIM1* knockdown, both of which are involved in DNA repair or DNA replication synthesis (134; 135). *POLD1* was further characterized as described below. *PRIM1* encodes the catalytic subunit of DNA primase synthesizing short RNA primers, which are extended in complex with DNA polymerase α (136). A polymerase switch to DNA polymerase δ harboring the catalytic and proofreading subunit POLD1 ensures primer elongation and DNA strand polymerization. Accordingly, both proteins, PRIM1 and POLD1, are involved in immediately consecutive DNA replication steps (137) explaining the synthetically lethal effects upon depletion of either protein in DLD1 $ATR^{s/s}$ cells. Mechanistically, RNA primer synthesis influences replication-dependent binding of ATR to chromatin, which is required for checkpoint

activation. Upon completion of DNA replication, dissociation of ATR from DNA triggers entry into mitosis (138). Impairment of either PRIM1 or POLD1 in combination with ATR impairment might thus be expected to cause first incomplete DNA replication, which is then followed by premature entry into mitosis due to checkpoint deficiency.

In addition to *POLD1* and *PRIM1*, *XRCC5* (*Ku80*) and *XRCC6* (*Ku70*) knockdown-induced proliferation inhibition in DLD1 $ATR^{s/s}$ cells were identified. Next to the role of XRCC5 and XRCC6 in non-homologous end joining DNA repair (139), the XRCC5/XRCC6 heterodimer complex associates with the essential hexamers MCM (140) and ORC (141) to form the pre-replication complex. Consistently, low expression levels of *XRCC6* and *XRCC5* lead to decreased DNA synthesis due to abortive DNA replication initiation (142), which in combination with impaired ATR-mediated checkpoint signaling might be expected to cause synthetic lethality between *ATR* and *XRCC5/XRCC6* through a similar mechanism as explained above. Clinically, *XRCC5* and *XRCC6* single nucleotide polymorphisms as well as epigenetic silencing of these genes can lead to the development of multiple cancers, such as CRC, breast and lung cancer (10). It will be interesting to investigate in future studies whether *XRCC5/XRCC6*-impaired tumors were sensitive towards ATR- or CHK1-inhibitors.

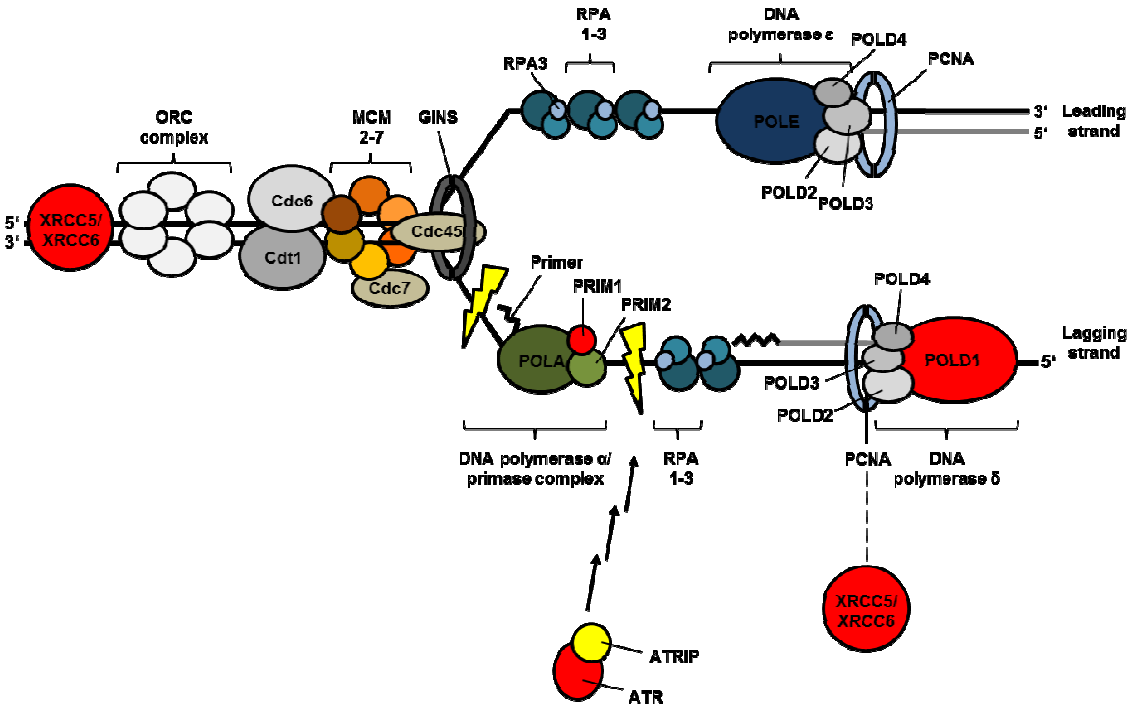

Figure 19: Schematic representation of DNA replication and DNA-repair proteins at the DNA replication fork. Due to replication stress and DNA single-strand breaks (yellow flash), ATR is activated and mediates DNA damage response (arrow). Knockdown of specific DNA replication and repair proteins (red) by classical gene knockdown and/or chemical inhibition induces a synthetic lethal effect with ATR depletion identified in the described siRNA library screen.

4.4. Pharmacological reproduction of the synthetic lethal interaction between *ATR* and *POLD1*

Additional studies are required to confirm and mechanistically characterize the synthetic lethal interactions between *ATR* and the DNA-repair genes identified in this study. As a start, *POLD1* was picked for in-depth characterization, as its knockdown elicited by far the strongest effects in DLD1 $ATR^{s/s}$ cells. After confirmation of time- and *siPOLD1* concentration-dependent cell killing specifically of DLD1 $ATR^{s/s}$ cells, these effects were demonstrated to be pharmacologically reproducible by using chemical ATR-inhibitors on POLD1-depleted DLD1 parental cells. Importantly, a general hypersensitivity phenotype of POLD1-depleted DLD1 parental cells was excluded by treatment with various chemotherapeutics including ICL- and non-ICL-agents, none of which elicited POLD1-dependent hypersensitivity. Clonally selected heterozygous DLD1 $ATR^{+/s}$ cells remained unaffected by POLD1 depletion excluding artefacts due to clonal variability.

Intracellular protection against DNA damage and replication stress is mediated by both ATR and its major downstream effector kinase CHK1. Both proteins are essential and appear to similarly promote tumorigenesis (28; 126; 143). As CHK1-inhibitors are currently further developed than ATR-inhibitors (144) and already undergoing testing in clinical trials (145), we analyzed whether the effects of ATR-inhibition could similarly be induced by targeting CHK1. The CHK1-inhibitor UCN-01 was applied for this purpose despite its rather low selectivity because it currently represents the only FDA-approved CHK1-inhibitor (145). Indeed, the inhibition of CHK1 by UCN-01 caused similar effects on POLD1-depleted DLD1 parental cells as ATR-inhibition did. Nevertheless, inhibition of ATR as the upstream kinase of CHK1 is expected to potentially elicit additional effects as compared to the specific inhibition of CHK1, as multiple other substrates are canonically phosphorylated by ATR in various tumor identities (5; 104; 146). Concomitantly, kinases other than ATR have been demonstrated to mediate compensatory ATR-independent CHK1 activation (147). Consistently, *ATR* and *CHK1* have been demonstrated to not function completely epistatically (148) and thus, ATR-inhibitors and CHK1-inhibitors are expected to not be readily interchangeable for cancer-therapeutic approaches.

In an effort to generalize these data beyond one single cell line, the effects of ATR- and CHK1-inhibitors were investigated in a panel of CRC cell lines including lines exhibiting a microsatellite instable (MSI) as well as those exhibiting a chromosomal instable (CIN) phenotype (125; 149). POLD1-depleted RKO, SW480 and LS513 cells displayed increased sensitivity towards ATR-/CHK1-inhibitors as compared to control cells.

Considering that siRNA-mediated *POLD1* knockdown was exclusively done once prior to inhibitor treatment, *POLD1* knockdown at multiple time points might further increase ATR- and CHK1-inhibitor effects in all cell lines. The fact that only some but not all ATR-/CHK1-

inhibitors elicited *POLD1*-dependent effects might be ascribable to the additional unspecific inhibition of other targets inherent to chemical inhibitors along with the heterogeneous genotype of the tested CRC lines. Nevertheless, inhibition of the ATR/CHK1-axis could be a generalizable therapeutic concept in patients with *POLD1* low-or non-expressing tumors.

4.5. Mechanistic characterization of the synthetic lethal interaction between *ATR* and *POLD1*

To investigate the underlying mechanism of the synthetic lethal interaction between *ATR* and *POLD1*, cell cycle distribution was analyzed to detect cell cycle arrests along with the sub-G1 fraction as a surrogate marker for apoptosis. While no significant effects on cell cycle were observed, a significantly increased sub-G1 fraction was displayed in DLD1 $ATR^{s/s}$ cells upon *POLD1* knockdown. Apoptosis was further confirmed by the proteolytic cleavages of PARP, the initiator CASPASE9 and the executioner CASPASE3 (150) as well as by CASPASE3-attributable DEVDase activity (101). In general, these data are consistent with previous studies showing spontaneous apoptosis *in vivo* in $POLD1^{-/-}$ mice (151). More specifically, *POLD1* down-regulation has been demonstrated to mediate the reduction of DNA synthesis *in vitro* (152), which is expected to activate the DNA replication checkpoint (153). Disruption of this checkpoint by *ATR* deficiency might thus prevent cell cycle arrest in S-phase, a hypothesis supported by the absence of cell cycle disturbances in our experiments. Taken together, reduction of DNA synthesis caused by *POLD1* knockdown along with premature entry into mitosis caused by *ATR* deficiency provides a plausible mechanism for the apoptosis-mediated synthetic lethality of *POLD1* and *ATR* in our experiments.

Since POLD1 represents a DNA polymerase δ subunit with critical catalytic and proofreading activity in replicative DNA synthesis, recombination and especially repair processes (134), the effects of POLD1 depletion on DNA damage- and DNA repair-kinetics in DLD1 parental and DLD1 $ATR^{s/s}$ cells were investigated. Upon *POLD1* knockdown, DLD1 $ATR^{s/s}$ cells but not DLD1 parental cells displayed strongly increased levels of endogenous DNA DSBs, as illustrated by increased nuclear γ-H2AX focus formation (118). Upon exogenously induced DNA DSBs by IR or etoposide, sustained γ-H2AX focus accumulation (>120 h) was observed specifically in *siPOLD1*-transfected DLD1 $ATR^{s/s}$ cells but not in control DLD1 $ATR^{s/s}$ cells or control or *siPOLD1*-transfected DLD1 parental cells, strongly supporting an impaired or at least decelerated DNA-repair capacity. These data further support our above hypothesis that depletion of *POLD1* causing increased DNA-damage (152) and decreased DNA-repair in combination with deficient *ATR*-signaling causing DNA replication checkpoint disruption (153), premature entry into mitosis and eventually apoptosis mechanistically explains the synthetic lethality of these two genes.

Co-localization studies in DLD1 parental cells supported the existence of a synthetic lethal interaction of *ATR* with *POLD1* in the presence of DNA damage/repair. POLD1 relocalization to sites of DNA damage visualized by γ-H2AX focus formation was displayed upon IR. Consistently, POLD1 recruitment with γ-H2AX after exposure to UV was reported to almost 100% confirming our data (154). In concordance with the observed spatial overlap of ATR and POLD1 upon IR, DNA polymerase δ consisting of different subunits including POLD1 (134) was identified as a putative ATR-specific phosphorylation target (155).

4.6. Clinical significance of *POLD1* as prognostic and predictive marker for personal *ATR*-targeted therapies

POLD1 was previously described as a prognostic marker with conflicting data in different types of cancer. *POLD1* overexpression is associated with a poor prognosis in hepatocellular carcinomas and multiple myeloma (156; 157), whereas *POLD1* down-regulation is associated with a poor outcome in head and neck squamous cell carcinoma (158).

Sporadic *POLD1* sequence alterations have been already found in human colon cancer cell lines and patient tissue samples (159). A missense mutation (p.His506Arg) in the exonuclease domain III of DNA polymerase δ expected to cause a hypermutability phenotype has earlier been reported in human CRC lines (159). In addition, recently identified *POLD1* missense mutations predispose to CRC (p.Ser478Asn, p.Pro327Arg), endometrial cancer (p.Ser478Asn) and likely to brain (p.Ser478Asn) and kidney tumors (p.Val392Met) (160; 161). Equivalent mutations of the human *POLD1* p.Ser478Arg lead to an increased mutation rate in fission yeast and are mapped along with the human *POLD1* p.Pro327Arg mutation at the interface of the exonuclease active site predicting these mutations to have functional effects on DNA binding and exonuclease activity (161).

Regarding colorectal cancer, at least 12 known CRC cell lines have been reported to harbor either heterozygous or homozygous mutations in *POLD1* (162). As many of these mutations represent variants of unknown significance, future studies applying suitable syngeneic *POLD1* model systems are urgently needed to clarify the functional significance of these genetic changes in CRC as well as other tumor entities.

Thus, genetic alterations of *POLD1* affecting catalytic or proofreading activity represent predictive markers for the therapeutic response towards ATR- and CHK1-inhibitors in the clinical setting. Combination treatment with radiotherapy (exemplarily shown in POLD1-depleted DLD1 $ATR^{s/s}$ cells upon IR, **Fig. 13**) or chemotherapeutics targeting DNA directly (e.g. cisplatin, 5-FU) or indirectly by DNA replication or DNA repair proteins (exemplarily shown in POLD1-depleted DLD1 $ATR^{s/s}$ cells upon etoposide, **Fig. 14**) might increase ATR-/CHK1-inhibitor effect in cancer cells which could improve clinical outcome.

5. CONCLUSION AND FURTHER PERSPECTIVE

In conclusion, ATR-inhibition has recently been demonstrated to induce the elimination of CRCs (104; 106) but the underlying genetic determinants remained insufficiently defined. By screening of a DNA-repair gene siRNA library in a well-defined DLD1 *ATR* cancer cell model, *POLD1* as one critical determinant during ATR inhibition-mediated CRC cell killing was identified. Synthetic lethality induced by POLD1 depletion in DLD1 $ATR^{s/s}$ cells was mechanistically described by caspase-dependent apoptosis induced by DNA damage accumulation. Consistent with these data, spatial co-localization of POLD1 with ATR as well as of POLD1 with γ-H2AX at sites of DNA damage was shown. Further, *POLD1* knockdown-induced cell killing was pharmacologically reproducible with various ATR-/CHK1-inhibitors in a panel of other CRC cell lines. Thus, our data might have clinical implications, as inactivating *POLD1* mutations have recently been described in four families with multiple colorectal adenomas and CRC (161). In three of these *POLD1* families endometrial tumors were diagnosed. Currently, ongoing whole-genome and whole-exome sequencing studies are expected to determine the *POLD1* mutation rates in tumor entities other than CRC or endometrial cancer, which could then broaden the applicability of the identified synthetic lethality with ATR-inhibitors. Long-term, the development of selective POLD1- or DNA polymerase δ-targeted drugs should be considered to further extend the applicability of the proposed concept of this genotype-based anti-cancer therapy.

6. REFERENCES

1. Lindahl T. 1993. Instability and decay of the primary structure of DNA. *Nature* 362:709-15
2. Lindahl T, Barnes DE. 2000. Repair of endogenous DNA damage. *Cold Spring Harbor symposia on quantitative biology* 65:127-33
3. Ciccia A, Elledge SJ. 2010. The DNA damage response: making it safe to play with knives. *Molecular cell* 40:179-204
4. Cimprich KA, Cortez D. 2008. ATR: an essential regulator of genome integrity. *Nature reviews. Molecular cell biology* 9:616-27
5. Zhou BB, Elledge SJ. 2000. The DNA damage response: putting checkpoints in perspective. *Nature* 408:433-9
6. Jackson SP, Bartek J. 2009. The DNA-damage response in human biology and disease. *Nature* 461:1071-8
7. Sulli G, Di Micco R, d'Adda di Fagagna F. 2012. Crosstalk between chromatin state and DNA damage response in cellular senescence and cancer. *Nature reviews. Cancer* 12:709-20
8. Khanna KK, Jackson SP. 2001. DNA double-strand breaks: signaling, repair and the cancer connection. *Nature genetics* 27:247-54
9. Helleday T, Petermann E, Lundin C, Hodgson B, Sharma RA. 2008. DNA repair pathways as targets for cancer therapy. *Nature reviews. Cancer* 8:193-204
10. Curtin NJ. 2012. DNA repair dysregulation from cancer driver to therapeutic target. *Nature reviews. Cancer* 12:801-17
11. Dietlein F, Thelen L, Reinhardt HC. 2014. Cancer-specific defects in DNA repair pathways as targets for personalized therapeutic approaches. *Trends in genetics : TIG* 30:326-39
12. Reardon JT, Sancar A. 2005. Nucleotide Excision Repair. In *Progress in Nucleic Acid Research and Molecular Biology*, ed. M Kivie, Volume 79:183-235: Academic Press. Number of 183-235 pp.
13. Jiricny J. 2006. The multifaceted mismatch-repair system. *Nature reviews. Molecular cell biology* 7:335-46
14. Kunkel TA, Erie DA. 2005. DNA mismatch repair. *Annual review of biochemistry* 74:681-710
15. Damia G, D'Incalci M. 2007. Targeting DNA repair as a promising approach in cancer therapy. *European journal of cancer (Oxford, England : 1990)* 43:1791-801
16. Fong PC, Yap TA, Boss DS, Carden CP, Mergui-Roelvink M, et al. 2010. Poly(ADP)-ribose polymerase inhibition: frequent durable responses in BRCA carrier ovarian cancer correlating with platinum-free interval. *Journal of clinical oncology : official journal of the American Society of Clinical Oncology* 28:2512-9
17. Pollack IF, Kawecki S, Lazo JS. 1996. Blocking of glioma proliferation in vitro and in vivo and potentiating the effects of BCNU and cisplatin: UCN-01, a selective protein kinase C inhibitor. *Journal of neurosurgery* 84:1024-32
18. Zhao Y, Thomas HD, Batey MA, Cowell IG, Richardson CJ, et al. 2006. Preclinical evaluation of a potent novel DNA-dependent protein kinase inhibitor NU7441. *Cancer research* 66:5354-62
19. Lovejoy CA, Cortez D. 2009. Common mechanisms of PIKK regulation. *DNA repair* 8:1004-8
20. Brown EJ, Baltimore D. 2003. Essential and dispensable roles of ATR in cell cycle arrest and genome maintenance. *Genes & development* 17:615-28
21. Bartek J, Lukas C, Lukas J. 2004. Checking on DNA damage in S phase. *Nature reviews. Molecular cell biology* 5:792-804
22. Zou L, Elledge SJ. 2003. Sensing DNA damage through ATRIP recognition of RPA-ssDNA complexes. *Science (New York, N.Y.)* 300:1542-8

23. Ball HL, Ehrhardt MR, Mordes DA, Glick GG, Chazin WJ, Cortez D. 2007. Function of a conserved checkpoint recruitment domain in ATRIP proteins. *Molecular and cellular biology* 27:3367-77
24. MacDougall CA, Byun TS, Van C, Yee MC, Cimprich KA. 2007. The structural determinants of checkpoint activation. *Genes & development* 21:898-903
25. Kumagai A, Dunphy WG. 2000. Claspin, a novel protein required for the activation of Chk1 during a DNA replication checkpoint response in Xenopus egg extracts. *Molecular cell* 6:839-49
26. Osborn AJ, Elledge SJ, Zou L. 2002. Checking on the fork: the DNA-replication stress-response pathway. *Trends in cell biology* 12:509-16
27. Brown EJ, Baltimore D. 2000. ATR disruption leads to chromosomal fragmentation and early embryonic lethality. *Genes & development* 14:397-402
28. Bartek J, Mistrik M, Bartkova J. 2012. Thresholds of replication stress signaling in cancer development and treatment. *Nature structural & molecular biology* 19:5-7
29. O'Driscoll M, Ruiz-Perez VL, Woods CG, Jeggo PA, Goodship JA. 2003. A splicing mutation affecting expression of ataxia-telangiectasia and Rad3-related protein (ATR) results in Seckel syndrome. *Nature genetics* 33:497-501
30. Murga M, Campaner S, Lopez-Contreras AJ, Toledo LI, Soria R, et al. 2011. Exploiting oncogene-induced replicative stress for the selective killing of Myc-driven tumors. *Nature structural & molecular biology* 18:1331-5
31. Bartkova J, Horejsi Z, Koed K, Kramer A, Tort F, et al. 2005. DNA damage response as a candidate anti-cancer barrier in early human tumorigenesis. *Nature* 434:864-70
32. Sarkaria JN, Busby EC, Tibbetts RS, Roos P, Taya Y, et al. 1999. Inhibition of ATM and ATR kinase activities by the radiosensitizing agent, caffeine. *Cancer research* 59:4375-82
33. Fokas E, Prevo R, Pollard JR, Reaper PM, Charlton PA, et al. 2012. Targeting ATR in vivo using the novel inhibitor VE-822 results in selective sensitization of pancreatic tumors to radiation. *Cell death & disease* 3:e441
34. Foote KM, Blades K, Cronin A, Fillery S, Guichard SS, et al. 2013. Discovery of 4-{4-[(3R)-3-Methylmorpholin-4-yl]-6-[1-(methylsulfonyl)cyclopropyl]pyrimidin-2-y l}-1H-indole (AZ20): a potent and selective inhibitor of ATR protein kinase with monotherapy in vivo antitumor activity. *Journal of medicinal chemistry* 56:2125-38
35. Jones CD, Blades K, Foote KM, Guichard SM, Jewsbury PJ, et al. 2013. Discovery of AZD6738, a potent and selective inhibitor with the potential to test the clinical efficacy of ATR kinase inhibition in cancer patients. *Cancer research* 73:2348-
36. Peasland A, Wang LZ, Rowling E, Kyle S, Chen T, et al. 2011. Identification and evaluation of a potent novel ATR inhibitor, NU6027, in breast and ovarian cancer cell lines. *British journal of cancer* 105:372-81
37. Pires IM, Olcina MM, Anbalagan S, Pollard JR, Reaper PM, et al. 2012. Targeting radiation-resistant hypoxic tumour cells through ATR inhibition. *British journal of cancer* 107:291-9
38. Reaper PM, Griffiths MR, Long JM, Charrier JD, Maccormick S, et al. 2011. Selective killing of ATM- or p53-deficient cancer cells through inhibition of ATR. *Nature chemical biology* 7:428-30
39. Charrier JD, Durrant SJ, Golec JM, Kay DP, Knegtel RM, et al. 2011. Discovery of potent and selective inhibitors of ataxia telangiectasia mutated and Rad3 related (ATR) protein kinase as potential anticancer agents. *Journal of medicinal chemistry* 54:2320-30
40. Hall AB, Newsome D, Wang Y, Boucher DM, Eustace B, et al. 2014. Potentiation of tumor responses to DNA damaging therapy by the selective ATR inhibitor VX-970. *Oncotarget* 5:5674-85
41. Toledo LI, Murga M, Zur R, Soria R, Rodriguez A, et al. 2011. A cell-based screen identifies ATR inhibitors with synthetic lethal properties for cancer-associated mutations. *Nature structural & molecular biology* 18:721-7
42. Maira SM, Stauffer F, Brueggen J, Furet P, Schnell C, et al. 2008. Identification and characterization of NVP-BEZ235, a new orally available dual phosphatidylinositol 3-

kinase/mammalian target of rapamycin inhibitor with potent in vivo antitumor activity. *Molecular cancer therapeutics* 7:1851-63
43. Kaelin WG, Jr. 2005. The concept of synthetic lethality in the context of anticancer therapy. *Nature reviews. Cancer* 5:689-98
44. Chan DA, Giaccia AJ. 2011. Harnessing synthetic lethal interactions in anticancer drug discovery. *Nature reviews. Drug discovery* 10:351-64
45. Reinhardt HC, Jiang H, Hemann MT, Yaffe MB. 2009. Exploiting synthetic lethal interactions for targeted cancer therapy. *Cell cycle (Georgetown, Tex.)* 8:3112-9
46. Luo J, Solimini NL, Elledge SJ. 2009. Principles of cancer therapy: oncogene and non-oncogene addiction. *Cell* 136:823-37
47. Pino MS, Chung DC. 2010. The chromosomal instability pathway in colon cancer. *Gastroenterology* 138:2059-72
48. Farmer H, McCabe N, Lord CJ, Tutt AN, Johnson DA, et al. 2005. Targeting the DNA repair defect in BRCA mutant cells as a therapeutic strategy. *Nature* 434:917-21
49. Bryant HE, Schultz N, Thomas HD, Parker KM, Flower D, et al. 2005. Specific killing of BRCA2-deficient tumours with inhibitors of poly(ADP-ribose) polymerase. *Nature* 434:913-7
50. Sultana R, Abdel-Fatah T, Perry C, Moseley P, Albarakti N, et al. 2013. Ataxia telangiectasia mutated and Rad3 related (ATR) protein kinase inhibition is synthetically lethal in XRCC1 deficient ovarian cancer cells. *PloS one* 8:e57098
51. Mohni KN, Kavanaugh GM, Cortez D. 2014. ATR pathway inhibition is synthetically lethal in cancer cells with ERCC1 deficiency. *Cancer research* 74:2835-45
52. Gilad O, Nabet BY, Ragland RL, Schoppy DW, Smith KD, et al. 2010. Combining ATR suppression with oncogenic Ras synergistically increases genomic instability, causing synthetic lethality or tumorigenesis in a dosage-dependent manner. *Cancer research* 70:9693-702
53. Walther A, Johnstone E, Swanton C, Midgley R, Tomlinson I, Kerr D. 2009. Genetic prognostic and predictive markers in colorectal cancer. *Nature reviews. Cancer* 9:489-99
54. López PJT, Albero JS, Rodríguez-Montes JA. 2014. Primary and secondary prevention of colorectal cancer. *Clinical medicine insights. Gastroenterology* 7:33
55. Ferlay J, Steliarova-Foucher E, Lortet-Tieulent J, Rosso S, Coebergh JW, et al. 2013. Cancer incidence and mortality patterns in Europe: estimates for 40 countries in 2012. *European journal of cancer (Oxford, England : 1990)* 49:1374-403
56. Siegel R, Ma J, Zou Z, Jemal A. 2014. Cancer statistics, 2014. *CA: a cancer journal for clinicians* 64:9-29
57. Weitz J, Koch M, Debus J, Hohler T, Galle PR, Buchler MW. 2005. Colorectal cancer. *Lancet* 365:153-65
58. Eaden J, Abrams K, Mayberry J. 2001. The risk of colorectal cancer in ulcerative colitis: a meta-analysis. *Gut* 48:526-35
59. Markowitz SD, Bertagnolli MM. 2009. Molecular origins of cancer: Molecular basis of colorectal cancer. *The New England journal of medicine* 361:2449-60
60. Mundade R, Imperiale TF, Prabhu L, Loehrer PJ, Lu T. 2014. Genetic pathways, prevention, and treatment of sporadic colorectal cancer. *Oncoscience* 1:400-6
61. Fearon ER, Vogelstein B. 1990. A genetic model for colorectal tumorigenesis. *Cell* 61:759-67
62. de la Chapelle A, Hampel H. 2010. Clinical relevance of microsatellite instability in colorectal cancer. *Journal of clinical oncology : official journal of the American Society of Clinical Oncology* 28:3380-7
63. Sideris M, Papagrigoriadis S. 2014. Molecular biomarkers and classification models in the evaluation of the prognosis of colorectal cancer. *Anticancer research* 34:2061-8
64. Corso G, Pascale V, Flauti G, Ferrara F, Marrelli D, Roviello F. 2013. Oncogenic mutations and microsatellite instability phenotype predict specific anatomical subsite in colorectal cancer patients. *European journal of human genetics : EJHG* 21:1383-8
65. Simons CC, Hughes LA, Smits KM, Khalid-de Bakker CA, de Bruine AP, et al. 2013. A novel classification of colorectal tumors based on microsatellite instability, the CpG

island methylator phenotype and chromosomal instability: implications for prognosis. *Annals of oncology : official journal of the European Society for Medical Oncology / ESMO* 24:2048-56

66. Cheng YW, Pincas H, Bacolod MD, Schemmann G, Giardina SF, et al. 2008. CpG island methylator phenotype associates with low-degree chromosomal abnormalities in colorectal cancer. *Clinical cancer research : an official journal of the American Association for Cancer Research* 14:6005-13
67. Zambirinis CP, Theodoropoulos G, Gazouli M. 2009. Undefined familial colorectal cancer. *World journal of gastrointestinal oncology* 1:12-20
68. Jass JR. 2007. Classification of colorectal cancer based on correlation of clinical, morphological and molecular features. *Histopathology* 50:113-30
69. Weisenberger DJ, Siegmund KD, Campan M, Young J, Long TI, et al. 2006. CpG island methylator phenotype underlies sporadic microsatellite instability and is tightly associated with BRAF mutation in colorectal cancer. *Nature genetics* 38:787-93
70. Vogelstein B, Kinzler KW. 2004. Cancer genes and the pathways they control. *Nature medicine* 10:789-99
71. Lengauer C, Kinzler KW, Vogelstein B. 1997. Genetic instability in colorectal cancers. *Nature* 386:623-7
72. Geiersbach KB, Samowitz WS. 2011. Microsatellite instability and colorectal cancer. *Archives of pathology & laboratory medicine* 135:1269-77
73. Ogino S, Kawasaki T, Kirkner GJ, Loda M, Fuchs CS. 2006. CpG island methylator phenotype-low (CIMP-low) in colorectal cancer: possible associations with male sex and KRAS mutations. *The Journal of molecular diagnostics : JMD* 8:582-8
74. Wolpin BM, Mayer RJ. 2008. Systemic treatment of colorectal cancer. *Gastroenterology* 134:1296-310
75. Winder T, Lenz HJ. 2010. Molecular predictive and prognostic markers in colon cancer. *Cancer treatment reviews* 36:550-6
76. Bertagnolli MM, Redston M, Compton CC, Niedzwiecki D, Mayer RJ, et al. 2011. Microsatellite instability and loss of heterozygosity at chromosomal location 18q: prospective evaluation of biomarkers for stages II and III colon cancer--a study of CALGB 9581 and 89803. *Journal of clinical oncology : official journal of the American Society of Clinical Oncology* 29:3153-62
77. Thorstensen L, Lind GE, Lovig T, Diep CB, Meling GI, et al. 2005. Genetic and epigenetic changes of components affecting the WNT pathway in colorectal carcinomas stratified by microsatellite instability. *Neoplasia (New York, N.Y.)* 7:99-108
78. Andreyev HJ, Norman AR, Cunningham D, Oates J, Dix BR, et al. 2001. Kirsten ras mutations in patients with colorectal cancer: the 'RASCAL II' study. *British journal of cancer* 85:692-6
79. Richman SD, Seymour MT, Chambers P, Elliott F, Daly CL, et al. 2009. KRAS and BRAF mutations in advanced colorectal cancer are associated with poor prognosis but do not preclude benefit from oxaliplatin or irinotecan: results from the MRC FOCUS trial. *Journal of clinical oncology : official journal of the American Society of Clinical Oncology* 27:5931-7
80. Mayer A, Takimoto M, Fritz E, Schellander G, Kofler K, Ludwig H. 1993. The prognostic significance of proliferating cell nuclear antigen, epidermal growth factor receptor, and mdr gene expression in colorectal cancer. *Cancer* 71:2454-60
81. Popat S, Matakidou A, Houlston RS. 2004. Thymidylate synthase expression and prognosis in colorectal cancer: a systematic review and meta-analysis. *Journal of clinical oncology : official journal of the American Society of Clinical Oncology* 22:529-36
82. Lievre A, Bachet JB, Le Corre D, Boige V, Landi B, et al. 2006. KRAS mutation status is predictive of response to cetuximab therapy in colorectal cancer. *Cancer research* 66:3992-5
83. Amado RG, Wolf M, Peeters M, Van Cutsem E, Siena S, et al. 2008. Wild-type KRAS is required for panitumumab efficacy in patients with metastatic colorectal cancer.

Journal of clinical oncology : official journal of the American Society of Clinical Oncology 26:1626-34
84. Di Nicolantonio F, Martini M, Molinari F, Sartore-Bianchi A, Arena S, et al. 2008. Wild-type BRAF is required for response to panitumumab or cetuximab in metastatic colorectal cancer. *Journal of clinical oncology : official journal of the American Society of Clinical Oncology* 26:5705-12
85. Hitre E, Budai B, Adleff V, Czegledi F, Horvath Z, et al. 2005. Influence of thymidylate synthase gene polymorphisms on the survival of colorectal cancer patients receiving adjuvant 5-fluorouracil. *Pharmacogenetics and genomics* 15:723-30
86. Samowitz WS, Curtin K, Ma KN, Schaffer D, Coleman LW, et al. 2001. Microsatellite instability in sporadic colon cancer is associated with an improved prognosis at the population level. *Cancer epidemiology, biomarkers & prevention : a publication of the American Association for Cancer Research, cosponsored by the American Society of Preventive Oncology* 10:917-23
87. Popat S, Hubner R, Houlston RS. 2005. Systematic review of microsatellite instability and colorectal cancer prognosis. *Journal of clinical oncology : official journal of the American Society of Clinical Oncology* 23:609-18
88. Walther A, Houlston R, Tomlinson I. 2008. Association between chromosomal instability and prognosis in colorectal cancer: a meta-analysis. *Gut* 57:941-50
89. Constant S, Mas C, Wiszniewski L, Huang S. 2013. *Colon Cancer: Current Treatments and Preclinical Models for the Discovery and Development of New Therapies*. INTECH Open Access Publisher
90. Yoruker EE, Holdenrieder S, Gezer U. 2016. Blood-based biomarkers for diagnosis, prognosis and treatment of colorectal cancer. *Clinica chimica acta; international journal of clinical chemistry*
91. Ferrara N. 2004. Vascular endothelial growth factor: basic science and clinical progress. *Endocrine reviews* 25:581-611
92. Bardelli A, Siena S. 2010. Molecular mechanisms of resistance to cetuximab and panitumumab in colorectal cancer. *Journal of clinical oncology : official journal of the American Society of Clinical Oncology* 28:1254-61
93. Garcia-Carbonero R, Supko JG. 2002. Current perspectives on the clinical experience, pharmacology, and continued development of the camptothecins. *Clinical cancer research : an official journal of the American Association for Cancer Research* 8:641-61
94. Arango D, Wilson AJ, Shi Q, Corner GA, Aranes MJ, et al. 2004. Molecular mechanisms of action and prediction of response to oxaliplatin in colorectal cancer cells. *British journal of cancer* 91:1931-46
95. Adams J, Cory S. 2007. The Bcl-2 apoptotic switch in cancer development and therapy. *Oncogene* 26:1324-37
96. Hanahan D, Weinberg RA. 2011. Hallmarks of cancer: the next generation. *Cell* 144:646-74
97. Hurley PJ, Wilsker D, Bunz F. 2007. Human cancer cells require ATR for cell cycle progression following exposure to ionizing radiation. *Oncogene* 26:2535-42
98. Nicoletti I, Migliorati G, Pagliacci MC, Grignani F, Riccardi C. 1991. A rapid and simple method for measuring thymocyte apoptosis by propidium iodide staining and flow cytometry. *Journal of immunological methods* 139:271-9
99. Bradford MM. 1976. A rapid and sensitive method for the quantitation of microgram quantities of protein utilizing the principle of protein-dye binding. *Analytical biochemistry* 72:248-54
100. Laemmli UK. 1970. Cleavage of structural proteins during the assembly of the head of bacteriophage T4. *Nature* 227:680-5
101. Lauber K, Appel HA, Schlosser SF, Gregor M, Schulze-Osthoff K, Wesselborg S. 2001. The adapter protein apoptotic protease-activating factor-1 (Apaf-1) is proteolytically processed during apoptosis. *The Journal of biological chemistry* 276:29772-81

102. Towbin H, Staehelin T, Gordon J. 1979. Electrophoretic transfer of proteins from polyacrylamide gels to nitrocellulose sheets: procedure and some applications. *Proceedings of the National Academy of Sciences of the United States of America* 76:4350-4
103. Gallmeier E, Hucl T, Calhoun ES, Cunningham SC, Bunz F, et al. 2007. Gene-specific selection against experimental fanconi anemia gene inactivation in human cancer. *Cancer biology & therapy* 6:654-60
104. Gallmeier E, Hermann PC, Mueller MT, Machado JG, Ziesch A, et al. 2011. Inhibition of ataxia telangiectasia- and Rad3-related function abrogates the in vitro and in vivo tumorigenicity of human colon cancer cells through depletion of the CD133(+) tumor-initiating cell fraction. *Stem cells (Dayton, Ohio)* 29:418-29
105. Andreassen PR, D'Andrea AD, Taniguchi T. 2004. ATR couples FANCD2 monoubiquitination to the DNA-damage response. *Genes & development* 18:1958-63
106. Wagner JM, Kaufmann SH. 2010. Prospects for the use of ATR inhibitors to treat cancer. *Pharmaceuticals* 3:1311-34
107. Huntoon CJ, Flatten KS, Wahner Hendrickson AE, Huehls AM, Sutor SL, et al. 2013. ATR inhibition broadly sensitizes ovarian cancer cells to chemotherapy independent of BRCA status. *Cancer research* 73:3683-91
108. Hall AB, Newsome D, Wang Y, Boucher DM, Eustace B, et al. 2014. Potentiation of tumor responses to DNA damaging therapy by the selective ATR inhibitor VX-970. *Oncotarget* 5:5674
109. Sausville EA, Arbuck SG, Messmann R, Headlee D, Bauer KS, et al. 2001. Phase I trial of 72-hour continuous infusion UCN-01 in patients with refractory neoplasms. *Journal of clinical oncology : official journal of the American Society of Clinical Oncology* 19:2319-33
110. Ma CX, Ellis MJ, Petroni GR, Guo Z, Cai S-r, et al. 2013. A phase II study of UCN-01 in combination with irinotecan in patients with metastatic triple negative breast cancer. *Breast cancer research and treatment* 137:483-92
111. Kortmansky J, Shah MA, Kaubisch A, Weyerbacher A, Yi S, et al. 2005. Phase I trial of the cyclin-dependent kinase inhibitor and protein kinase C inhibitor 7-hydroxystaurosporine in combination with Fluorouracil in patients with advanced solid tumors. *Journal of clinical oncology* 23:1875-84
112. Elmore S. 2007. Apoptosis: a review of programmed cell death. *Toxicologic pathology* 35:495-516
113. Golstein P, Kroemer G. 2007. Cell death by necrosis: towards a molecular definition. *Trends in biochemical sciences* 32:37-43
114. Fulda S, Debatin KM. 2006. Extrinsic versus intrinsic apoptosis pathways in anticancer chemotherapy. *Oncogene* 25:4798-811
115. Arda-Pirincci P, Bolkent S. 2011. The role of glucagon-like peptide-2 on apoptosis, cell proliferation, and oxidant-antioxidant system at a mouse model of intestinal injury induced by tumor necrosis factor-alpha/actinomycin D. *Molecular and cellular biochemistry* 350:13-27
116. Robertson JD, Enoksson M, Suomela M, Zhivotovsky B, Orrenius S. 2002. Caspase-2 acts upstream of mitochondria to promote cytochrome c release during etoposide-induced apoptosis. *The Journal of biological chemistry* 277:29803-9
117. Rogakou EP, Pilch DR, Orr AH, Ivanova VS, Bonner WM. 1998. DNA double-stranded breaks induce histone H2AX phosphorylation on serine 139. *The Journal of biological chemistry* 273:5858-68
118. Fernandez-Capetillo O, Lee A, Nussenzweig M, Nussenzweig A. 2004. H2AX: the histone guardian of the genome. *DNA repair* 3:959-67
119. Olive PL, Banath JP. 2009. Kinetics of H2AX phosphorylation after exposure to cisplatin. *Cytometry. Part B, Clinical cytometry* 76:79-90
120. Rogakou EP, Boon C, Redon C, Bonner WM. 1999. Megabase chromatin domains involved in DNA double-strand breaks in vivo. *The Journal of cell biology* 146:905-16
121. Svetlova M, Solovjeva L, Tomilin N. 2010. Mechanism of elimination of phosphorylated histone H2AX from chromatin after repair of DNA double-strand

breaks. *Mutation Research/Fundamental and Molecular Mechanisms of Mutagenesis* 685:54-60
122. Tanaka T, Halicka HD, Traganos F, Seiter K, Darzynkiewicz Z. 2007. Induction of ATM activation, histone H2AX phosphorylation and apoptosis by etoposide: relation to cell cycle phase. *Cell cycle (Georgetown, Tex.)* 6:371-6
123. Fujiwara T, Stolker JM, Watanabe T, Rashid A, Longo P, et al. 1998. Accumulated clonal genetic alterations in familial and sporadic colorectal carcinomas with widespread instability in microsatellite sequences. *The American journal of pathology* 153:1063-78
124. Herman JG, Umar A, Polyak K, Graff JR, Ahuja N, et al. 1998. Incidence and functional consequences of hMLH1 promoter hypermethylation in colorectal carcinoma. *Proceedings of the National Academy of Sciences of the United States of America* 95:6870-5
125. Oliveira C, Pinto M, Duval A, Brennetot C, Domingo E, et al. 2003. BRAF mutations characterize colon but not gastric cancer with mismatch repair deficiency. *Oncogene* 22:9192-6
126. Cortez D, Guntuku S, Qin J, Elledge SJ. 2001. ATR and ATRIP: partners in checkpoint signaling. *Science (New York, N.Y.)* 294:1713-6
127. Wilsker D, Bunz F. 2007. Loss of ataxia telangiectasia mutated- and Rad3-related function potentiates the effects of chemotherapeutic drugs on cancer cell survival. *Molecular cancer therapeutics* 6:1406-13
128. Zhang J-H, Chung TD, Oldenburg KR. 1999. A simple statistical parameter for use in evaluation and validation of high throughput screening assays. *Journal of biomolecular screening* 4:67-73
129. Menezes DL, Holt J, Tang Y, Feng J, Barsanti P, et al. 2015. A synthetic lethal screen reveals enhanced sensitivity to ATR inhibitor treatment in mantle cell lymphoma with ATM loss-of-function. *Molecular cancer research : MCR* 13:120-9
130. Mohni KN, Thompson PS, Luzwick JW, Glick GG, Pendleton CS, et al. 2015. A Synthetic Lethal Screen Identifies DNA Repair Pathways that Sensitize Cancer Cells to Combined ATR Inhibition and Cisplatin Treatments. *PloS one* 10:e0125482
131. Yonemasu R, Minami M, Nakatsu Y, Takeuchi M, Kuraoka I, et al. 2005. Disruption of mouse XAB2 gene involved in pre-mRNA splicing, transcription and transcription-coupled DNA repair results in preimplantation lethality. *DNA repair* 4:479-91
132. Lu LY, Wood JL, Minter-Dykhouse K, Ye L, Saunders TL, et al. 2008. Polo-like kinase 1 is essential for early embryonic development and tumor suppression. *Molecular and cellular biology* 28:6870-6
133. Higgins GS, Prevo R, Lee YF, Helleday T, Muschel RJ, et al. 2010. A small interfering RNA screen of genes involved in DNA repair identifies tumor-specific radiosensitization by POLQ knockdown. *Cancer research* 70:2984-93
134. Prindle MJ, Loeb LA. 2012. DNA polymerase delta in DNA replication and genome maintenance. *Environmental and molecular mutagenesis* 53:666-82
135. Michael WM, Ott R, Fanning E, Newport J. 2000. Activation of the DNA replication checkpoint through RNA synthesis by primase. *Science (New York, N.Y.)* 289:2133-7
136. Yotov WV, Hamel H, Rivard GE, Champagne MA, Russo PA, et al. 1999. Amplifications of DNA primase 1 (PRIM1) in human osteosarcoma. *Genes, chromosomes & cancer* 26:62-9
137. Pellegrini L. 2012. The Pol alpha-primase complex. *Sub-cellular biochemistry* 62:157-69
138. Hekmat-Nejad M, You Z, Yee MC, Newport JW, Cimprich KA. 2000. Xenopus ATR is a replication-dependent chromatin-binding protein required for the DNA replication checkpoint. *Current biology : CB* 10:1565-73
139. Pfeiffer P, Goedecke W, Kuhfittig-Kulle S, Obe G. 2004. Pathways of DNA double-strand break repair and their impact on the prevention and formation of chromosomal aberrations. *Cytogenetic and genome research* 104:7-13

140. Burckstummer T, Bennett KL, Preradovic A, Schutze G, Hantschel O, et al. 2006. An efficient tandem affinity purification procedure for interaction proteomics in mammalian cells. *Nature methods* 3:1013-9
141. Sibani S, Price GB, Zannis-Hadjopoulos M. 2005. Ku80 binds to human replication origins prior to the assembly of the ORC complex. *Biochemistry* 44:7885-96
142. Rampakakis E, Di Paola D, Zannis-Hadjopoulos M. 2008. Ku is involved in cell growth, DNA replication and G1-S transition. *Journal of cell science* 121:590-600
143. Liu Q, Guntuku S, Cui X-S, Matsuoka S, Cortez D, et al. 2000. Chk1 is an essential kinase that is regulated by Atr and required for the G2/M DNA damage checkpoint. *Genes & development* 14:1448-59
144. Weber AM, Ryan AJ. 2014. ATM and ATR as therapeutic targets in cancer. *Pharmacology & therapeutics*
145. Ma CX, Janetka JW, Piwnica-Worms H. 2011. Death by releasing the breaks: CHK1 inhibitors as cancer therapeutics. *Trends in molecular medicine* 17:88-96
146. Matsuoka S, Ballif BA, Smogorzewska A, McDonald ER, Hurov KE, et al. 2007. ATM and ATR substrate analysis reveals extensive protein networks responsive to DNA damage. *Science (New York, N.Y.)* 316:1160-6
147. Buisson R, Boisvert JL, Benes CH, Zou L. 2015. Distinct but Concerted Roles of ATR, DNA-PK, and Chk1 in Countering Replication Stress during S Phase. *Molecular cell* 59:1011-24
148. Luciani MG, Oehlmann M, Blow JJ. 2004. Characterization of a novel ATR-dependent, Chk1-independent, intra-S-phase checkpoint that suppresses initiation of replication in Xenopus. *Journal of cell science* 117:6019-30
149. Ahmed D, Eide PW, Eilertsen IA, Danielsen SA, Eknaes M, et al. 2013. Epigenetic and genetic features of 24 colon cancer cell lines. *Oncogenesis* 2:e71
150. Chen M, Wang J. 2002. Initiator caspases in apoptosis signaling pathways. *Apoptosis : an international journal on programmed cell death* 7:313-9
151. Uchimura A, Hidaka Y, Hirabayashi T, Hirabayashi M, Yagi T. 2009. DNA polymerase delta is required for early mammalian embryogenesis. *PloS one* 4:e4184
152. Song J, Hong P, Liu C, Zhang Y, Wang J, Wang P. 2015. Human POLD1 modulates cell cycle progression and DNA damage repair. *BMC biochemistry* 16:14
153. Roos WP, Kaina B. 2013. DNA damage-induced cell death: from specific DNA lesions to the DNA damage response and apoptosis. *Cancer letters* 332:237-48
154. Chea J, Zhang S, Zhao H, Zhang Z, Lee EY, et al. 2012. Spatiotemporal recruitment of human DNA polymerase delta to sites of UV damage. *Cell cycle (Georgetown, Tex.)* 11:2885-95
155. Kim ST, Lim DS, Canman CE, Kastan MB. 1999. Substrate specificities and identification of putative substrates of ATM kinase family members. *The Journal of biological chemistry* 274:37538-43
156. Sanefuji K, Taketomi A, Iguchi T, Sugimachi K, Ikegami T, et al. 2010. Significance of DNA polymerase delta catalytic subunit p125 induced by mutant p53 in the invasive potential of human hepatocellular carcinoma. *Oncology* 79:229-37
157. Kassambara A, Gourzones-Dmitriev C, Sahota S, Reme T, Moreaux J, et al. 2014. A DNA repair pathway score predicts survival in human multiple myeloma: the potential for therapeutic strategy. *Oncotarget* 5:2487-98
158. Ceder R, Haig Y, Merne M, Hansson A, Zheng X, et al. 2012. Differentiation-promoting culture of competent and noncompetent keratinocytes identifies biomarkers for head and neck cancer. *The American journal of pathology* 180:457-72
159. Flohr T, Dai JC, Büttner J, Popanda O, Hagmüller E, Thielmann HW. 1999. Detection of mutations in the DNA polymerase δ gene of human sporadic colorectal cancers and colon cancer cell lines. *International journal of cancer* 80:919-29
160. Church DN, Briggs SE, Palles C, Domingo E, Kearsey SJ, et al. 2013. DNA polymerase epsilon and delta exonuclease domain mutations in endometrial cancer. *Human molecular genetics* 22:2820-8

161. Palles C, Cazier JB, Howarth KM, Domingo E, Jones AM, et al. 2013. Germline mutations affecting the proofreading domains of POLE and POLD1 predispose to colorectal adenomas and carcinomas. *Nature genetics* 45:136-44
162. COSMIC, Cell, Line, Project. 2015. http://cancer.sanger.ac.uk/cell_lines.

7. SUPPLEMENTARY

7.1. List of siRNA library genes

Table 11: siRNA library of 288 genes involved in DNA repair.

ABCF2	*DNASE2*	*G3BP1*	*MMS19*	*POLB*	*RDM1*	*TK1*
ACLY	*DNMT1*	*HDAC1*	*MNAT1*	*POLD1*	*RECQL*	*TK2*
AHCY	*DNMT3A*	*HDAC2*	*MPG*	*POLE*	*RECQL4*	*TMEM30A*
ALKBH2	*DNMT3B*	*HDAC4*	*MRE11A*	*POLG*	*RECQL5*	*TOP1*
ALKBH3	*DOT1L*	*HDAC6*	*MRPL3*	*POLH*	*REV1*	*TOP1MT*
APEX1	*DUT*	*HDAC10*	*MRPS12*	*POLI*	*REV3L*	*TOP2A*
APEX2	*DVL3*	*HDAC11*	*MSH2*	*POLK*	*RFC2*	*TOP2B*
APTX	*EHMT1*	*HELQ*	*MSH3*	*POLL*	*RFC4*	*TOP3A*
ATM	*EIF4A3*	*HLTF*	*MSH4*	*POLM*	*RPA1*	*TP53*
ATR	*EME1*	*HNRNPA2B1*	*MSH5*	*POLN*	*RPA2*	*TP53BP1*
BLM	*ELN*	*HSPD1*	*MSH6*	*POLQ*	*RPA3*	*TPX2*
BRCA1	*ENDOG*	*HSPE1*	*MUS81*	*PPP2R5C*	*RPA4*	*TRAF4*
BRCA2	*ENDOV*	*HSP90B1*	*MTHFD2*	*PRDX2*	*RPL13*	*TRDMT1*
BRIP1	*ERCC1*	*HUS1*	*MUTYH*	*PRDX4*	*RPL27*	*TREX2*
CANX	*ERCC2*	*H2AFX*	*NBN*	*PRIM1*	*RPL35*	*TREX1*
CARM1	*ERCC3*	*H2AFZ*	*NCBP2*	*PRKDC*	*RRM1*	*TSTA3*
CBX3	*ERCC4*	*IARS*	*NEIL1*	*PRMT1*	*RRM2*	*TUBB*
CCNH	*ERCC5*	*IFNGR2*	*NEIL2*	*PSMA1*	*RRM2B*	*UBE2A*
CCT4	*ERCC6*	*ILF2*	*NEIL3*	*PSMC4*	*SDHC*	*UBE2B*
CCT5	*ERCC8*	*IL7R*	*NHEJ1*	*PSME2*	*SEPTIN9*	*UBE2N*
CDK1	*EXO1*	*INO80C*	*NME1*	*PTMA*	*SETD7*	*UBE2S*
CDK2	*EZH2*	*IP6K3*	*NONO*	*PTTG1*	*SETD8*	*UBE2V1*
CDK7	*E2F5*	*KDELR2*	*NTHL1*	*RAD1*	*SHFM1*	*UBE2V2*
CDKN3	*FANCA*	*KIAA0101*	*NT5E*	*RAD9A*	*SMARCA4*	*UNG*
CETN2	*FANCB*	*KPNA2*	*NUDT1*	*RAD17*	*SMC1A*	*WRN*
CHAF1A	*FANCC*	*LDHA*	*NUP205*	*RAD18*	*SMC3*	*XAB2*
CHEK1	*FANCD2*	*LIG1*	*OGG1*	*RAD21*	*SMUG1*	*XPA*
CHEK2	*FANCE*	*LIG3*	*OGT*	*RAD23A*	*SND1*	*XPC*
CKS2	*FANCF*	*LIG4*	*ORC6*	*RAD23B*	*SNRPE*	*XRCC1*
COL1A2	*FANCG*	*MAD2L2*	*PAFAH1B3*	*RAD50*	*SNRPF*	*XRCC2*
COPB2	*FANCL*	*MANF*	*PARP1*	*RAD51*	*SOX4*	*XRCC3*
CRIP2	*FANCM*	*MBD1*	*PARP2*	*RAD51AP1*	*SPO11*	*XRCC4*
CRY1	*FAP*	*MBD2*	*PARP3*	*RAD51B*	*SPRTN*	*XRCC5*
CRY2	*FBXO18*	*MBD3*	*PARP4*	*RAD51C*	*SSBP1*	*XRCC6*
CXCL6	*FEN1*	*MBD4*	*PCNA*	*RAD51D*	*SSR1*	*ZDHHC17*
C10orf2	*GINS2*	*MCM3*	*PLK1*	*RAD52*	*SUV39H1*	*ZNF607*
DCLRE1A	*GMNN*	*MECP2*	*PMS1*	*RAD54B*	*SUV39H2*	
DCLRE1B	*GTF2H1*	*MGMT*	*PMS2*	*RAD54L*	*TARS*	
DCLRE1C	*GTF2H2*	*MLH1*	*PMS2P3*	*RAG1*	*TDG*	
DDB1	*GTF2H3*	*MLH3*	*PMS2P5*	*RAG2*	*TDP1*	
DDB2	*GTF2H4*	*MLL*	*PNKP*	*PAICS*	*TERT*	
DMC1	*GTF2H5*	*MMP9*	*POLA1*	*RBM4*	*TGIF1*	

8. APPENDIX

8.1. Publications

Hocke S, Guo Y, Job A, Orth M, Ziesch A, et al. 2016. A synthetic lethal screen identifies ATR-inhibition as a novel therapeutic approach for POLD1-deficient cancers. *Oncotarget.*

De Toni E, Ziesch A, Rizzani A, Török H, Hocke S, et al. 2016. Inactivation of BRCA2 in human cancer cells identifies a subset of tumors with enhanced sensitivity towards death receptormediated apoptosis. *Oncotarget*

Guo Y, Ziesch A, Hocke S, Kampmann E, Ochs S, et al. 2015. Overexpression of heat shock protein 27 (HSP27) increases gemcitabine sensitivity in pancreatic cancer cells through S-phase arrest and apoptosis. *Journal of cellular and molecular medicine* 19:340-50

8.2. Abstract

Hocke S, Guo Y, Orth M, Lauber K, De Toni E, et al. 2015. Identifikation genetischer Determinanten für das Ansprechen auf ATR-Inhibition als tumortherapeutischer Ansatz. *Zeitschrift für Gastroenterologie* 53:KG226

8.3. Oral Presentation

Hocke S, Guo Y, Orth M, Lauber K, De Toni EN, et al. 2015. Identifikation genetischer Determinanten für das Ansprechen auf ATR-Inhibition als tumortherapeutischer Ansatz. 70. Jahrestagung DGVS, September, 16-19, 2015, Leipzig, Germany

8.4. Acknowledgement

First of all, I would like to express my special appreciation and thanks to PD Dr. Eike Gallmeier for giving me the opportunity to do my PhD thesis in his lab. Although his time was usually limited, he contributed great ideas and gave me a lot of scientific advice to push the project forward. I appreciated our discussions about how to solve scientific problems. I also thank him for his excellent support and endless endurance during the writing process of my paper.

Equally, I would like to deeply thank PD Dr. Andreas Herbst for having his door always open for any kind of scientific and non-scientific questions and his excellent support during the writing process of my thesis.

Thanks to the members of the Gallmeier lab, especially to Albert Job in Marburg for supporting me during the rebuttal process of my paper and Dr. Yang Guo for supporting me in all respects and reminding me not to lose focus on the important things. I really appreciated that.

In regards to my irradiation and apoptosis experiments, I thank Prof. Dr. Kirsten Lauber and Dr. Michael Orth for their unselfish help, the technical support in their lab and their constructive discussions for my project and beyond.

I also thank the members of the Medical Clinic II, especially Verena, Tatjana and Julian for their help in scientific questions and for a lot of great conversations at lunch and never-ending lab days.

Special thanks to Martin for always being at my side, his unconditional encouragement and endless motivation.

Last but not least, I would like to deeply thank my family for giving me the opportunity to go my own way. Thanks Mum and Dad for all your encouragement, trust and love.